Development of Responsive Nano/Microgels For Materials Application

By

Ting Zhou

A dissertation submitted to the Graduate Faculty in Chemistry in partial fulfillment of the requirements for the degree of Doctor of Philosophy, The City University of New York

2012

This manuscript has been read and accepted for the
Graduate Faculty in Chemistry in satisfaction of the
dissertation requirement for the degree of Doctor of Philosophy.

Shuiqin Zhou

Date

Chair of Examining Committee

Maria C. Tamargo

Date

Executive Officer

Michal Kruk

Yujia Xu

Supervisory Committee

THE CITY UNIVERSITY OF NEW YORK

Abstract

Development of Responsive Nano/Microgels for Materials Application

By

Ting Zhou

Adviser: Professor Shuiqin Zhou

Stimulus-responsive polymer microgels swell and shrink reversibly upon exposure to various environmental stimuli such as change in pH, temperature, ionic strength or magnetic fields. Therefore, they become ideal candidates for biomaterial applications. This work covers the general areas of responsive microgels and their application on controlled and targeted drug release. According to the therapy purpose, this work can be classified to two parts.

The first part of this thesis (chapter 3-5) focused on the development of biocompatible microgels–based drug delivery systems as anticancer drug carrier. These microgels are constructed from thermo-responsive and/or pH-responsive biocompatible materials, such as, oligo(ethylene glycol) and chitosan. The effects of pH values and temperatures on drug release behaviors of these stimulus-responsive microgels have been discussed. In chapter 5, hybrid ZnO quantum dots (QDs) encapsulated pH and temperature dual-responsive core-shell structure microgels has been prepared, which can not only be applied as targeting drug release system, but also can act as optical sensor for imaging in therapeutic application.

The latter part of this thesis (chapter 6, 7) investigated the synthesis, functionalization and characterization of glucose-responsive microgels for diabetes therapy purpose. CdS QDs immobilized glucose-sensitive microgels exhibit fluorescence quenching in the physiologically

important glucose concentration range 1–25 mM, which shows promise for a continuous non-invasive in vivo glucose sensing system. In another chapter, core-shell microgels with the P(NIPAM-AAm-PBA) microgel as core and the P(MEO_5MA) gel layer as shell were prepared for biocompatibility purpose. The presence of P(MEO_5MA) shell could prevent the glucose-sensitive core network from swelling due the hydrogen bonding between oxygens from P(MEO_5MA) side chains and glucose molecules, resulting in a shift of glucose sensitivity of core-shell microgels to higher glucose concentration in comparison with the free parent core microgels. Therefore, the set point of glucose sensitivity of microgels could be adjusted possibly and result in potential biomedical applications.

Acknowledgements

I first wish to express my deepest appreciation to my supervisor, Professor Shuiqin Zhou, who not only served as my supervisor but also encouraged and challenged me throughout my academic program. Without her help, this dissertation would not have been written.

I am most grateful for having had the opportunity to work with wonderful people in our group. Thanks to Dr. Weitai Wu, who used to be Post-Doctoral in our group and gave me a lot of great suggestions on my research projects. Thanks to Jing Shen and Yingyu Li, they helped me a lot to develop my work.

I am also grateful to Professor Michal Kruk, Professor Zhonghua Yu and Professor Yujia Xu for being on my Supervisory committee, and for their valuable insights and helpful discussion.

I wish to thank my family and friends who have been supportive and kind throughout all my years as a graduate student. Special thanks to my parents and my husband.

We gratefully acknowledge the financial support from the USAID (PGA-P280422) and PSC-CUNY research award.

Table of Contents

List of Figures

Chapter 5

List of Tables and Schemes

List of Abbreviations

5-FU	5-Fluorouracil
AA	Acrylic acid
AAm	Acryamide
AIBN	2,2′-azobisisobutyronitrile
APBA	3-aminophenylboronic Acid
APS	Ammonium Persulfate
BIS	N,N'-methylenebisacrylamide
$Cd(ClO_4)_2 \cdot H_2O$	Cadmium Perchlorate Hydrate
CdS	Cadmium Sulfide
CH_3CSNH_2	Thioacetamide
CHI	Chitosan
CMC	Critical Micelle Concentration
CNS	Central Nervous System
Con A	Concanavalin A
CSM	Core-shell Microgels
DIP	Dipyridamole
DLS	Dynamic Laser Scattering
DMEM	Dulbecco's Modified Eagle Medium
DNA	Deoxyribonucleic Acid
DTMP	Deoxythymidine monophosphate
DUMP	Deoxyuridine monophosphate
DVB	Divinylbenzene

EDC	N-(3-dimethylaminopropyl)-N'-ethyl-carbodiimide Hydrochloride
FBS	Foetal Bovine Serum
GOx	Glucose Oxidase
LCST	Lower Critical Solution Temperature
MBAAm	N,N'-methylenebisacrylamide
MEO_2MA	2-(2-methoxyethoxy)ethyl methacrylate
MEO_5MA	Oligo(ethylene glycol)methyl ether methacrylate (M_n = 300 g/mol)
MEO_9MA	Oligo(ethylene glycol) methacrylate (Mn = 475 g/mol)
MAA	Methacrylic Acid
MTT	3-(4,5-dimethyl-2-thiazolyl)-2,5-diphenyltetrazolium Bromide
Na_2S	Sodium Sulfide
NaOH	Sodium Hydroxide
NPs	Nanoparticles
PA	Polyalanine
PANI	Polyaniline
PBA	Phenylboronic Acid
PEG	Poly(ethylene glycol)
PEGDMA	Poly(ethylene glycol) Dimethacrylate
POEGMA	Poly(oligo(ethylene glycol) methacrylate
PNIPAM	Poly(N-isopropylacrylamide)
PS	Polystyrene
QDs	Quantum Dots
Rhb	Rhodamine B

RNA	Ribonucleic acid
SDS	Sodium Dodecyl Sulfate
Semi-IPN	Semi-interpenetrating Polymer Networks
SFPP	Surfactant Free Precipitation Polymerization
SiRNA	Small Interfering RNA
TEM	Transmission Electron Microscopy
TS	Thymidylate Synthase
VPTT	Volume Phase Transition Temperature

Chapter 1

Introduction of Responsive Polymer Microgels

1. 1 Definition of Microgels

Polymer microgels are cross-linked latex particles with a network structure that can swell in a suitable solvent.[1] The term microgel was first introduced by Baker in 1949,[2] however, the first microgel poly(divinylbenzene) (poly(DVB)) was prepared by Staudinger and Husemann over 70 years ago.[3] They polymerized highly diluted DVB in good solvent to achieve cross-linked polymer particles. So far, poly(N-isopropylacrylamide) (PNIPAM) is the most well studied water-swellable microgel system, while the best example of an organic swellable microgel is poly(styrene) (PS) that can swell in aromatic solvents (e.g. toluene). There is considerable scope for variation of microgel properties by changes in the structure of the monomers. The ionic microgel particles are frequently prepared by combining carboxylate groups derived from the acrylic acid (AA) or methacrylic acid (MAA) monomers. This work aims at water-swellable microgels system for the potential applications on biomaterial fields.

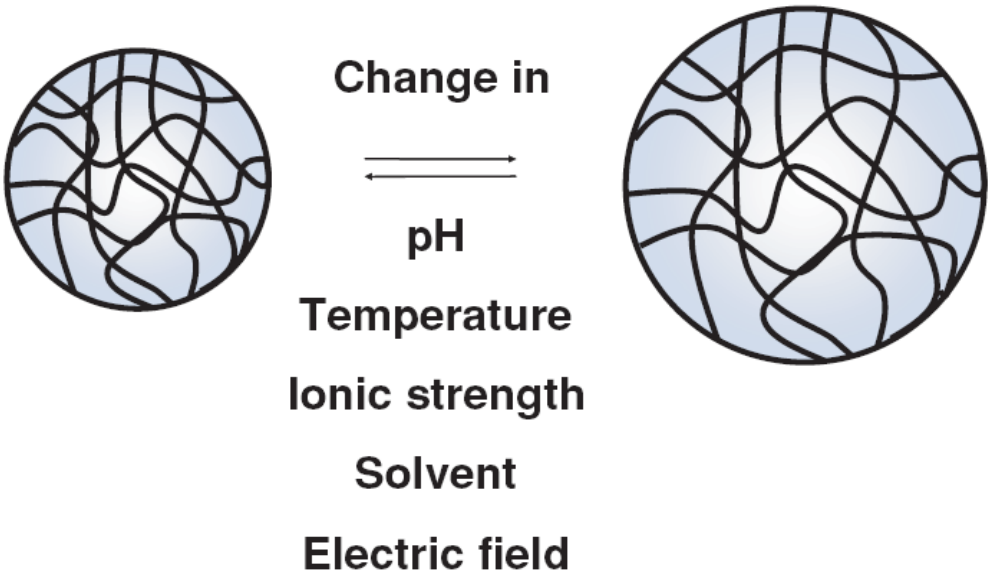

Figure 1-1 Schematic of change in microgel size in response to environmental stimuli.[4]

The responsive behavior of polymer microgels in a solvent is related to the balance between repulsive and attractive forces acting in the particles. Swelling occurs when ionic repulsion and osmotic forces exceed attractive forces, such as hydrogen bonding, van der Waals interactions, hydrophobic and specific interactions among the polymer chains.[4,5] Take thermo-sensitive polymers as an example, at higher temperatures, the hydrogen bonds to the water molecules break and there is an entropically favored release of bound and structured water, leading to the formation of a globular polymer chain conformation. In such a case, the polymer-polymer hydrophobic interactions become stronger than the polymer-solvent interactions, and the polymer phase separates from the water solvent. The temperature at which this phase separation occurs is called the lower critical solution temperature (LCST).[6] Compared to bulk gels, microgels have several advantages. First, they can respond very quickly to the environmental change. Second, the mono-dispersed microgel particles, as building blocks, can be readily assembled to meet various application requirements. Third, microgels are able to undergo a reversible volume phase transition in response to the environmental change, such as pH[7],

temperature[8], ionic strength, light, and electric field (figure 1-1).[9] Therefore, microgels have attracted much attention during the past several decades.

1. 2 Classification of microgels

Generally, microgels can be classified in two categories. First, they can be grouped based on cross-linking method, either physical method or chemical method. Second, they can be sorted by their responsive properties, which are determined by the functional groups incorporated within the microgel particles.[4,10]

1. 2. 1 Classification based on cross-linking method

Polymer molecules could be cross-linked by either chemical bonds or physical interactions. Chemically cross-linked microgels are more stable than their physically crosslinked counterparts due to their covalent nature. These microgels usually maintain a permanent structure unless a labile functionality has been intentionally added to the network.

For chemical bonding, functional groups like -OH, -COOH, -NH_2 of polymer chains can be used to prepare microgels by forming covalent linkages between the polymer chains and complementary reactivity.[7] The use of cross-linker is vital because this agent can prevent the microgels from dissolving in water at low temperatures. The most widely studied microgels are PNIPAM-based derivatives. The typical synthesis involved free radical precipitation polymerization of NIPAM monomers cross-linked with N, N-methylene-bisacrylamide (MBAAm).[11]

For physically cross-linked microgels, network formed via non-covalent attractive forces such as hydrophobic or ionic interactions. The latter is more prevalent. This physical gelation is

ideal for biodegradable systems that can reversibly go from the solution state to the gel state. Besides, physical cross-linking can avoid the potential toxicity originated from cross-linker. Physically crosslinked microgels are often constructed from biopolymers. Alginate is a well-known example which could be crosslinked by calcium ions.[12] The crosslinking can be carried out at room temperature and physiological pH. Hence, alginate gels are often used as matrix for the encapsulation of living cells[13] and the release of proteins[14]. However, physically cross-linked systems are extremely sensitive to many factors and may lose stability and fall apart to yield individual polymer molecules under particular conditions. These factors include polymer composition, temperature, ionic strength of the medium, as well as the concentrations of the polymer and cross-linking agent.

1. 2. 2 Classification based on responsive properties

Microgels can also be classified as pH sensitive, temperature sensitive, enzyme sensitive and electrically sensitive based on their nature. Temperature-induced volume phase transitions have been most widely studied for PNIPAM and related copolymers.[15,16] Above their volume phase transition temperature (VPTT), the hydrogen bonds between the amide groups and water molecules are broken and the PNIPAM chains undergo a coil to globule transition, thus the volume of microgel particles are decreased dramatically. The VPTT can be adjusted by the copolymerization of NIPAM with other monomers based on the hydrophobic-hydrophilic balance in the polymer matrix. Typically, incorporation of hydrophilic moieties increases and broadens the VPTT of microgels, conversely, incorporation of hydrophobic groups decreases the VPTT. For pH-sensitive microgels, copolymerization of NIPAM with ionic monomers such as acrylic acids, methacrylic acid, vinyl pyridine and vinyl imidazole leads to pH-responsive

property. In ionic microgels, the driving force for swelling arises from the electrostatic interactions between the ionic groups. The presence of ionizable functional groups like carboxylic acid, sulfonic acid, or amine groups renders the polymer more hydrophilic and result in high solvent uptake. The combination of different environmental stimuli responses results in multi-responsive microgels.

1. 3 Microgels Preparation

Microgels are usually prepared by precipitation polymerization and emulsion polymerization in the presence or absence of surfactant molecules.

1. 3. 1 Precipitation polymerization

Precipitation polymerization could be the most frequently used method to prepare microgels.[17] During free-radical precipitation polymerization, all ingredients are dissolved in a solvent (water) to form a homogeneous mixture, including monomers, crosslinker, surfactant and initiator. This method is very powerful for the preparation of thermo-sensitive microgels. The formation of microgel particles occurs by a homogeneous nucleation mechanism (figure 1-2). Water-soluble initiator decomposes to generate free radicals at reaction temperature, then the free radicals will attack water-soluble monomers followed by radical propagation and chain growth. When the polymerization temperature is far above the LCST of formed polymers, the growing polymer chains start to collapse to form precursor particles. [1, 18]

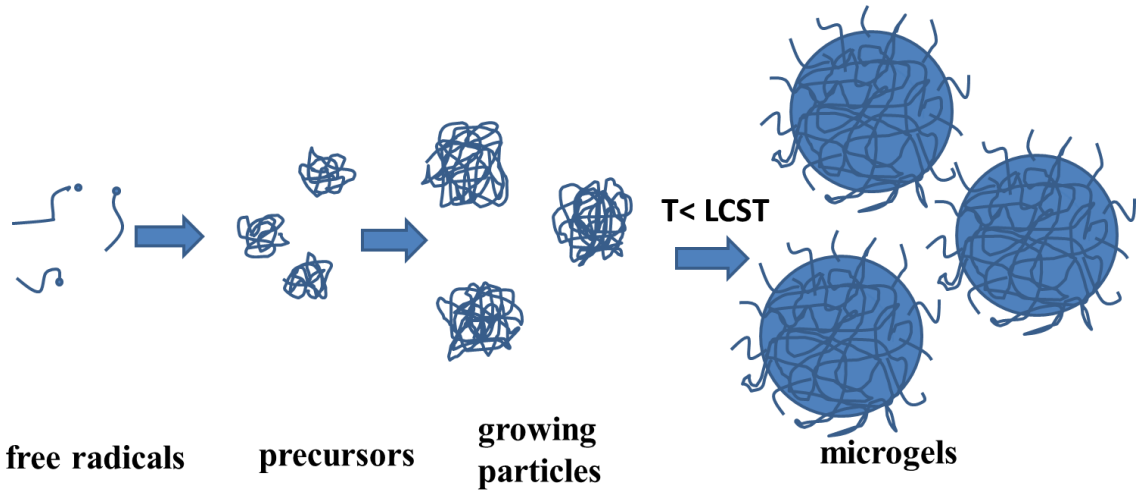

Figure 1-2 Mechanism of precipitation polymerization.

The precursor particles can grow by different mechanisms. Firstly, precursor particles aggregate to form a large colloidally stable polymer particle; secondly, they deposit on the surface of existing polymer particles; thirdly, they grow by addition of monomers or macroradicals. When microgel particles reach a critical size, they become stabilized by surfactant molecules. After the polymerization is completed and the reaction mixture is cooled down, microgel particles will swell. At temperatures below VPTT, microgels start to swell due to the formation of hydrogen bonds between polymer segments and water molecules. Hu and co-workers have prepared P(MEO_2MA-co-OEGMA) microgels by free radical precipitation polymerization in aqueous medium[19,20] and with the similar method OEGMA-based core-shell microgels were prepared as well.[21] They investigated the physical properties of the polymer microgels extensively, such as, the swelling kinetics of microgel shell and the melting kinetics of microgels after self-assembling. It is also demonstrated that OEGMA-based microgels can be self-assembled in aqueous medium to form crystalline structures with iridescent colors.[20,21] It is believed that these colloidal crystals are stabilized by interparticle crosslinking.[22]

However, there is a certain concern that surfactant molecules may not be completely removed through the repeated centrifugation/dialysis purification process. The presence of surfactant may limit the potential applications of microgels, therefore, surfactant free precipitation polymerization (SFPP) has been developed as an alternative. The colloidal stability is attributed to the charged initiator fragments residing at the particle surface.

1. 3. 2 Emulsion polymerization

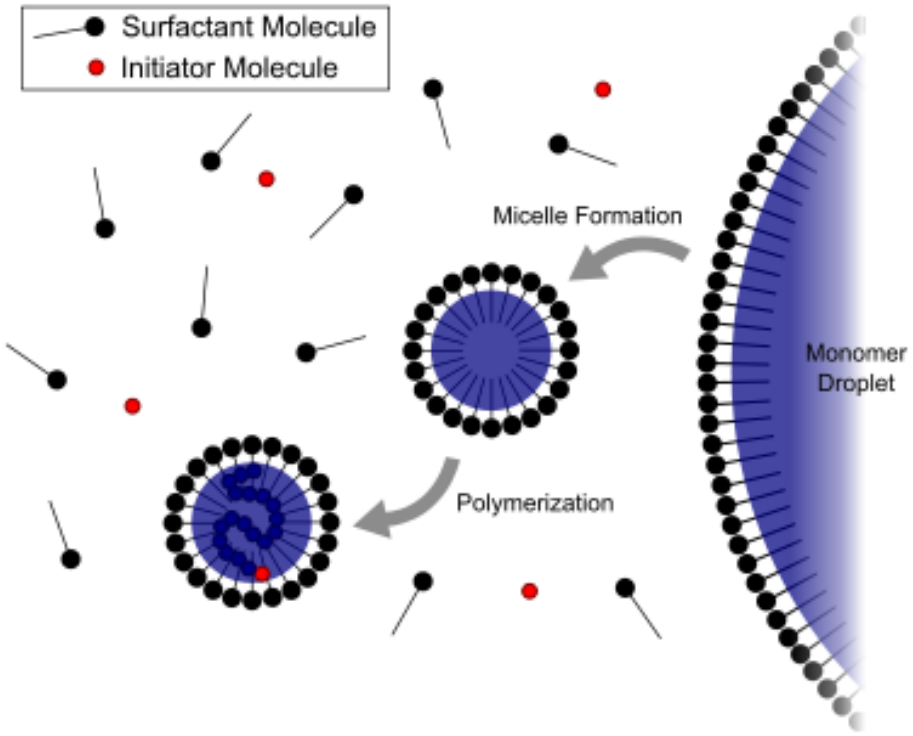

Figure 1-3 Mechanism of emulsion polymerization.

The term emulsion polymerization encompasses several related processes: (1) conventional emulsion polymerization, (2) inverse emulsion polymerization, (3) miniemulsion polymerization, (4) dispersion polymerization, and (5) microemulsion polymerization.[23] Conventional emulsion polymerization accounts for the majority of the world's production of

commercial polymers, such as PS. The most common type of conventional emulsion polymerization is an oil-in-water emulsion (figure 1-3), in which surfactant dissolved in water until micelle has been formed, droplets of monomer (the oil) are emulsified by surfactant in a continuous phase of water. The polymerization will take place in the micelle when free radicals migrate into the micelle and react with monomers. Monomer migrates in the large monomer droplets of the micellar core to sustain polymerization until all the monomer is consumed.

1. 4 Characterization

Several techniques are used to characterize microgel particles. They include light scattering, fluorometry, UV-VIS spectrophotometry, TEM and confocal imaging technique. Dynamic light scattering (DLS) has been the most widely used technique to study the solution behavior of microgels, especially the volume phase transitions and size distribution. A dilute dispersion of microgels appears transparent because the microgels are swollen with water at T < VPTT and the contrast in refractive indices of the polymer and the solvent is small. At T > VPTT, the expulsion of water from the particles causes an increase in refractive index contrast between the polymer and the solvent, and the dispersion appears turbid. TEM could show the morphology of microgel product. More details of this experimental technique are provided in Chapter 2.

1. 5 Applications of Microgels

Since the discovery of thermal de-swelling properties of nearly monodispersed PNIPAM microgels (when the temperature increased above the LCST i.e. 32 ^{o}C in water) in early 1990s, intensive research efforts have been focused on PNIPAM-based microgels.[24-40] In order to control the volume phase transitions and introduce other environmental sensitivities, various

functionalized PNIPAM microgels have been designed to accommodate the application requirement.[3-5, 8, 9]

Besides PNIPAM-based system, other polymer microgels have also discovered with responsive properties. Lutz and coworkers have reported thermo-responsive properties of poly-oligo (ethylene glycol) methacrylates (POEGMA) in 2006.[41,42] They found that the copolymers of 2-(2-methoxyethoxy)ethyl methacrylate (MEO_2MA) with oligo(ethylene glycol) methacrylate (Mn=475 g/mol, MEO_9MA) showed a similar thermo-responsive behavior as PNIPAM. Poly(ethylene glycol) PEG is an ideal material for bioapplication, with many excellent properties such as uncharged, water-soluble, biocompatible, nontoxic, and nonimmunogenic, which makes it undoubtedly the most studied and applied synthetic polymer in the biomedical field . In further research, it has been found that the LCST of the copolymer of P(MEO_2MA-co-MEO_9MA) can be adjusted by varying the comonomer ratios.[43,44] Lutz et al. also reported that P(MEO_2MA-co-MEO_9MA) modified bovine pancreas typsin have improved thermo-responsiveness and enzymatic activity.[45] Therefore, thermo-responsive polymers containing short oligo(ethylene glycol) side chains are regarded as an attractive alternative to PNIPAM. Many previous applications of responsive PNIPAM mircogels could be replaced by POEGMA polymers to improve biocompatibility.

As a result, these responsive microgels have gained much attention in the field of materials science. Their potential applications include drug delivery,[24-28] sensing and imaging,[29-32] fabrication of photonic crystals,[33-37] template-based synthesis of inorganic nanoparticles,[38] and separations and purification technologies.[39,40] In the following part, several important main applications of microgels have been introduced, which include their uses as microreactors for the

synthesis of inorganic nanoparticles (NPs), as optical sensors, and as carriers for targeted drug delivery.

1. 5. 1 Templates for Synthesis of Nanoparticles

Compared with inorganic compounds, inorganic nanoparticles exhibit strongly different properties. Therefore, inorganic nanoparticles showed promising applications in electronic and optical devices, magnetic recording media, biological labeling, catalysis and quantum computing. However, the stability of these inorganic nanoparticles in solution has to be considered since they tend to aggregate, which will limit their applications.[46] In this case, suitable carrier systems, such as microgels, dendrimers, block copolymer micelles, and latex particles, may be used as "microreactors" in which the metal nanoparticles can be immobilized and used for the purpose at hand.

In comparison with other polymer templates, microgels have several important advantages as the microreactors for nanoparticles formation: (1) simple synthesis and good control over particle size, (2) easy functionalization to provide stimulus-responsive behavior, (3) good stability, (4) relatively large size comparable to the wavelength of visible light.[1] The last one is important for optical applications of microgels. Figure 1-4 shows a typical schematic of NP synthesis in carboxylated microgels. When pH value is above the pKa of carboxylic acid groups in the network chains, the positively charged metal precursors were then introduced into the microgel networks through the electrostatic attractions. After reduction, the inorganic nanoparticles can be formed in situ in the interior of the microgels. In the case of Cadmium

Sulfide (CdS) synthesis, Sodium Sulfide (Na_2S) aqueous solution could be added into the dispersion to form nanoparticles.

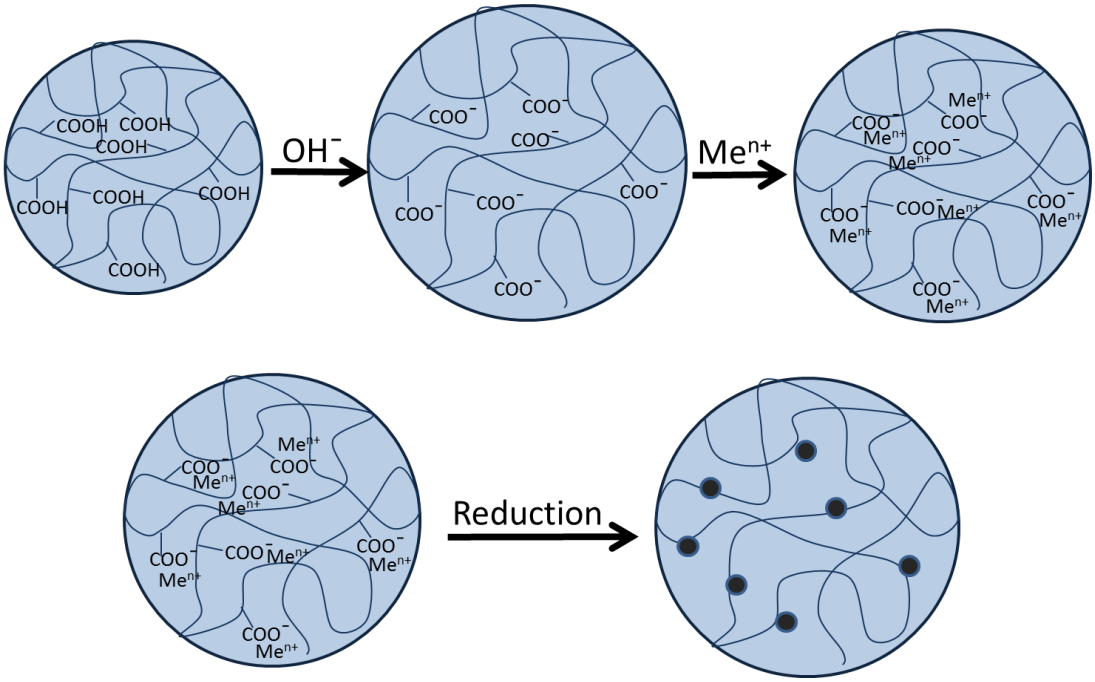

Figure 1-4 Schematic of microgel-based synthesis of nanoparticles.

The ionization of the carboxylic groups can increase the driving force for incorporation of metal ions into the microgels dramatically. In addition, the decrease in cross-linking density of microgels can increase the swelling ratio of microgels, resulting in the increase in the loading capacity of NPs as well.

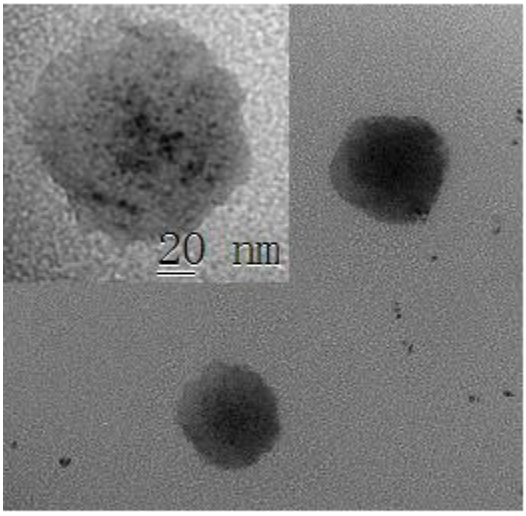

Figure 1-5 Typical TEM image of P(EG-co-Acrylic acid) microgels loaded with CdS nanoparticles.

Figure 1-5 shows representative transmission electron microscopy (TEM) images of hybrid microgel particles embedded with CdS nanoparticles. The small black nanoparticles inside the microgels network were clearly observed. These hybrid microgels retained their stimuli-responsiveness.

The template-based synthesis of NPs in microgels yields two important applications: the use of polymer particles as micro-reactors for NPs (that can be ultimately removed from microgels) and the production of hybrid microgel system. Our group prepared a class of NPs incorporated hybrid microgels, such as, ZnO-Au immobilized PEG-based nanogels[47] and ZnO QDs encapsulated semi-IPN PEG/Chitosan microgels. The presence of these inorganic nanoparticles enables the in vivo cell imaging, which is very helpful for us to understand the targeting efficiency and distribution of the microgels in living cell.

1. 5. 2 Optical sensor

Real-time measurements of biological/chemical/physical processes in live cells, with no interferences, are an ultimate goal for in vivo intracellular studies. Significant progress has been achieved by the continuous development of analyte-specific fluorescent probes, such as, organic dyes, semiconductor quantum dots and noble metal nanoparticles. However, the cytotoxicity of some available probes is a big problem and these moieties may affect immunological response of cells. Besides, non-specific binding and short lifetime of these molecular probes have to be considered as well. To overcome these problems, the integration of small molecule probes into other matrices such as polymers microgels could be a suitable choice. First, this matrix can eliminate the toxicity problem by protecting the cellular contents from the probes. The cell viability after sensor delivery can reach 99%, relative to control cells, indicating negligible physical and chemical perturbation to the cell. Second, microgels show some physical properties similar to living tissues, including a soft and rubbery consistency and low interfacial tension with water or biological fluids. The elastic nature of hydrated gels has been found to minimize irritation to the surrounding tissues after implantation. The low interfacial tension between the gel surface and body fluid minimizes protein adsorption and cell adhesion, which reduces the chances of a negative immune reaction. The inert protective matrix of the gel networks also eliminates interferences such as protein binding and/or membrane/organelle sequestration. Third, the hybrid micro-/nanogels with the optical moieties immobilized in polymer gel networks, combining the properties from both optical moieties and polymer gels.[48] The presence of specific functional groups on microgels enable the possibilities of environmental responsiveness and targeting delivery of optical probes to cells, in other word, selectivity and sensitivity of small molecule probes have been improved.[49]

Generally, a hybrid micro-/nanogel-based optical probe is composed of two components: optical moieties and a three-dimensional polymer scaffold. Under this consideration, such hybrid micro-/nanogel probes can be classified into three types (Figure 1-6). [2]

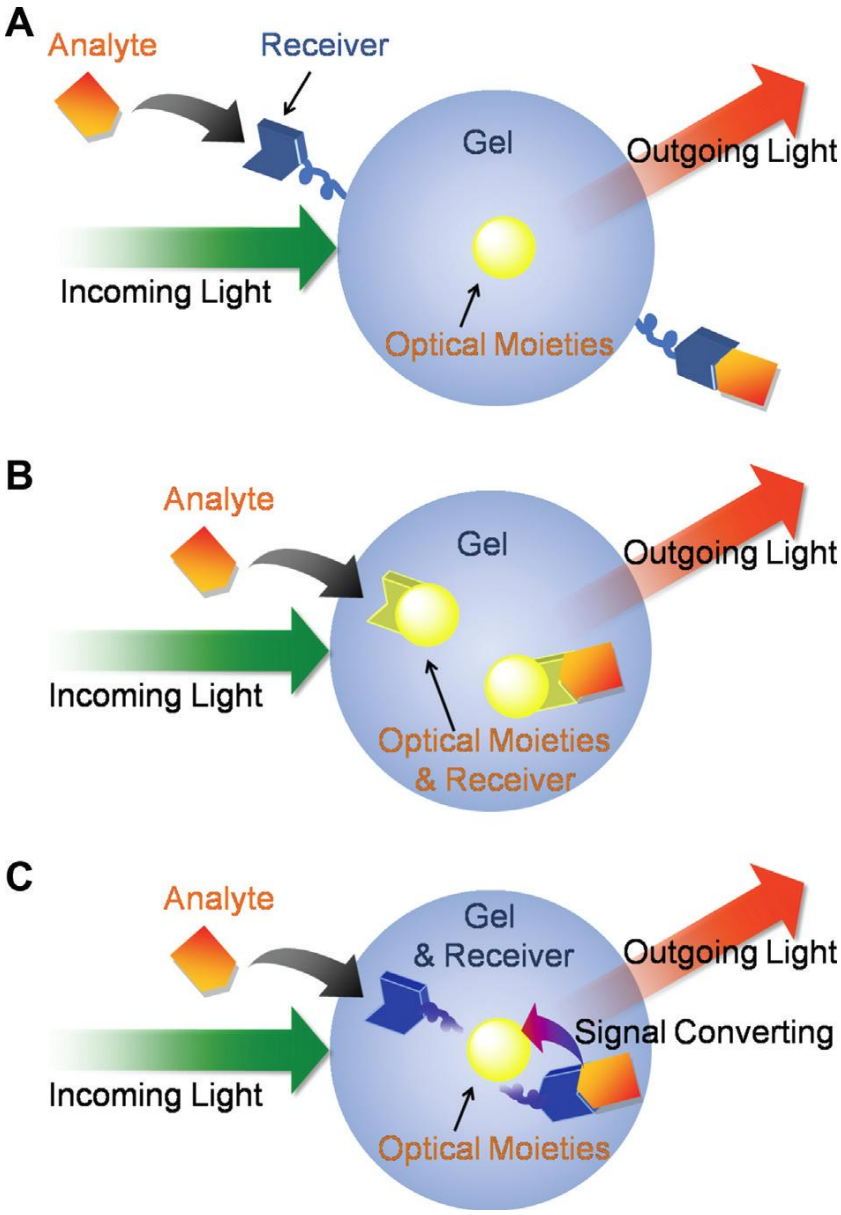

Figure 1-6 Schematic diagrams showing three types of hybrid micro-/nanogel-based optical probes: (A) Type 1 where the antibody or specific targeting ligand acts as a chemical/biochemical signal receiver; (B)Type 2 where an optical moiety acts directly as the

chemical / biochemical signal receiver; and (C) Type 3 where a responsive polymer gel network chain acts as the chemical/biochemical signal receiver, which will undergo a volume phase transition, change the physicochemical environment of the optical moieties, and convert the received signal into an optical signal.

In a Type 1 probe, the specific antibodies, aptamers, or other selective analyte-recognition ligands are covalently linked to the hybrid micro-/nanogels. Binding of the analyte to the hybrid micro-/nanogels would not affect the optical properties of the optical moieties, but the apparent color may change upon colocalization of the probes. In a Type 2 probe, the optical moiety acts directly as the chemical/biochemical signal receiver. The optical properties of the optical moieties (such as indicator dye and conjugated polymer) would change upon the binding of analyte. In a Type 3 probe the stimuli-responsive polymer gel network chains act as the chemical/biochemical signal receiver. Upon receiving the external stimulus, the gel network will undergo a volume phase transition and change the physicochemical environment of the optical moieties, converting the received signal into optical signal.

Sensors could be grouped into several main types according to their analytes.

TEMPERATURE SENSOR

Recently, Fangmao Ye et al. developed an ultrabright single-nanoparticle ratiometric temperature sensor based on polymer dots.[50] The polymer dots attached with a temperature sensitive dye –Rhodamine B(Rhb), whose emission intensity decreases with increasing temperature. This as-prepared polymer dots showed excellent temperature sensitivity and could be employed for measuring intracellular temperatures in a live cell imaging mode.

IONS SENSOR

The polyacrylamide nanoparticle has been used exclusively for this type of ion sensor because of its neutral and hydrophilic nature, which allows ions to readily permeate polymer matrix and interact with the indicator dye. Sensors for cobalt, copper, hydrogen, nickel, potassium, silver, sodium, zinc, and chloride ions have been developed.

PH SENSOR

A pH sensor was developed by coating a pH-insensitive fluorescent polystyrene bead (200 nm in diameter) with a layer of polyaniline (PANI) of only a few nanometers thick.[51] Plain PANI films display no fluorescence in the visible and near-IR range, but they do display characteristic pH-dependent absorption spectra that are due to protonation and deprotonation, respectively, of the emeraldine form of the PANI. Because of the fluorescence spectra of the beads being overlapped with the absorption spectra of PANI, the fluorescence intensity changes in accordance with the changes in pH.

GLUCOSE SENSOR

For the application in glucose detection, CdS QDs immobilized PNIPAM-based glucose-sensitive microgels have been designed as optical glucose sensor by our group. The PL intensity of CdS QDs can be quenched gradually when microgels gradually swelled up with the addition of D-glucose. Therefore, such hybrid microgels exhibit excellent sensitivity in physiologically important glucose concentration range (1-25 mM).[52] Wu et al. in our group designed hybrid nanogels made of Ag nanoparticle (NP) cores covered by a copolymer gel shell of poly(4-vinylphenylboronic acid-co-2-(dimethylamino)ethyl acrylate) as well. These hybrid microgels can also be used as optical glucose sensor and show regulate release of preloaded insulin at physiological pH.[53]

1. 5. 3 Intelligent Drug Delivery Systems

Polymer-based drug delivery system for site-specific delivery and controlled release of therapeutics has attracted great interest from the chemical, materials science, and pharmaceutical communities because they can dramatically improve drug efficiency and reduce side effects.[54-63] Microgels are particularly attractive as drug delivery carriers: their size can be easily varied from 100 nm to several micrometers, their interior network structure can be used for the incorporation of drugs to protect the drug from hydrolysis and potential biocompatibility, and their surface can be conjugated to receptor-specific molecules to achieve targeting ability. In addition, microgels carrying specific functional groups can undergo large swelling-deswelling transitions in response to changes in pH, ionic strength, or temperature, which commonly occur in many biological events.

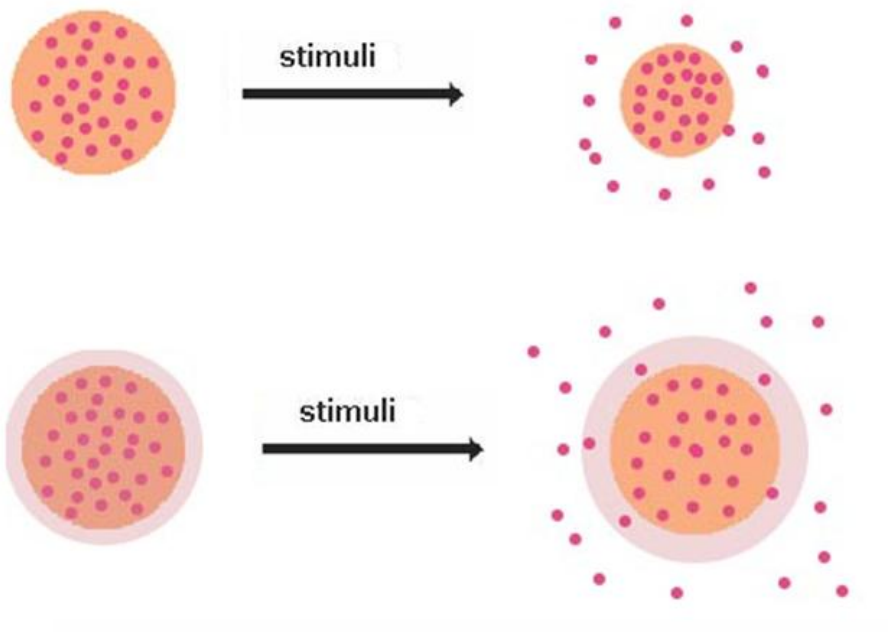

Figure 1-7 Model of triggerable drug release from the responsive microgels or shell-responsive core-shell structure microgels with drug in the core.

Generally, two systems could be applied on drug delivery (figure 1-7). The first one is functionalized microgels. Therefore, drug loaded microgels are able to undergo shrinkage or swelling when the environment has been changed, which can trigger the release of the drug. Second, core-shell structure microgels could be used as well. In this case, the shell of microgels will act as a switch and drugs are incorporated within core. As the change of environment, responsive shell start to swell along with the increased pore size, hence, drugs can diffuse to exterior. Lyon's group has focused on the investigation of PNIPAM-based microgels since 1999. They were the first group to explore the synthesis of core-shell particle composed entirely of hydrogel.[64] Besides, they have investigated particles with multi-shell structure,[65] hollow structure[66] or erodible property[67-69]as well. These microgels particles functionalized with target ligands (e. g. 12 amino acid peptide sequence) were applied for targeting drug delivery.[70] Recently, they started to investigate microgels as carriers for small interfering RNA (siRNA) in cancer therapy. SiRNA can induce gene silencing, which is helpful for the investigation in the development of new disease therapies. So far, they already achieved some impressive progresses, such as, efficient delivery of RNA to cytosol controlled by temperature change.[71]

Different from these reported work on microgels, we focus on the design of oligo(ethylene glycol)-based biocompatible microgels and their applications as drug carrier in biomedical fields. We designed oligo(ethylene glycol)-based microgels with core-shell structures and investigated the interactions between core and shell with respect to volume phase transition of the microgels. Additionally, the correlation of shell thickness with drug loading efficiency has been studied. Ideally, multi-responsive microgels are required for therapy in tumor tissue since the process in pathological zone always accompanied with pH and/or temperature change. Dual-responsive semi-interpenetrated PEG/Chitosan microgels have been prepared accordingly, which

show good biocompatibility, high drug loading capacity, and triggerable drug release kinetics under the in vitro conditions similar to the environments in pathological zone. We have further fabricated a series of core-shell structured microgels with ZnO quantum dots in the core and PEG/chitosan gel layer as shell to provide potential multifunctions for simultaneous imaging, pH/temperature sensing, and controlled drug release, which is important to monitor the therapeutic effects of drugs and the pathology. We have also fabricated oligo(ethylene glycol) gel shell on the glucose-sensitive gel core to tune the onset of glucose-induced volume phase transition of the microgels for potential self-regulated insulin delivery. We found that the thicker the oligo(ethylene glycol) gel shell, the higher the glucose concentration required to induce the swelling of the core-shell microgels. Therefore, the insulin can be released only after the blood glucose level is beyond the normal condition in human body as designed.

1. 6 Conclusion

Stimulus-responsive polymer microgels swell and shrink reversibly upon exposure to various environmental stimuli such as change in pH, temperature, glucose concentration, ionic strength or magnetic fields. They could be synthesized by precipitation polymerization. Due to the stimuli responsive properties, they become ideal candidates for biomaterial applications. Significant areas of development include the use of microgels for the templated synthesis of nanoparticles with pre-determined properties, as optical sensors and imaging agents, and as primary carriers in site-specific and controlled drug delivery systems. Facile synthesis and functionalization of microgel particles provide a broad range of variables for tuning their properties and favorably distinguishes them from other particulate polymer materials used for similar applications.

1. 7 References

(1) Saunders *Advances in Colloid and Interface Science* **1999**, *80*, 1-25.

(2) Baker, W. O. *Ind. Eng. Chem.* **1949**, *41*, 511-520.

(3) Staudinger, H.; Huseman, E. *Ber.* **1935**, *68*, 1618.

(4) Das, M.; Zhang, H.; Kumacheva, E. *Annu. Rev. Mater. Res.* **2006**, *36*, 117-142.

(5) Saunders, B. R.; Laajam, N.; Daly, E.; Teow, S.; Hu, X.; Stepto, R. *Adv Colloid Interface Sci* **2009**, *147-148*, 251-262.

(6) Nayak, S.; Lyon, L. A. *Angewandte Chemie International Edition* **2005**, *44*, 7686-7708.

(7) Dalmont, H.; Pinprayoon, O.; Saunders, B. R. *Langmuir* **2008**, *24*, 2834-2840.

(8) Pelton, R. *Adv Colloid Interface Sci* **2000**, *85*, 1-33.

(9) Zhang, Y.; Guan, Y.; Zhou, S. *Biomacromolecules* **2006**, *7*, 3196-3201.

(10) Hennink, W. E.; van Nostrum, C. F. *Adv. Drug Deliv. Rev* **2002**, *54*, 13-36.

(11) Wang, D.; Liu, T.; Yin, J.; Liu, S. *Macromolecules* **2011**, *44*, 2282-2290.

(12) Peter, G. *Carbohydrate Polymers* **1988**, *8*, 161-182.

(13) Goosen, M. F. A.; O'Shea, G. M.; Gharapetian, H. M.; Chou, S.; Sun, A. M. *Biotechnology and Bioengineering* **1985**, *27*, 146-150.

(14) Wee; Gombotz, W. *Advanced Drug Delivery Reviews* **1998**, *31*, 267-285.

(15) Wu, C.; Zhou, S. *Macromolecules* **1995**, *28*, 8381-8387.

(16) Zhou, S.; Chu, B. *J. Phys. Chem. B* **1998**, *102*, 1364-1371.

(17) Pich, A.; Richtering, W. In *Chemical Design of Responsive Microgels*; Pich, A.; Richtering, W., Eds.; Springer Berlin Heidelberg: Berlin, Heidelberg, 2010; Vol. 234, pp. 1-37.

(18) Welsch, N.; Ballauff, M.; Lu, Y. In Chemical Design of Responsive Microgels; Pich, A.; Richtering, W., Eds.; Springer Berlin Heidelberg: Berlin, Heidelberg, 2010; Vol. 234, pp. 129-163.

(19) Hu, Z. B.; Cai, T.; Chi, C.L. *Soft Matter* **2010**, 6, 2115-2123.

(20) Cai, T.; Marquez, M.; Hu, Z. *Langmuir* **2007**, 23, 8663-8666.

(21) Chi, C.; Cai, T.; Hu, Z. *Langmuir* **2009**, 25, 3814-3819.

(22) Cai, T.; Wang, G.; Thompson, S.; Marquez, M.; Hu, Z. *Macromolecules* **2008**, 41, 9508-9512.

(23) Asua, J. M. *Journal of Polymer Science Part A: Polymer Chemistry* **2004**, *42*, 1025-1041.

(24) Lally, S.; Mackenzie, P.; LeMaitre, C. L.; Freemont, T. J.; Saunders, B. R. *J Colloid Interface Sci* **2007**, *316*, 367-375.

(25) Kashyap, N.; Kumar, N.; Kumar, M. N. V. R. *Crit Rev Ther Drug Carrier Syst* **2005**, *22*, 107-149.

(26) Peppas, N. A.; Wood, K. M.; Blanchette, J. O. *Expert Opin Biol Ther* **2004**, *4*, 881-887.

(27) Shivakumar, H.; Satish, C.; Satish, K. *Indian J Pharm Sci* **2006**, *68*, 133.

(28) Vinogradov, S. V. *Curr Pharm Des* **2006**, *12*, 4703-4712.

(29) Wu, W.; Zhou, S. *Nano Reviews* **2010**, *1*.

(30) Chan, Y.-H.; Wu, C.; Ye, F.; Jin, Y.; Smith, P. B.; Chiu, D. T. *Analytical Chemistry* **2011**, *83*, 1448-1455.

(31) Liu, T.; Hu, J.; Yin, J.; Zhang, Y.; Li, C.; Liu, S. *Chemistry of Materials* **2009**, *21*, 3439-3446.

(32) Yin, J.; Guan, X.; Wang, D.; Liu, S. *Langmuir* **2009**, *25*, 11367-11374.

(33) Suzuki, D.; McGrath, J. G.; Kawaguchi, H.; Lyon, L. A. *J. Phys. Chem. C* **2007**, *111*, 5667-5672.

(34) Green, N. L.; Kaya, D.; Maloney, C. E.; Islam, M. F. *Phys. Rev. E* **2011**, *83*, 051404.

(35) Xu, S.; Zhang, J.; Paquet, C.; Lin, Y.; Kumacheva, E. *Advanced Functional Materials* **2003**, *13*, 468-472.

(36) Lyon, L. A.; Debord, J. D.; Debord, S. B.; Jones, C. D.; McGrath, J. G.; Serpe, M. J. *J. Phys. Chem. B* **2004**, *108*, 19099-19108.

(37) Zhang, J.; Sun, Z.; Yang, B. *Current Opinion in Colloid & Interface Science* **2009**, *14*, 103-114.

(38) Zhang, J.; Xu, S.; Kumacheva, E. *J. Am. Chem. Soc.* **2004**, *126*, 7908-7914.

(39) Bromberg, L.; Temchenko, M.; Hatton, T. A. *Langmuir* **2003**, *19*, 8675-8684.

(40) Mizrahi, B.; Irusta, S.; McKenna, M.; Stefanescu, C.; Yedidsion, L.; Myint, M.; Langer, R.; Kohane, D. S. *Advanced Materials* **2011**, *23*, H258-H262.

(41) Lutz, J. F.; Hoth, A. *Macromolecules* **2006**, 39, 893-896.

(42) Lutz, J. F.; Okdemir, O.; Hoth, A. *J. Am. Chem. Soc.* **2006**, 128, 13046-13047.

(43) Lutz, J. F.; Weichenhan, K.; Akemir, O.; Hoth, A. *Macromolecules* **2007**, 40, 2503-2508.

(44) Lutz, J. F.; Hoth, A.; Schade, K. *Des. Monomers Polym.* **2009**, 12, 343-353.

(45) Zarafshani, Z.; Obata, T.; Lutz, J. F. *Biomacromolecules* **2010**, 11, 2130-2135. (28) Jones, C. D.; Lyon, L. A. *Macromolecules* **2000**, 33, 8301-8306.

(46) Welsch, N.; Ballauff, M.; Lu, Y. In *Chemical Design of Responsive Microgels*; Pich, A.; Richtering, W., Eds.; Springer Berlin Heidelberg: Berlin, Heidelberg, **2010**; Vol. 234, pp. 129-163.

(47) Wu, W.; Shen, J.; Banerjee, P.; Zhou, S. *Adv. Func. Material.* **2011**, 21, 2830-2839.

(48) Hu, J.; Liu, S. *Macromolecules* **2010**, *43*, 8315-8330.

(49) Lee, Y. K.; Kopelman, R. *Wiley Interdisciplinary Reviews: Nanomedicine and Nanobiotechnology* **2009**, *1*, 98-110.

(50) Ye, F.; Wu, C.; Jin, Y.; Chan, Y.-H.; Zhang, X.; Chiu, D. T. *Journal of the American Chemical Society* **0**, *0*.

(51) Pringsheim, E.; Zimin, D.; Wolfbeis, O. S. *Advanced Materials* **2001**, *13*, 819-822. (52) Wu, W.; Zhou, T.; Shen, J; Zhou, S. *Chem. Comm.* **2009**, 4390-4392.

(53) Wu, W.; Mitra, N.; Yan, E. C. Y.; Zhou, S. *ACS Nano* **2010**, 4, 4831-4839.

(54) Honarkar, H.; Barikani, M. *Monatshefte für Chemie Chemical Monthly* **2009**, *140*, 1403-1420.

(55) Das, M.; Mardyani, S.; Chan, W. C. W.; Kumacheva, E. *Advanced Materials* **2006**, *18*, 80-83.

(56) Biondi, M.; Ungaro, F.; Quaglia, F.; Netti, P. A. *Advanced Drug Delivery Reviews* **2008**, *60*, 229-242.

(57) Zhang, H.; Mardyani, S.; Chan, W. C. W.; Kumacheva, E. *Biomacromolecules* **2006**, *7*, 1568-1572.

(58) Das, M.; Zhang, H.; Kumacheva, E. *Annual Review of Materials Research* **2006**, *36*, 117-142.

(59) Van Thienen, T. G.; Raemdonck, K.; Demeester, J.; De Smedt, S. C. *Langmuir* **2007**, *23*, 9794-9801.

(60) Kost, J.; Langer, R. *Advanced Drug Delivery Reviews* **2001**, *46*, 125-148.

(61) Malmsten, M. *Soft Matter* **2006**, *2*, 760-769.

(62) Alvarez-Lorenzo, C.; Concheiro, A.; Dubovik, A. S.; Grinberg, N. V.; Burova, T. V.; Grinberg, V. Y. *Journal of Controlled Release* **2005**, *102*, 629-641.

(63) Oh; Drumright, R.; Siegwart, D. J.; Matyjaszewski, K. *Progress in Polymer Science* **2008**, *33*, 448-477.

(64) Jones, C. D.; Lyon, L. A. *Macromolecules* **2000**, 33, 8301-8306.

(65) Hu, X.; Tong, Z.; Lyon, L. A. *J. Am. Chem. Soc.* **2010**, 132, 11470-11472.

(66) Nayak, S.; Gan, D.; Serpe, M.; Lyon, L. A. *Small* **2005**, 1, 416-421.

(67) Smith, M. H.; Herman, E. S.; Lyon, L. A. *J. Phys. Chem. B* **2011**, 115, 3761-3764.

(68) Smith, M. H.; South, A. B.; Gaulding, J. C.; Lyon, L. A. *Anal. Chem.* **2009**, 82, 523-530.

(69) South, A. B.; Lyon, L. A. *Chem. Mater.* **2010**, 22, 3300-3306.

(70) Nayak, S.; Lee, H.; Chmielewski, J.; Lyon, L. A. *J. Am. Chem. Soc.* **2004**, 126, 10258-10259.

(71) Duracher, D.; Sauzeddde, F.; Elaissari, A.; Pichot, C.; Nabzar, L. *Colloid, Polym. Sci.* **1998**, 276, 920-929.

Chapter 2

Materials and Methods

This chapter presents the basic synthetic and characterization methods used in this work. The standard synthetic method for preparation of microgels by free radical precipitation polymerization was discussed. The typical method for preparation of inorganic nanoparticles was provided. The techniques used for particle characterization are also available.

2. 1 Preparation of Microgels

2. 1. 1 Reagents

All reagents were purchased from Sigma-Aldrich. 2-(2-methoxyethoxy)ethyl methacrylate (MEO_2MA, 95%), oligo(ethylene glycol)methyl ether methacrylate (M_n = 300 g/mol, MEO_5MA), and poly(ethylene glycol) dimethacrylate (PEGDMA, $M_n \approx$ 550 g/mol, crosslinker) were purified with neutral Al_2O_3. Chitosan (CHI) was dissolved in acetic acid, then pass through a filter and dialysed against distilled water for three days to remove free acetic acid. Acrylic acid (AA) was distilled under reduced pressure; N-isopropylacryamide (NIPAM) was recrystallized from the mixture of hexane and acetone (1:1) prior to use. Sodium dodecyl sulfate (SDS) and ammonium persulfate (APS) were used as received. Deionized water with a resistance

of 18.2 MΩ (Millipore Milli-Q) was used. Figure 2-1 shows the structure and functions of the reactants used for microgels synthesis in this work.

Structure	Name	Function
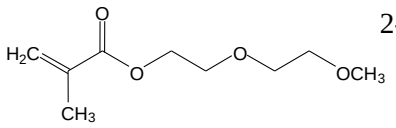	2-(2-methoxyethoxy)ethyl methacrylate (MEO_2MA)	Major monomer Thermo-responsive component
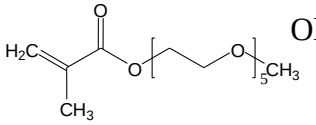	Oligo(ethylene glycol)methyl ether ethacrylate (MEO_5MA)	Major monomer Thermo-responsive component
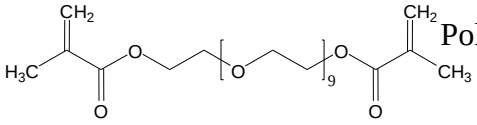	Poly(ethylene glycol) dimethacrylate (PEGDMA)	Crosslinker
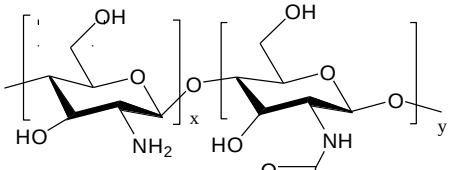	Chitosan (CHI)	pH-sensitive biopolymer
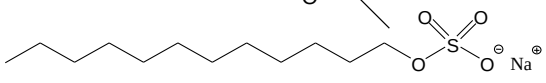	Sodium dodecyl sulfate (SDS)	Surfactant
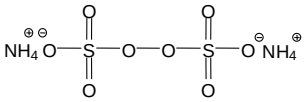	Ammonium persulfate (APS)	Initiator
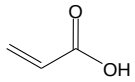	Acrylic acid (AA)	pH-sensitive ionic Comonomer
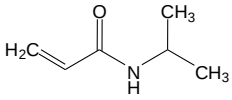	N-isopropylacrylamide(NIPAM)	Neutral Comonomer Thermo-responsive component

Figure 2-1 Structures and function of reactants used in free radical precipitation polymerization for the synthesis of microgels in this work.

2. 1. 2 Synthesis of Microgels

The microgels in this work were synthesized by free radical precipitation polymerization.[1] Typically, the proper amount of primary monomers 2-(2-methoxyethoxy)ethyl methacrylate (MEO_2MA), oligo(ethylene glycol)methyl ether methacrylate (MEO_5MA) and cross-linker PEGDMA were dissolved in 80 mL deionized water, together with comonomers and surfactant with a concentration under critical micelle concentration (CMC) in water. Then, the mixture was transferred to a three-neck round bottom flask equipped with condenser and nitrogen inlet. The solution was heated to 65 ℃ under a N_2 purge under stirring to remove oxygen dissolved in the mixture. After 1h, the initiator solution of ammonium persulfate (APS) (3.0×10^{-4} mol) was added to start the polymerization. The reaction was allowed to proceed for 5 hrs under continuous stirring. After the reaction finished, the obtained microgels were cooled and purified by 3 days of dialysis (Spectra/Por® molecularporous membrane tubing, cutoff 12000-14000) against very frequently changed water at room temperature (~ 22 °C). Figure 2-2 showed the scheme for preparation of microgels. The resultant microgel product displayed very narrow polydispersity according to the characterization by dynamic laser scattering (DLS) and transmission electron microscopy (TEM) imaging.

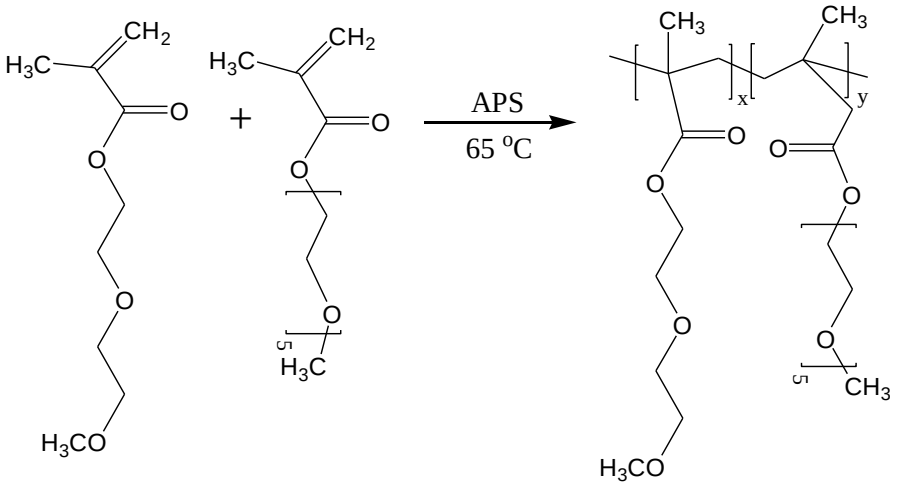

Figure 2-2 Synthetic scheme for the thermo-sensitive nonlinear PEG-based microgels. Comonomers with different functional groups can be added into solutions to anticipate the polymerization as well.

Figure 2-3 demonstrates the mechanism of free radical precipitation polymerization. One initiator molecule decomposed into two free radicals under reaction temperature, which can initiate polymerization in the homogenous solution phase; therefore, the water-soluble oligomers start to grow. As oligomers reach a critical chain length, the growing chain condenses to form precursor particles because the phase separation occurs at the polymerization temperature higher than the LCST of the polymer. The precursors may then either aggregate with other precursor particles or deposit onto an existing, colloidally stable microgel particles. Surfactant was used to prevent precursors from aggregating; therefore, the precursors formed in the early stage of reaction can be stabilized to form nuclei particles. The more surfactant, the more nuclei particles will be formed. The growing chains prefer to deposit onto these existing precursor microgel particles. Hence, the higher concentration of surfactant, the smaller the particle size is. Beside surfactants, the growing polymer particles can also achieve colloidal stability by the presence of electrostatic stabilization provided by the ionic groups originating from the initiator.

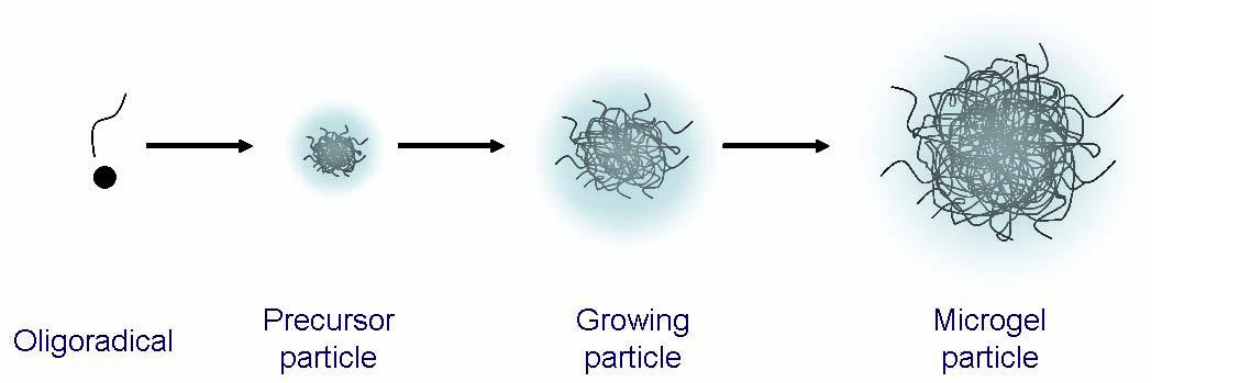

Figure 2-3 Mechanism of precipitation polymerizations. After initiation, the oligoradical grows to a critical length before precipitating itself to form a precursor particle. The precursor particle continues to grow either by aggregating with other precursor particles or with growing oligomers until the polymerization is completed.

2. 1. 3 Purification of Microgels

After polymerization, the solutions will contain surfactant molecules and a certain amount of linear or slightly branched polymer segments. Generally, there are two ways to purify the microgels. First, effectively repeated centrifugation, decantation, and redispersion of the microgels in water can be applied. Depending on the property of microgels, centrifugation conditions may be varied. Second, unreacted monomers and excess surfactant can be removed by dialysis against daily changes of water for a long enough time. However, dialysis even over extended periods of time is not always sufficient to remove all linear polymers or sol from microgel dispersions, a combination of dialysis and repeated centrifugation, decantation and redispersion techniques at appropriate pH values can effectively remove linear polymers from a dispersion of microgels. In the present work, microgels were typically purified by first

centrifugation and redispersion, then followed by dialysis for 3-5 days against daily changes of deionized water.

2. 2 Characterization of microgels

2. 2. 1 Size and Size Distribution

A standard light scattering spectrometer (BI-200SM) equipped with a BI-9000 AT digital time correlator (Brookhaven Instrument, Inc.) was used to monitor the size and size distribution of the microgels under different conditions. The schematic layout of the instrument is shown in figure 2-4. A Nd: YAG laser (150 mW, 532 nm) was used as the light source. The solutions were passed through 0.45 μm Millipore Millex-HV filters to remove dust. In DLS, the Laplace inversion of each measured intensity–intensity time correlated function can result in a characteristic line width distribution G(Γ). For a purely diffusive relaxation, Γ is related to the translational diffusion coefficient D by $(\Gamma/q2)_{C\rightarrow 0,q\rightarrow 0} = D$, where $q = (4\pi n/\lambda)\sin(\theta/2)$, with n, λ, and θ being the solvent refractive index, the wavelength of the incident light in vacuum, and the scattering angle, respectively. G(D) can be further converted to a hydrodynamic radius (R_h) distribution by using the Stokes–Einstein equation, $R_h = (k_BT/6\pi\eta)D^{-1}$, where T, k_B, and η are the absolute temperature, the Boltzmann constant, and the solvent viscosity, respectively.[2]

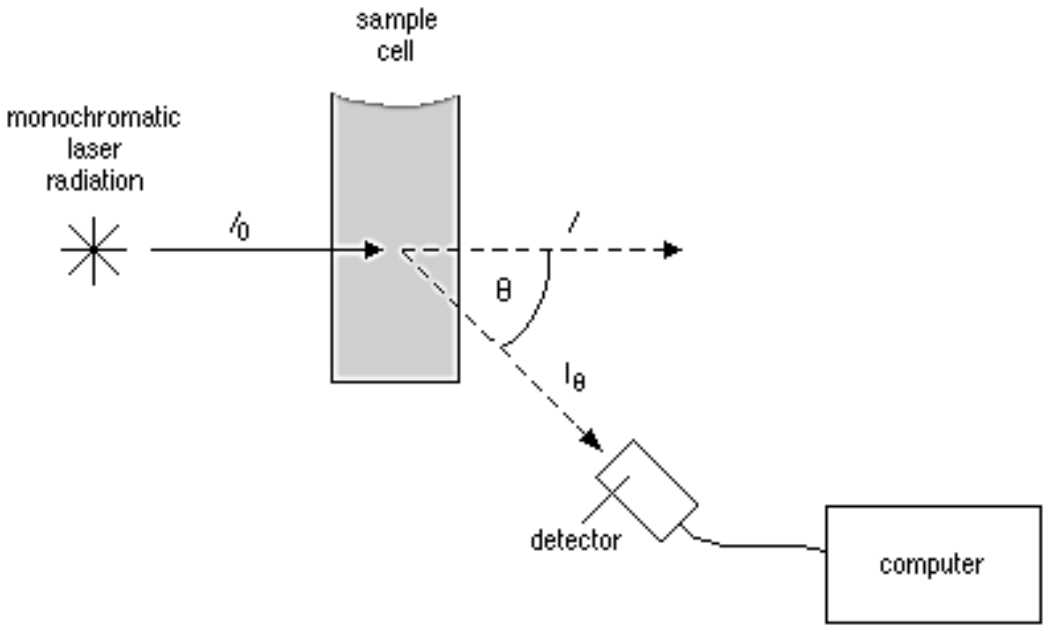

Figure 2-4 Schematic diagram of a conventional light scattering instrument setup.

2. 2. 2 Transmission electron microscopy

The morphology of microgels was characterized with transmission electron microscopy (TEM). Detailed information on the theory of TEM can be found elsewhere.[3] Briefly, a beam of electrons are focused on a single, pinpoint spot or element on the sample being studied. The electrons interact with the sample and only those that go past unobstructed hit the phosphor screen on the other side. At this point, the electrons are converted to light and an image is formed. The basic set up for TEM is schematically shown in figure 2-5. The TEM images were taken on a Zeiss EM 902 transmission electron microscope operating at an accelerating voltage of 100 kV. Approximately 10 μL of the diluted microgel suspension was dropped on a Formvar-covered copper grid (300 meshes) and dried in the air.

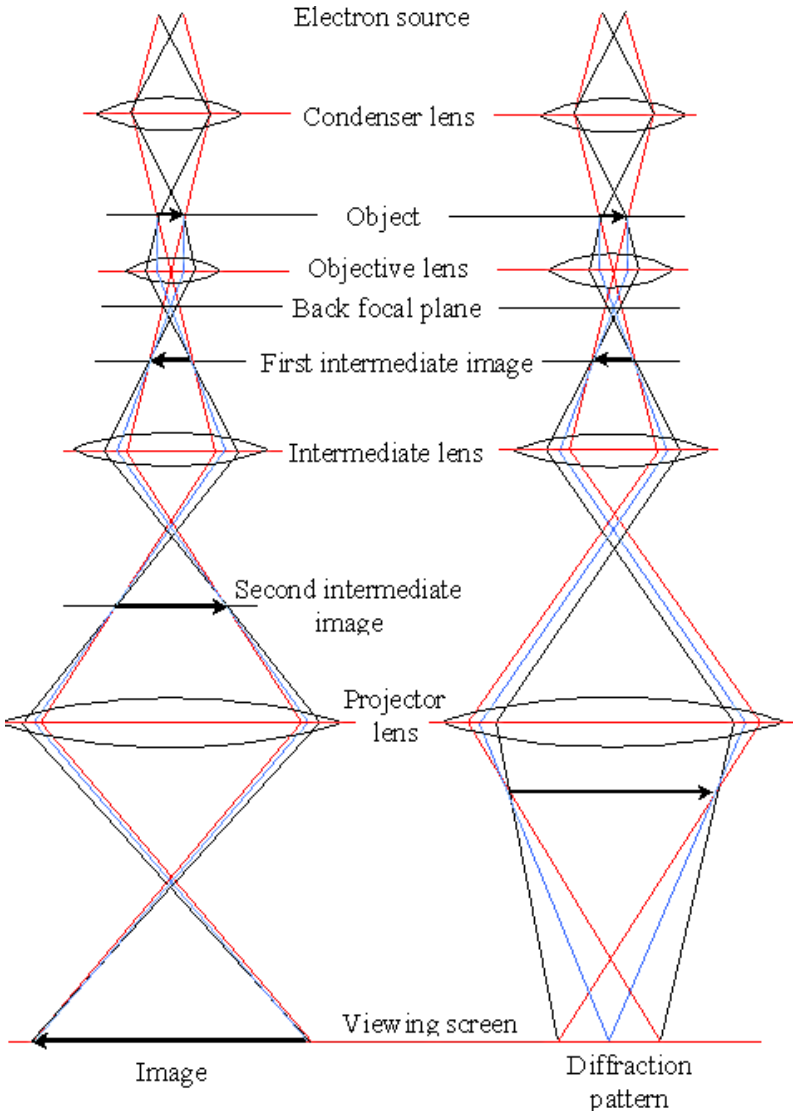

Figure 2-5 Schematic illustration of Transmission Electron Microscope.

The dark areas of the image correspond to areas on the specimen where fewer electrons were able to pass through (they were either absorbed or scattered upon impact); the lighter areas are where more electrons pass through, although the varying amounts of electrons in these areas enable the user to see structures and gradients.

The 'lenses' in a TEM are not the same as lenses in a conventional microscope. These are actually the EM devices that can 'focus' the electron beam to the desired wavelength or size. In

much the same way as a light microscope, however, the amount of power used to generate electrons allows for higher magnification or better resolutions.[3]

2. 2. 3 Confocal Microscopes

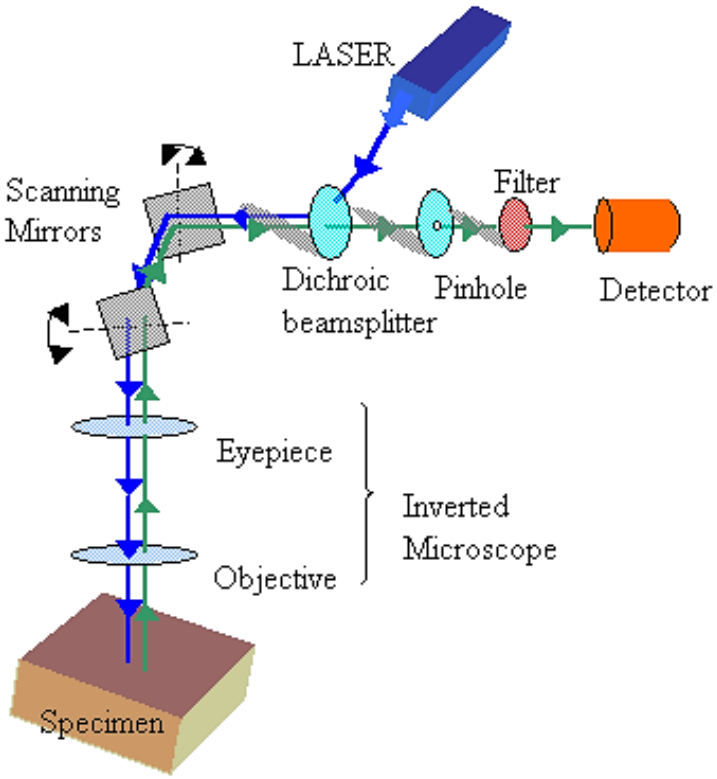

Figure 2-6 Schematic of confocal microscope.

A laser is used to provide the excitation light (in order to get very high intensities). The laser light (blue) reflects off a dichroic mirror. From there, the laser hits two mirrors which are mounted on motors; these mirrors scan the laser across the sample. The labeling molecules (e.g., dye, quantum dots) in the sample fluoresce, and the emitted light (green) gets descanned by the same mirrors that are used to scan the excitation light (blue) from the laser. The emitted light

passes through the dichroic and is focused onto the pinhole. The light that passes through the pinhole is measured by a detector.[4]

2. 2. 4 Cell toxicity

B16F10 cells (2000 cell/well) were cultured in DMEM containing 10% FBS and 1% penicillin-streptomycin in two 96-well plates, and exposed to free 5-FU, drug-free PEG-chitosan nanogels, and 5-FU loaded PEG-chitosan nanogels. To cover the high concentrations, the nanogels were concentrated and adjusted to an appropriate concentration in DMEM right before feeding into the well. One plate was incubated at 37 ℃ for 2 h and another plate was incubated for 24 h. The medium was then aspirated, and these wells were washed using fresh serum-free DMEM. After that, 25.0 mL of 3-(4,5-dimethyl-2-thiazolyl)-2,5-diphenyltetrazolium bromide (MTT) solution (5.0 mg/mL in PBS) were added to the wells. After incubation for 2 h, the solution was aspirated. 100.0 mL of dimethyl sulfoxide was then added to each well and the plate was sealed and incubated for 30 min at 37 ℃ with gentle mixing. Three portions of the solution obtained from each well were transferred to three respective wells of a 96-well plate. Cell viability was measured using a microplate reader at 570 nm. Positive controls contained no 5-FU or nanogels, and negative controls contained MTT.[5]

2. 3 In situ synthesis of Quantum Dots (QDs) in the microgels

2. 3. 1 Synthesis of ZnO QDs

0.04 g of 2,2′-azobisisobutyronitrile (AIBN), 0.30 g zinc methacrylate and 6 mL of poly(ethylene glycol) methyl ether methacrylate PEGMEMA (M_n=300) were dissolved in 30 mL absolute ethanol. The solution was stirred and heated at 80 ℃ for 30 min under purge of nitrogen. Then 0.06 g of AIBN and 500 μL of 10 M sodium hydroxide (NaOH) aqueous solution were added into the reaction system and refluxed for 1 h. After cooling to room temperature, the solution was dialyzed against deionized water for 3 days.[6]

2. 3. 2 Synthesis of CdS quantum dots

The mixture of 0.1431 g $Cd(ClO4)_2 \cdot H_2O$ with 20 mL microgel dispersions was stirred at room temperature for 1 day under a N_2 purge. After that, excess Cd^{2+} ions were removed by centrifugation (20,000 rpm, 10 min), decantation, and dialysis against water for 2 days. The purified microgels loaded with Cd^{2+} ions were heated to 60 ℃ under a N_2 purge. After 30 min, 5 mL thioacetamide solution (0.0146 g/mL) was added dropwise. The temperature was raised to 85 °C and the color gradually turned to brilliant yellow. The mixture was further stirred for 1 h under N_2 atmosphere. The resulted microgels incorporated with in situ grown CdS QDs were then purified by centrifugation, decantation, and dialysis against very frequently changed water for 3 days.[7]

2. 3. 3 Characterizations of QDs

QDs in this work were characterized by their photoluminescence spectrum, obtained on a Jobin Yvon Co FluoroMax-3 spectrofluorometer equipped with a Hamamatsu R928P photomultiplier tube.

2. 4 References

(1) Pich, A.; Richtering, W. In *Chemical Design of Responsive Microgels*; Pich, A.; Richtering, W., Eds.; Springer Berlin Heidelberg: Berlin, Heidelberg, 2010; Vol. 234, pp. 1-37.

(2) Schärtl, W. *Light scattering from polymer solutions and nanoparticle dispersions*; Springer, 2007.

(3) Williams, D. B.; Carter, C. B. In *Transmission Electron Microscopy*; Springer US: Boston, MA, 2009; pp. 3-22.

(4) Fujimoto, J. G.; Farkas, D.; Farkas, D. L. *Biomedical Optical Imaging*; Oxford University Press, 2009.

(5) Wu, W.; Aiello, M.; Zhou, T.; Berliner, A.; Banerjee, P.; Zhou, S. *Biomaterials* **2010**, *31*, 3023-3031.

(6) Xiong, H.-M.; Xu, Y.; Ren, Q.-G.; Xia, Y.-Y. *Journal of the American Chemical Society* **2008**, *130*, 7522-7523.

(7) Wu, W.; Zhou, T.; Aiello, M.; Zhou, S. *Biosensors and Bioelectronics* **2010**, *25*, 2603-2610.

Chapter 3

Oligo(ethylene glycol)-Based core-shell Microgels for Drug Delivery Applications

3. 1 Introduction

Microgel particles as drug delivery carriers for biological and biomedical applications have received increasing attention during the last decade due to their unique chemical and physical versatility [1-6]. Microgels offer several advantages over other polymer based drug delivery systems: simple synthesis, tunable size from nanometers to micrometers, large surface area for effective bioconjugation to add target ligands for site-specific delivery, an interior network structure for the incorporation of drug molecules to protect the drug from hydrolysis and other type of chemical degradation, and potential biocompatibility. Among the various approaches used to enhance the efficacy of chemotherapy is the use of smart carrier systems that can release a drug in response to stimuli, such as changes in pH, temperature, light, or the presence of specific enzymes that are selectively encountered in relevant cell organelles.[7-10]

So far, the thermo-responsive PNIPAM-based microgels have been most extensively studied for applications in drug delivery,[8-20] including the introduction of other environmental sensitivities such as pH, glucose, and light sensitive components into the PNIPAM microgels to control the drug release. However, the well-studied PNIPAM-based microgels have not been translated into a biomedical breakthrough although a recent study on the microgels containing NIPAM and AA indicated no adverse effects.[16] To meet the general requirement in biocompatibility of the materials used for drug delivery systems, an important challenge is to develop biocompatible polymers which have similar properties to PNIPAM.[4] Thermo-responsive polymers containing short oligo(ethylene glycol) side chains were recently proposed as an attractive alternative to PNIPAM.[22-28] The LCST of these graft polymers are tunable through the control in the compositions of the oligo(ethylene glycol) side chains. Lutz et al. have reported that the LCST of the copolymers composed of MEO_2MA with MEO_9MA can be adjusted by varying the comonomer ratios.[22-24] Ishizone et al. found that the LCST of the poly[oligo(ethylene glycol) alkyl ether methacrylates] is tunable by varying the oligo(ethylene glycol) side chain length.[26, 27] The longer the oligo(ethylene glycol) side chain, the higher the LCST of the graft polymer. In addition, the star-block copolymers of these oligo(ethylene glycol) methyl ether methacrylate with star PEG exhibit thermoreversible sol-gel transitions in physiological media.[28] Although the graft structure composed of a carbon-carbon backbone and multiple oligo(ethylene glycol) side chains is different from the standard linear PEG, these nonlinear PEG analogues are mainly composed of oligo(ethylene glycol) segments and are, in most cases, water-soluble and biocompatible.[25] Hence, these thermo-sensitive nonlinear PEG analogue polymers are very promising for biomedical applications.

Based on the free radical precipitation polymerization technique used to synthesize PNIPAM microgels, Hu's group has successfully synthesized monodisperse copolymer microgels from the comonomers of MEO_2MA and MEO_9MA at different ratios.[29] With the same two-step polymerization method used for the preparation of PNIPAM-based core-shell microgels, they also successfully synthesized core-shell microgels with the poly[oligo(ethylene glycol) ethyl ether methacrylate (M_n = 246 g/mol, EEO_3MA)] as core and the copolymer of EEO_3MA, MEO_5MA (M_n = 300 g/mol) and acrylic acid as shell. Similar to PNIPAM microgels, these nonlinear PEG analogue polymer microgels can self-assemble into interesting colloidal crystalline phases, depending on the concentration and temperature .[30]

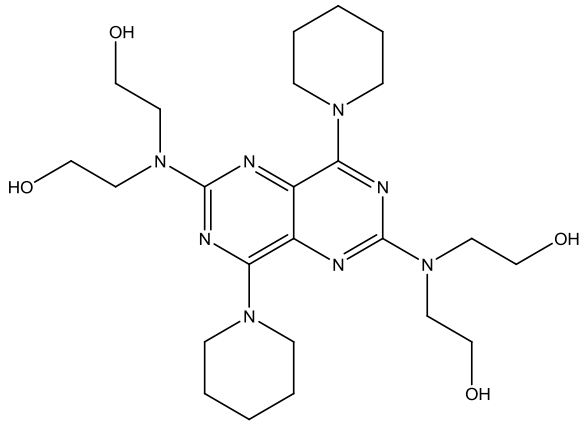

Figure 3-1 Chemical Structure of model drug DIP.

The aim of this work is to develop a series of monodisperse oligo(ethylene glycol)-based temperature sensitive core-shell microgels with different shell thickness, and study their potential application as delivery vehicles of hydrophobic drugs. The structures and volume phase transitions of PNIPAM-based core-shell microgels have been well studied.[31-34] The core-shell microgels can provide unique internal structures and multi-responsive properties due to the mutual influence of core and shell swelling, which enables us to explore the possibility to control the uptake and release of drug molecules in the microgels. In our design, the poly[2-(2-

methoxyethoxy)ethyl methacrylate] [P(MEO_2MA)] microgels with a VPTT ~22 °C is used as a hydrophobic core and the crosslinked copolymer of P(MEO_2MA-co-MEO_5MA) with the comonomer ratio of MEO_2MA:MEO_5MA = 1:2 and a VPTT of ~55 °C is used as a hydrophilic shell. In addition to the good biocompatibility, the hydrophilic P(MEO_2MA-co-MEO_5MA) shell can influence the core swelling. Although the free P(MEO_2MA) core chain network is hydrophobic and collapsed at temperature above its VPTT, the addition of hydrophilic shell can mechanically expand the collapsed core. As the shell thickness increases to certain extent, the hydrophobic core network can be almost fully expanded even at temperature above the VPTT of core microgels.[33, 34] We expect that the hydrophobic core with an open network structure should load hydrophobic drug molecules much more effectively compared to the collapsed structure. To demonstrate this concept, a hydrophobic drug dipyridamole (DIP) (see figure3-1) was studied as model drug. The effects of shell thickness and temperature on the drug loading efficiency were investigated. The sustained drug release behavior and cytotoxicity of the drug-free/drug-loaded microgels were evaluated. The results presented in this work provide important guidelines for the rational design of biocompatible PEG analogue-based core-shell microgels for drug delivery vehicles.

3. 2 Experimental

3. 2. 1 Materials

All reagents were purchased from Sigma-Aldrich. 2-(2-methoxyethoxy)ethyl methacrylate (MEO_2MA, 95%), oligo(ethylene glycol)methyl ether methacrylate (M_n = 300 g/mol, MEO_5MA), and poly(ethylene glycol) dimethacrylate (PEGDMA, $M_n \approx$ 550 g/mol,

crosslinker) were purified with neutral Al_2O_3. Dipyridamole (DIP), sodium dodecyl sulfate (SDS) and ammonium persulfate (APS) were used as received.

3. 2. 2 Synthesis of Oligo(ethylene glycol)-based Core-Shell Microgels

The P(MEO_2MA) core microgels were respectively synthesized according to the compositions listed in Table 3-1. Typically, the monomers, PEGDMA crosslinker, and SDS (5.0×10^{-5} mol) were dissolved in 200 mL deionized water. The mixture was heated to 70 ℃ under a N_2 purge. After 1 h, APS (3.0×10^{-4} mol) was added to the solution to initiate the polymerization. The reaction was allowed to proceed for 5 h. The obtained core microgels were purified by centrifugation (Thermo Electron Co. SORVALL® RC-6 PLUS superspeed centrifuge), decantation, and redispersion in deionized water for three cycles to remove the unreacted small molecules and SDS surfactant molecules. The size of the core microgels is controllable by varying the amount of SDS.

Table 3-1 Feeding Compositions for Synthesis of the Core-Shell Microgels

Sample	Core Solution (mol)		Shell Solution (mol)		
	MEO_2MA	PEGDMA (550)	MEO_2MA	MEO_5MA	PEGDMA (550)
Core Microgel	0.0008	0.8×10^{-5}			
Shell Microgel			0.001	0.002	0.3×10^{-4}
CSM1	0.0008	0.8×10^{-5}	0.001	0.002	0.3×10^{-4}
CSM2	0.0008	0.8×10^{-5}	0.002	0.004	0.6×10^{-4}
CSM3	0.0008	0.8×10^{-5}	0.004	0.008	1.2×10^{-4}
CSM4	0.0008	0.8×10^{-5}	0.008	0.016	2.4×10^{-4}

The P(MEO_2MA-co-MEO_5MA) shell was synthesized using core microgel particles as nuclei for subsequent precipitation polymerization. The shell precursors of MEO_2MA and MEO_5MA monomer mixture in 1:2 molar ratio, PEGDMA crosslinker, and SDS were dissolved in deionized water (for details see Table 3-1), then the core microgels were added. The mixture was heated to 70 ℃ under a N_2 purge. After 1 h, the APS initiator was added to start the polymerization. The synthesis was allowed to proceed for 5 h. The resulted core-shell microgels were purified with centrifugation/redispersion in water for three cycles, followed by 3 days of dialysis (Spectra/Por® molecularporous membrane tubing, cutoff 12000-14000) against very frequently changed water at room temperature (~ 22 °C).

3. 2. 3 Drug Uptake Experiments

8 ml DIP solution (0.5 mg/mL, pH = 2.0) was added into the 10 mL microgel suspensions at a core microgel concentration of 1.0 mg/mL, resulting in a final pH around 3. After being stirred for 20 min, the pH of the mixture was adjusted to 8.0 by an addition of NaOH solution and the mixture was continuously stirred overnight. The DIP-microgel complexes were then removed from suspension by ultracentrifugation at 20,000 rpm and 22 ℃ for 40 min and redispersed in 10 mL of pH = 8.0 NaOH solution. The supernatant solution of residual DIP was collected and dissolved adequately with 0.1 N HCl to form uniform solution with a final pH being controlled at 3. The concentrations of the residual DIP were determined by fluorescence emission intensity at 480 nm with the excitation wavelength of 414 nm,[36-38] based on the linear calibration curve with $R^2 > 0.99$ measured using the DIP solutions with known concentrations under the same condition. The excitation at 414 nm gives an intensive emission band at 480 nm, which allows the detection of DIP in the nanomolar range based on the calibration curve. The drug loading efficiency of microgels was calculated as follows:

$$\textit{Drug loading efficiency (\%)} = 100\ (W_{feed\ drug} - W_{free\ drug})/W_{feed\ drug}$$

3. 2. 4 In Vitro Drug Release

The release of model drug from the microgel was evaluated by the dialysis method.[36, 39] The purified DIP-loaded microgel dispersions (1 mL) were transferred into dialysis tubes with a molecular weight cutoff of 12000-14000 and then immersed into 100 mL 0.005 M phosphate buffer solutions at different pHs. The aliquots outside of the dialysis bag were sampled at time intervals. The released drug concentrations were assayed using the fluorescence spectrometry for

DIP, as outlined for the drug uptake measurements. Cumulative release is expressed as the total percentage of drug released through the dialysis membrane over time.

3. 2. 5 In Vitro Cytotoxicity

Mouse melanoma cells B16F10 (2000 cell/well) were cultured in Dulbecco's Modified Eagle Medium (DMEM) containing 10% FBS and 1% penicillin-streptomycin in a 96-well plate, and exposed to free DIP, DIP-free microgels, and DIP-loaded microgels. To cover the high concentrations, the microgels were concentrated and adjusted to an appropriate concentration in DMEM right before feeding into the well. The plate was incubated at 37 ℃ for 2 h. The medium was then aspirated, and these wells were washed using fresh serum-free DMEM. After that, 25 μL of 3-(4,5-dimethyl-2-thiazolyl)-2,5-diphenyltetrazolium bromide (MTT) solution (5 mg/mL in PBS) were added to the wells. After incubation for 2 h, the solution was aspirated and 100 μL of DMSO was added to each well to dissolve the formazan crystal, and the plate was sealed and incubated overnight at 37 ℃ with gentle mixing. Cell viability was measured using a microplate reader at 570 nm. Positive controls contained no drug or microgels, and negative controls contained MTT. Results are expressed as a percentage of the absorbance of the positive control.

3. 2. 6 Characterization

The morphology of the core-shell microgels was characterized with transmission electron microscopy (TEM). The TEM images were taken on a Zeiss EM 902 transmission electron microscope operating at an accelerating voltage of 100 kV. Approximately 10 μL of the diluted microgel suspension was dropped on a Formvar-covered copper grid (300 meshes) and then air-dried at room temperature for the TEM measurements. The PL spectra were obtained on a

JOBIN YVON Co. FluoroMax®-3 Spectrofluorometer equipped with a Hamamatsu R928P photomultiplier tube, calibrated photodiode for excitation reference correction from 200-980 nm. The pH values were obtained on a METTLER TOLEDO SevenEasy pH meter.

The size and size distribution of the microgels under different conditions were measured using a standard light scattering spectrometer (BI-200SM) equipped with a BI-9000 AT digital time correlator (Brookhaven Instrument, Inc.). A He-Ne laser (35 mW, 633 nm) was used as the light source. The diluted microgel dispersion solutions were passed through 0.45 μm Millipore Millex-HV filters to remove dust.

3. 3 Results and Discussion

3. 3. 1 Synthesis of Oligo(ethylene glycol)-based Core-Shell Microgels

Our strategy to prepare the oligo(ethylene glycol)-based core-shell microgels involves the first synthesis of a P(MEO_2MA) core microgel, followed by the synthesis of P(MEO_2MA-co-MEO_5MA) gel layer on the core microgel. The P(MEO_2MA) core microgels were synthesized at 70 °C (well above the LCST of P(MEO_2MA)) based on the well-established precipitation polymerization method. Figure 3-2 shows the size distributions of the P(MEO_2MA) microgels, in terms of the hydrodynamic radius (R_h) measured at T = 25 °C and θ = 45°, synthesized with different concentrations of SDS surfactant. All the obtained P(MEO_2MA) microgel particles have a very narrow size distribution. The DLS characterization indicated that the obtained microgels are nearly monodispersed with a polydispersity index of $\mu_2/\langle\Gamma\rangle^2 = 0.001$. The particle size decreases with the increase in SDS concentration, which enables us to control the size of core microgel by a simple change in the amount of surfactant as the application needs. For the P(MEO_2MA) core microgels, the hydrodynamic diameter below 100 nm can be easily obtained

in the presence of small amount of SDS (e.g., 1-2 mM, well below the critical micelle concentration of SDS). The P(MEO_2MA) microgels with R_h = 110 nm at 22 °C was chosen as core model for the further synthesis of core-shell microgels using the method developed by Lyon's group.[31]

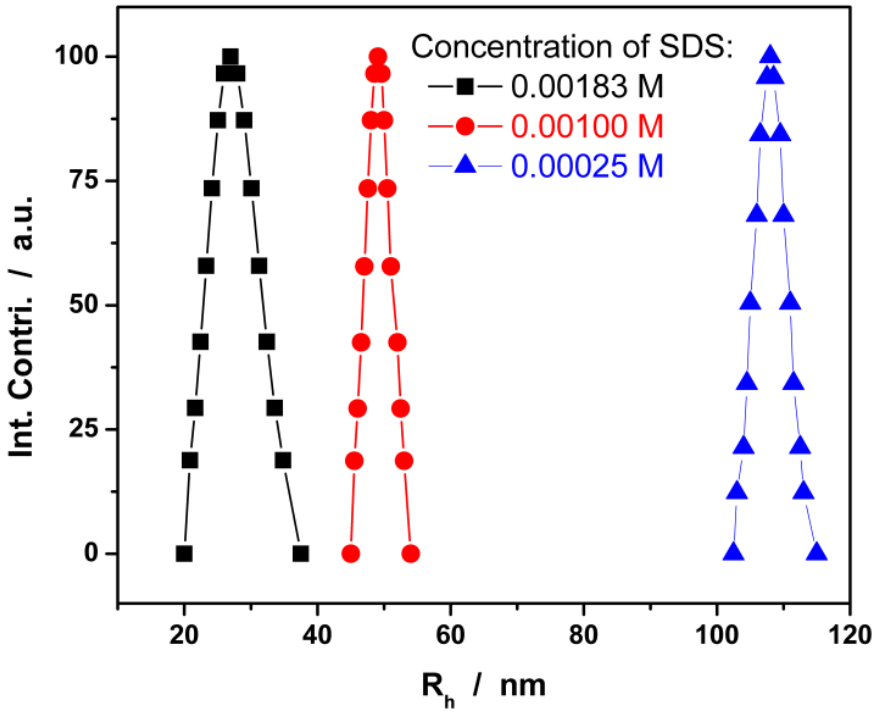

Figure 3-2 Size distributions of P(MEO_2MA) core microgels synthesized with different SDS concentrations, measured at 22 °C and a scattering angle of θ = 45°.

The further synthesis of P(MEO_2MA-co-MEO_5MA) gel shell was performed at 70 °C, at which the P(MEO_2MA) core microgels are fully collapsed. The collapsed core can not only serve as nuclei for further polymerization of shell, resulting in preferential growth of the existing particles over the nucleation of new ones, but also prevent the penetration of shell polymer into the core area.[31a] Figure 3-3 shows the typical TEM image of dried core-shell microgels CSM3 (see Table 3-1). The resulting core-shell microgels have a clear boundary between the core and

shell. The core-shell structure can be clearly observed with a dark condensed core and a light contrast shell. The low contrast of shell is due to the highly swollen state of the P(MEO_2MA-co-MEO_5MA) gel layer at sample preparation temperature. To observe the low contrast shell, the microgel suspension was mixed with citric acid-capped gold nanoparticles (~ 33 nm). The gold nanoparticles can be readily anchored onto the surface of microgels through the hydrogen bonding between the –COOH groups and the ethylene oxide (EO) units. It is clear that the gold nanoparticles anchored on the shell region give us an easy visualization of the whole core-shell microgel particles. On the basis of the core-shell structure as demonstrated, the thickness of shell can be controlled by adding different amount of shell monomers relative to a fixed amount of core particles. This is similar to the synthesis of PNIPAM-based core-shell microgels.[33]

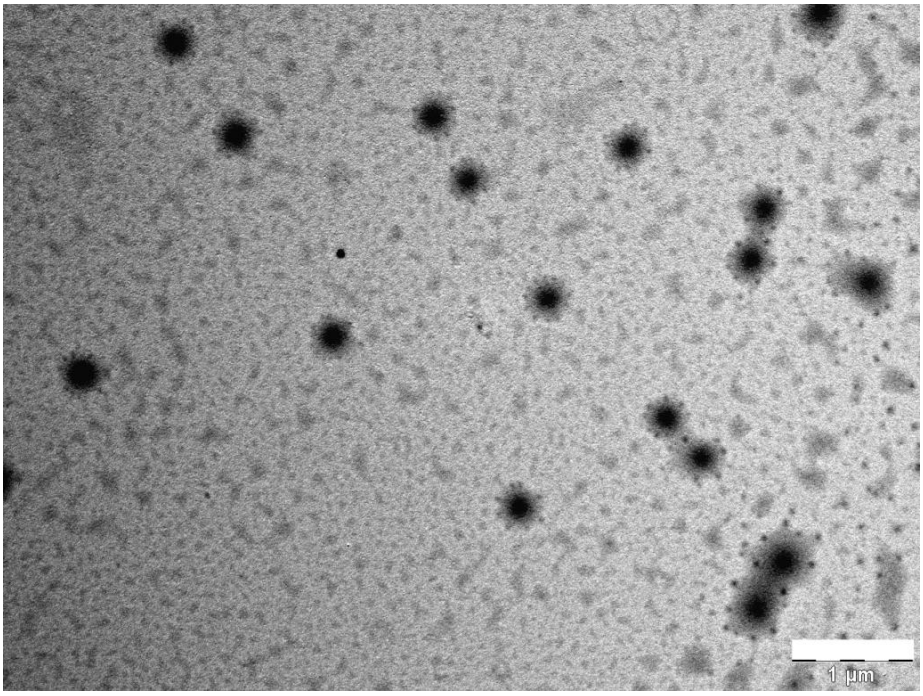

Figure 3-3 Typical TEM image of the core-shell microgels (CSM3). The citric acid-capped gold nanoparticles are attached onto the shell surface for easy visualization of the core-shell structure. The scale bar is 1 µm.

3. 3. 2 Temperature-Responsive Volume Phase Transitions of the Core-Shell Microgels

Figure 3-4A shows the thermo-responsive volume phase transitions of the core microgels of P(MEO_2MA) and the pure shell-composed microgels of P(MEO_2MA-co-MEO_5MA), respectively. The volume phase transition of core microgels begins around 13 ℃. The core microgels are nearly collapsed at room temperature, and completely collapsed at body temperature. In contrast, the shell-composed P(MEO_2MA-co-MEO_5MA) microgels show a very broad transition temperature beginning at around 40 ℃. However, at the experimental temperature limit of ~55 ℃, the shell-composed microgels still have not reached the collapsing limit. Thus, the shell-composed microgels are highly swollen and very hydrophilic at the temperatures below 40 ℃.

Figure 3-4B shows the temperature-dependent average R_h of the four core–shell microgels. Two features should be noted. Firstly, the increase in the feeding amount of shell components increases the thickness of the resultant shells. The size difference between the core-shell microgels and the parent core microgels can be attributed to the shell layer. Thus the thickness of the shell was estimated for the core-shell microgels. For example, at 7.5 ℃, the increase of R_h from 157 nm for the core microgel to 165 nm (CSM1), 176 nm (CSM2), 190 nm (CSM3) and 256 nm (CSM4), respectively, corresponds to a shell thickness of 8 nm, 19 nm, 33 nm, and 99 nm. Secondly, the core-shell microgels with different shell thickness exhibited different volume phase transition temperatures (VPTT). The increase in shell thickness shifts the VPTT of the core microgels toward higher temperatures, which is consistent with the results observed in the PNIPAM-based core-shell microgels.[31-33] For CSM1 and CSM2 with thinnest shells, these microgels start to shrink at temperature above 15 ℃, which is slightly higher than the VPTT of the core microgels. When the shell thickness is increased to 33 nm, the CSM3

microgels begins to shrink around 24 ℃, indicating a shift of the VPTT of core with 11 °C higher compared to the core microgels. For the CSM4 microgels with the thickest shell of 99 nm, no significant volume phase transition was observed within the experimental temperature range, indicating that the phase behavior of the CSM4 microgels is almost similar to that of the pure shell-composed microgels of P(MEO_2MA-co-MEO_5MA), in terms of VPTT.

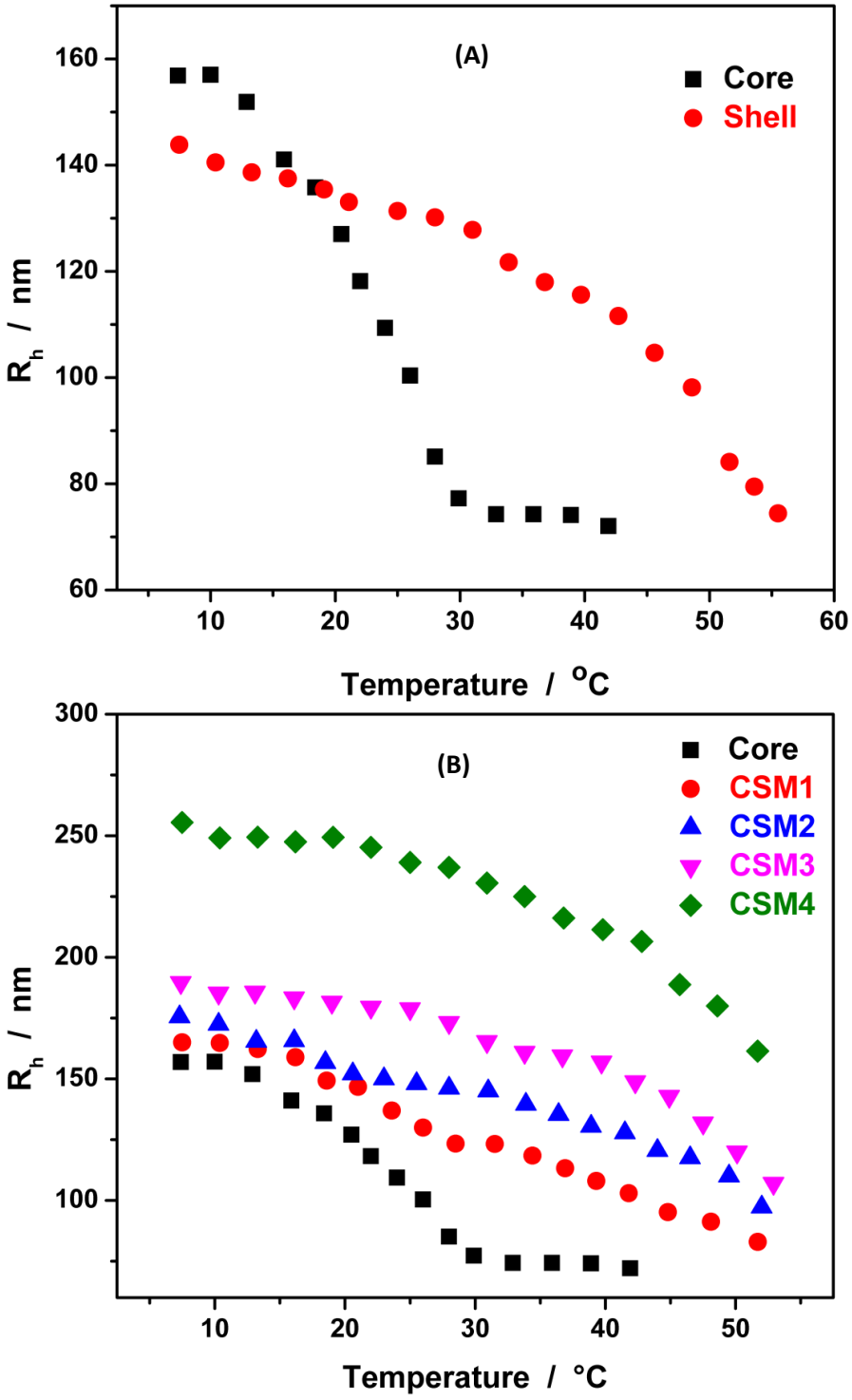

Figure 3-4 (A) Average R_h values of P(MEO_2MA) core and P(MEO_2MA-co-MEO_5MA) shell microgels as a function of temperature, respectively, measured at θ = 45°. (B) Temperature

dependence of average R_h values of core-shell microgels with different shell thickness, respectively, measured at $\theta = 45°$. The parent core is shown for comparison.

In addition to the VPTT shift, the shell thickness can also dramatically affect the collapsing degree of the core region in the core-shell microgels. As temperature increased from 10 to 32 ℃, the full collapse of the free core microgels resulted in a decrease of 83 nm in R_h, while the R_h of the CSM1, CSM2, CSM3, and CSM4 only reduced 42, 28, 20, and 18 nm, respectively. Obviously, the shell can significantly restrict the shrinking of the core at the elevated temperature. The thicker the shell is, the less the collapsing degree of core network has. It was known that the swelling behavior of a core–shell microgel is not a simple addition of the individual core and shell components. The mutual interaction between the shell and the core has been studied for PNIPAM-based core-shell microgels.[31-33] In our systems, at temperatures below the VPTT (e.g., < 40 °C) of the core-shell microgels, the hydrophilic shell will try to maintain its swollen state (Figure 3-4A). Although water is a poor solvent for the P(MEO_2MA) core network chains at temperature above 30 ℃, the thick and swollen P(MEO_2MA-co-MEO_5MA) copolymer gel shell will mechanically pull up the lightly crosslinked core network. The final equilibrium collapsing degree of the core networks in the core-shell microgels depends on the counterbalance of the expanding (hydrophilic shell) and retracting forces (hydrophobic core). Under this consideration, it allows us to control the collapsing degree (mesh size of network) of the hydrophobic core simply by tailoring the thickness of the shell. When modified with a P(MEO_2MA-co-MEO_5MA) gel shell of sufficient thickness, it is expected that the hydrophobic P(MEO_2MA) core networks can be stretched up to nearly a full expansion even at the high temperatures above the VPTT of the core but below that of the shell-composed microgels, e.g. 40

°C. Indeed, the collapsing degree ($R_{h,40°C}/R_{h,10°C}$ = 0.84) of the CSM4 microgels with the thickest shell of 99 nm is nearly the same as that ($R_{h,40°C}/R_{h,10°C}$ = 0.82) of pure shell-composed microgels, which indicates that the core in CSM4 microgels has no contribution to the size reduction of the CSM4 microgels in this specific temperature range and the core is almost fully expanded. This unique shell thickness-dependent collapsing degree of the hydrophobic core in our core-shell microgels is a key parameter for the storage and delivery of hydrophobic drugs, because the equilibrium collapsing degree (or mesh size) influences the loading capacity and drug diffusion coefficient.

3. 3. 3 Drug Loading Efficiency of the P(MEO_2MA-co-MEO_5MA) Core-Shell Microgels

The hydrophobic P(MEO_2MA) core of our core-shell microgels offer the capability for storage of hydrophobic drugs. DIP was chosen as the model drug. DIP is a known platelet inhibitor, coronary vasodilator[40] and a coactivator of antitumor compounds[41, 42]. As a poor soluble weak base with a reported pKa of 6.4, the solubility of DIP can be significantly different in different digestive fluids. For example, DIP dissolves readily in the stomach but incompletely in the intestine. Therefore, an effective carrier for such a drug is required.

Figure 3-5 shows the effect of shell thickness on the drug loading efficiency of the core-shell microgels measured at a constant number concentration of microgel particles together a fixed feeding concentration of drug and 22 ℃. It is clear that the loading efficiency increases with the increase in shell thickness, and then reaches a nearly plateau slope, which indicates that the loading efficiency only increases slightly with the further increase in shell thickness after the shell thickness reaches a certain value. These results imply that the shell may contribute very little to the overall drug loading. Control experiment confirmed that the pure shell-composed

microgels of P(MEO_2MA-co-MEO_5MA) did show an extremely low loading capacity of 8.5 mg DIP/g dry microgel. Although the free P(MEO_2MA) core microgels also demonstrate a low drug loading efficiency with 20% for DIP (equivalent to 80.5 mg DIP/g dry microgel), which is still one order of magnitude higher in loading capacity than the pure shell-composed microgels. Therefore, the loading of DIP into the core-shell microgels mainly depends on the hydrophobic interactions between the drug and the P(MEO_2MA) core.

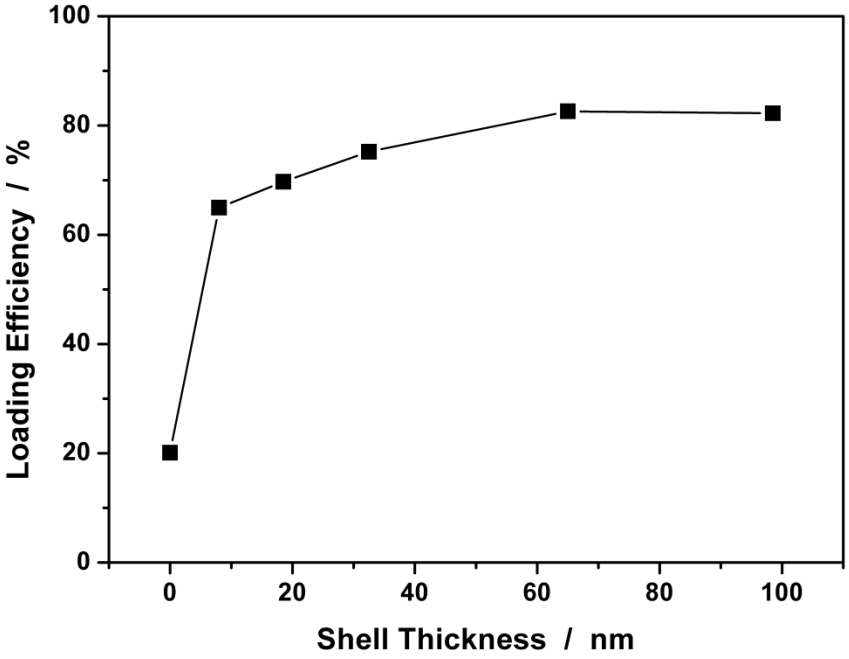

Figure 3-5 DIP loading efficiency of the core-shell microgels as a function of shell thickness, measured at a fixed number concentration of microgel particles and 22 °C.

Upon demonstrating the important role of the hydrophobic interactions in DIP loading, it is noteworthy that the free P(MEO_2MA) core microgels, when compared with the core-shell microgels, still exhibit low loading efficiency. We speculate that the collapsing degree (mesh size of network) of the hydrophobic core is another important factor related to the drug loading capacity. The low loading efficiency of the free core microgels could be attributed to their fully

collapsed structure. The core microgels is nearly collapsed at 22 ℃ and the P(MEO_2MA) network chains are hydrophobic and densely sticked together. Such a collapsed structure is difficult for the drug molecules to diffuse into the interior of the core particles. The core-shell structure can increase the drug loading efficiency dramatically. As we have discussed above (Figure 3-4B), the hydrophilic and swollen shell layer can restrict the collapsing of the P(MEO_2MA) core. Although the P(MEO_2MA) core network chains are still very hydrophobic, but the swollen shell will pull up and stretch the core network. In such a case, the hydrophobic core has open network with large mesh size for drug molecules diffusing into the core area. The thicker swollen shell has larger pulling force to prevent the collapsing of the hydrophobic core network chains, thus the mesh size of the core in CSM2 and CSM3 is larger than those of CSM1 and parent core at 22 ℃, which can hold more hydrophobic drug molecules in the interior of the hydrophobic core. When the shell thickness is increased to a certain value, the mesh size of the hydrophobic core network chains will no longer increase due to the limitation of chemical crosslinking, thus the loading capacity of the core can reach to a maximum and the overall loading efficiency of the core-shell microgels can only increase very slightly with further increase in shell thickness due to the very low loading capacity of shell (Figure 3-5). Therefore, certain shell thickness in the core-shell microgels is necessary to achieve maximum drug loading.

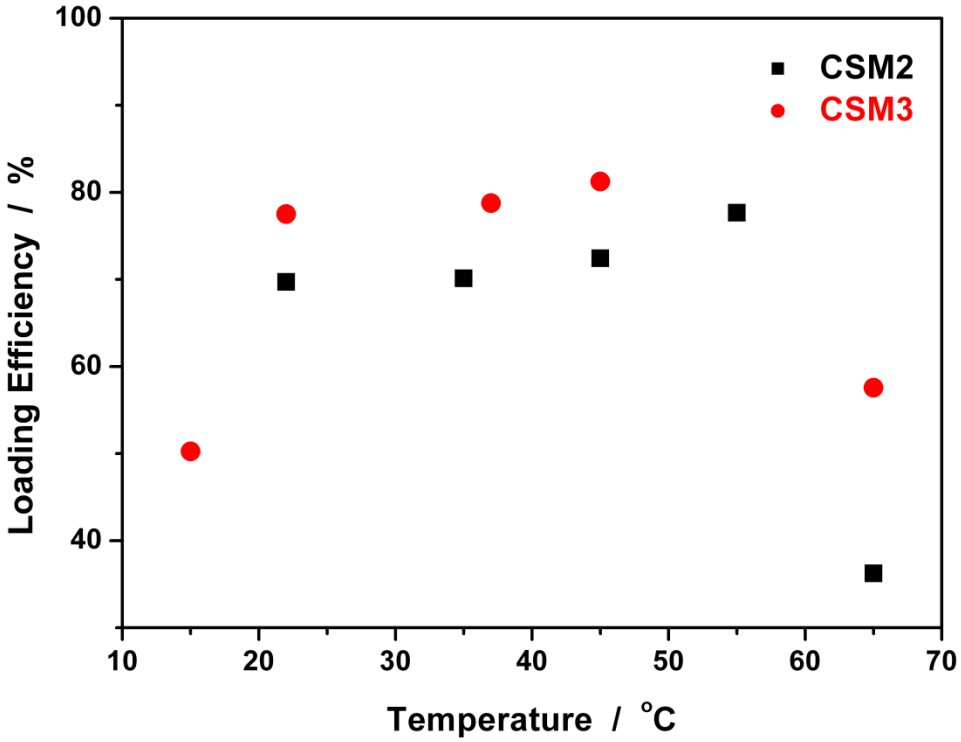

Figure 3-6 The temperature dependence of the DIP loading efficiency of the core-shell microgels CSM2 and CSM3.

The hypothesis can be further supported by the temperature effect on the drug loading efficiency. Figure 3-6 shows the DIP loading efficiency of the CSM2 and CSM3 core-shell microgels at different temperatures. At the temperature window between the VPTT of the core microgels and the shell-composed microgels (e.g. 22-40 °C, Figure 3-4A and 3-6), the hydrophilic shell restricts the collapse of core network chains, which can maintain the mesh size of hydrophobic core to hold hydrophobic drug molecules. As a consequence, the loading efficiency for drug molecules remains nearly a constant. When the temperature is further increased (> 40 °C), the shell will continuously shrink and gradually becomes hydrophobic, thus both hydrophobic core and partial hydrophobic shell layer can hold hydrophobic drug molecules, and a higher loading efficiency can be expected. However, when temperature is increased to ~ 65

°C, a dramatic decrease in drug loading efficiency was observed. Although both core and shell are very hydrophobic to interact with hydrophobic drug molecules, the shell is collapsed and loses its function for pulling up the network at such a high temperature, resulting in a collapsed P(MEO_2MA) core without the restriction of swollen shell. The very small mesh size of both core and shell gel limits the loading amount of drug molecules. Clearly, in addition to the drug-polymer hydrophobic interactions, the mesh size of the hydrophobic core is also very important to determine the loading capacity of hydrophobic drugs. These results indicate that the temperature range between the VPTT of core microgels and the shell-composed microgels is the most suitable condition to achieve high loading efficiency of hydrophobic drugs.

3. 3. 4 In Vitro Release Studies

Figure 3-7 shows the cumulative release profiles of DIP from the CSM2 core-shell microgels to buffer solutions at different pH values and 22 °C. It was anticipated that the drug molecules trapped in the hydrophobic core could gradually diffuse into the hydrophilic shell and then diffuse out of the shell to be released. At pH = 7.4, only ~14% of the loaded DIP can be released after 28 h. When the pH was decreased to 3, ~35% of the loaded DIP can be released after 25 h due to the partial protonation of DIP. The results were further analyzed to understand the release mechanism of the drug release from the core-shell microgels. The analysis was performed on the basis of the empirical equation proposed by Peppas et al.[43]:

$$M_t / M_\infty = kt^n$$

where M_t and M_∞ is the amount of drug released up to any time t and the final amount of drug; k is a structural/geometric constant and n is a release exponent related to the intimate mechanism of release. The power law is easy to use and can be applied to most diffusion-controlled release

systems, even if it is too simple to offer a robust prediction for complicated release phenomena. The advantage of this approach is that it yields a convenient measure of the constancy of release rate in the value of *n*. It also provides a quick way to check the releasing mechanisms, as values of $n < 0.43$ or $n > 0.85$ for spheres or sphere-like device indicate another controlling process in addition to the diffusion process.

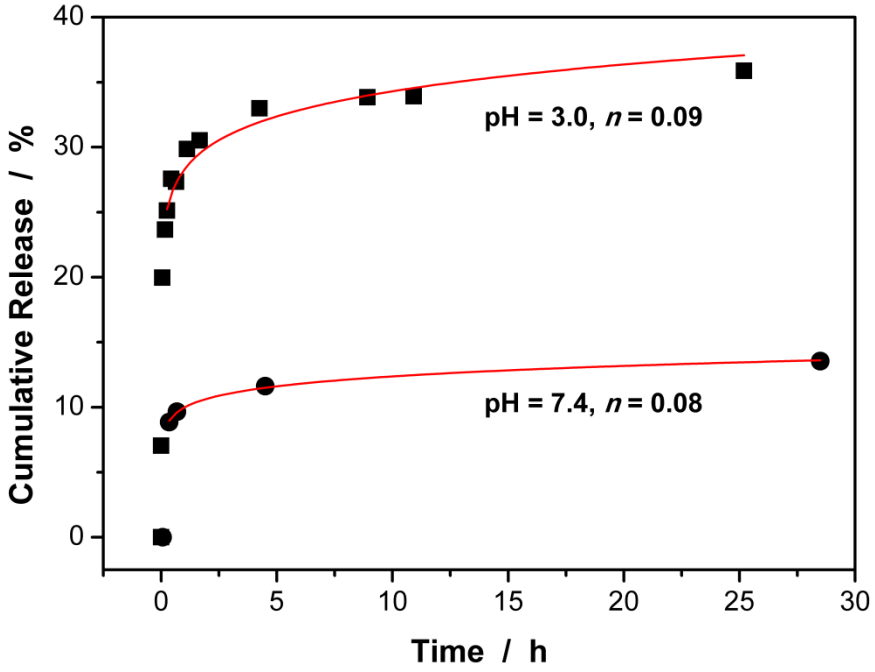

Figure 3-7 Cumulative DIP release from the core-shell microgels (CSM2) to buffer solutions at different pH values and 22 ℃.

The *n* values presented in Figure 3-7 are obtained from the best fitting of our experimental curves. DIP is soluble at pH = 3.0, but the unionized DIP molecules have a very low water solubility ($\leq 5\times10^{-6}$ g/mL) at pH = 7.4.[44, 45] Despite of the difference in the solubility of DIP, the exponent *n* was found to be nearly the same at the two pH values. The low *n* values exclude the simple diffusion controlled delivery mechanism. The investigated pH variable affects the release rate, but essentially does not change the drug release mechanism. These results confirm that the release of DIP molecules trapped in the core-shell microgels obeys to two

correlated processes within the delivery matrix. One is controlled through the breakage of coordinate hydrogen bonds between the drug and the polymer chains. Another is a diffusion-controlled step.

3. 3. 5 In Vitro Cytotoxicity

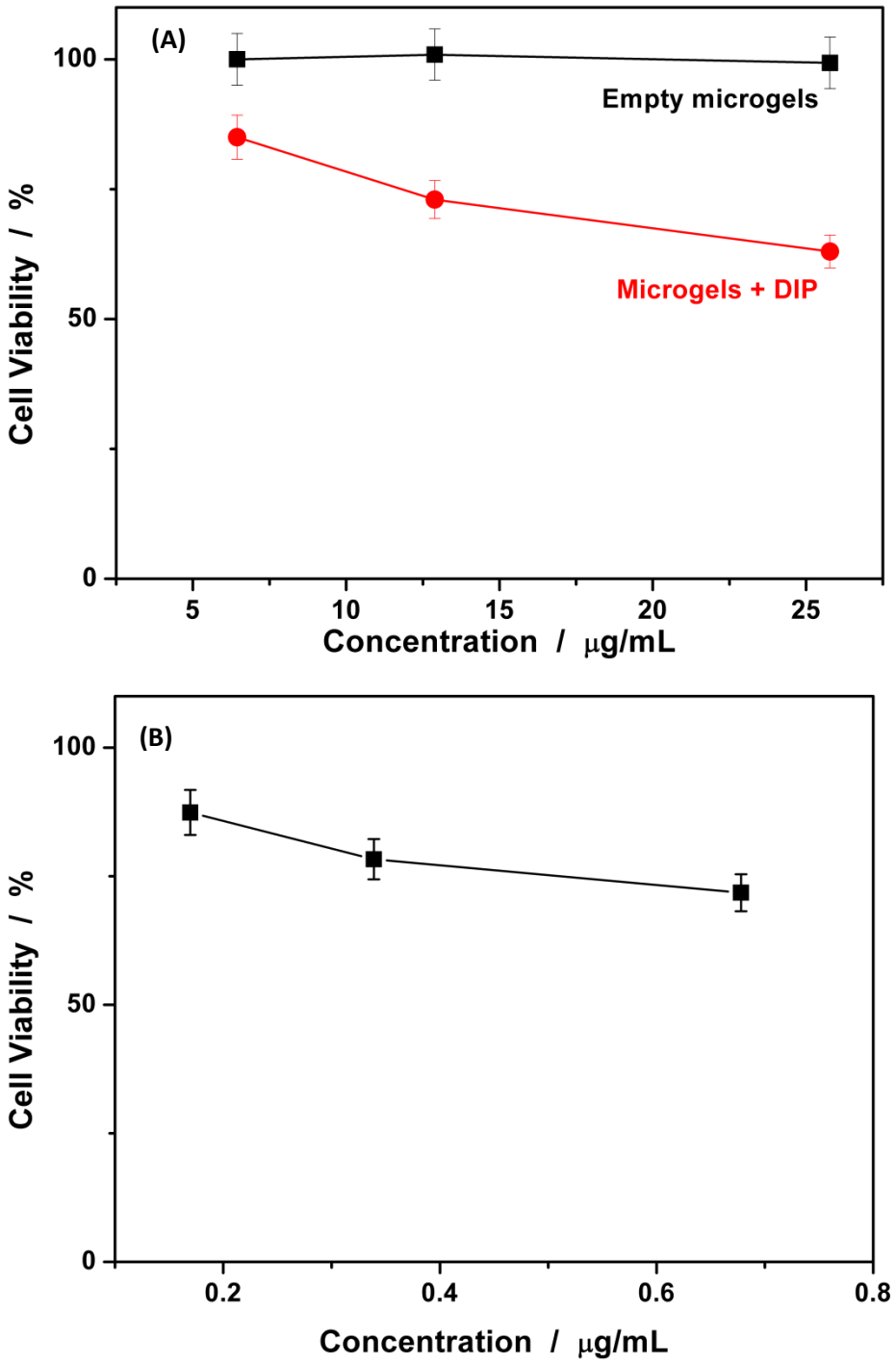

Figure 3-8 (A) In vitro cytotoxicity of empty CSM3 microgels, and DIP-loaded microgels against B16F10 cells. (B) The control experiment on the free DIP solution was presented for

comparison. The concentrations of DIP used for the control study are equal to DIP-loaded in the interior of the CSM3 microgels correspondingly.

For future biological applications, materials should be non- or low-cytotoxic. To evaluate the cytotoxicity of the core-shell microgels, *in vitro* cytotoxicity tests were conducted against mouse melanoma B16F10 cells. As shown in Figure 3-8, the empty core-shell microgels were non-cytotoxic to B16F10 cells in concentrations of up to 25.8 μg/mL. These results indicate that our microgels based on the oligo-(ethylene glycol) macromonomers exhibit an excellent *in vitro* biocompatibility. In contrast, when the cells were incubated with DIP-loaded microgels even at a concentration as low as 6.44 μg/mL (equivalent to about 0.17 μg/mL free DIP), the cell viability drastically decreased, which indicates that the DIP-loaded microgels can interact with cells and are pharmacologically active. DIP is a known coactivator of antitumor compounds, and the formation of metastatic tumors could be inhibited by such inhibitors of platelet aggregation.[41] Despite of these encouraging preliminary results and a compelling biochemical rationale, we cannot conclude whether the DIP drug would be pharmacologically active for cancer treatment because very limited information exists on the clinical use of anticoagulants for the prevention or treatment of cancer.[42] Nevertheless, the increase in cytotoxicity in the presence of DIP-loaded microgels can be attributed to the cellular uptake of DIP-loaded microgels and possibly their sustained-release property.

3. 4 Conclusion

Well-defined oligo(ethylene glycol)-based doubly thermosensitive core-shell microgels with the P(MEO_2MA) microgel as a hydrophobic core and the P(MEO_2MA-co-MEO_5MA) gel layer as a hydrophilic shell could be successfully synthesized via precipitation polymerization.

The presence of P(MEO_2MA-co-MEO_5MA) hydrophilic shell could prevent the hydrophobic core network from collapsing, resulting in a shift of the VPTT of P(MEO_2MA) core to higher temperatures in comparison with the free parent core microgels. The simple synthesis also allows us to tailor the shell layer to different thickness. When the shell thickness increases to a certain extent, the hydrophobic core network can be fully expanded. This unique structure of hydrophobic core with the open network (or large mesh size) in the core-shell microgels can dramatically improve the loading capacity for hydrophobic drugs, which indicates that both the drug-core hydrophobic interactions and the mesh size of core networks are important to determine the drug loading efficiency. These nontoxic core-shell microgels provide well-controlled drug loading yield and sustained drug release profiles. The DIP-loaded core-shell microgels significantly enhanced the in vitro cytotoxicity against tumor cells. Although DIP was selected as a specific model drug in this study, the concept and technique of developing nontoxic polymeric drug carriers by loading drug molecules into polymer chain networks through stimuli-responsive gel engineering can be generalized to deliver many other types of therapeutic or diagnostic agents.

3. 5 References

(1) Das M, Zhang H, Kumacheva E. *Annu. Rev. Mater. Res.* **2006,** 36: 117–42.

(2) Malmsten M. *Soft Matter* **2006**, 2: 760-9.

(3) Oh JK, Drumright R, Siegwart DJ, Matyjaszewski K. *Prog. Polym. Sci.* **2008**, 33: 448-77.

(4) Saunders BR, Laajam N, Daly E, teow S, Hu X, Stepto R. *Adv. Colloid Interface Sci.* **2009**, 147-8: 251-62.

(5) Das M, Mardyani S, Chan WCW, Kumacheva E. *Adv. Mater.* **2006**, 18: 80-3.

(6) Thienen TG, Raemdonck K, Demeester J, De Smedt SC. *Langmuir* **2007**, 23: 9794-801.

(7) Shi L, Khondee S, Linz TH, Berkland C. *Macromolecules* **2008**, 41: 6546-54.

(8) Ghugare S, Mozetic P, Paradossi G. *Biomacromolecules* **2009**, 10: 1589-96.

(9) Nolan CM, Serpe MJ, Lyon LA. *Biomacromolecules* **2004**, 5: 1940-6.

(10) Das M, Sanson N, Fava D, Kumacheva E. *Langmuir* **2007**, 23: 196-201.

(11) Nolan CM, Reyes C, Debord J, Garcia A, Lyon LA. *Biomacromolecules* **2005**, 6: 2032-9

(12) Nolan C, Gelbaum LT, Lyon LA. *Biomacromolecules* **2006**, 7:2918-22.

(13) Snowden M J. *J Chem Soc Chem Comm* **1992**, 11: 803-4.

(14) Huo D, Li Y, Kobayashi T. *Adv Mat Res* **2006**, 11-12: 299-302.

(15) Wu JY, Liu SQ, Heng PW, Yang YY. *J Controlled Release* **2005**, 102: 361-72.

(16) Zhou J, Wang G, Zou L, Tang L, Marquez M, Hu Z. *Biomacromolecules* **2008**, 9: 142-8.

(17) Hoare T, Pelton R. *Langmuir* **2008**, 24: 1005-12.

(18) Pelton R. *Adv. Colloid Interface Sci.* **2000**, 85: 1-33.

(19) Castro-Lopez V, Hadgraft J, Snowden MJ. *Int. J Pharm.* **2005**, 292: 137-47.

(20) Zhang Y, Guan Y, Zhou S. *Biomacromolecules* **2007**, 8: 3842–7.

(21) Harsh DC, Gehrke SH. *J Controlled Release* **1991**, 17: 175-85.

(22) Lutz JF, Hoth A. *Macromolecules* **2006**, 39:893-6.

(23) Lutz JF, Akdemir O, Hoth A. *J. Am. Chem. Soc.* **2006**, 128: 13046-7.

(24) Lutz JF, Weichenhan K, Akdemir O, Hoth A. *Macromolecules* **2007**, 40: 2503-8.

(25) Lutz JF. *J Polym. Sci. Part A: Polym. Chem.* **2008**, 46: 3459-70.

(26) Han S, Hagiwara M, Ishizone T. *Macromolecules* **2003**, 36: 8312-9.

(27) Ishiznoe T, Seki A, Hagiwara M, Han S, Yokoyama H, Oyane A, Deffieux A, Carlotti S. *Macromolecules* **2008**, 41: 2963-7.

(28) Badi N, Lutz JF. *J Controlled Release* **2009**, 140: 224-9.

(29) Cai T, Marquez M, Hu Z. *Langmu*ir **2007**, 23: 8663-6.

(30) Chi C, Cai T, Hu Z. *Langmuir* **2009**, 25: 3814-9.

(31) (a) Jones CD, Lyon A. *Macromolecules* **2000**, 33: 8301-6. (b) Jones CD, Lyon A. *Macromolecules* **2003**, 36: 1988-93. (c) Jones CD, Lyon A. *Langmuir* **2003**, 19: 4544-7.

(32) (a)Gan D, Lyon A. *J. Am. Chem. Soc.* **2001,** 123: 8203-9. (b) Jones CD, McGrath JG, Lyon A. *J. Phys. Chem. B* **2004**, 108: 12652-7.

(33) Berndt I, Richtering W. *Macromolecules* **2003**, 36: 8780-5.

(34) Berndt I, Pedersen JS, Lindner P, Richtering W. *Langmuir* **2006,** 22: 459-68.

(35) Chu B. *Laser Light Scattering*, 2nd ed, Academic Press: New York, **1991**.

(36) Tang Y, Liu SY, Armes SP, Billinghan NC. *Biomacromolecules* **2003**, 4: 1636-45.

(37) Giacomelli C, Le ML, Borsali R, Lai-Kee-Him J, Brisson A, Armes SP, Lewis A. *Biomacromolecules* **2006**,7: 817-28.

(38) Vertzoni M, Pastelli E, Psachoulias D, Kalantzi L, Reppas C. *Pharm. Res.* **2007**, 24: 909-17.

(39) Jiang X, Ge Z, Xu J, Liu H, Liu S. *Biomacromolecules* **2007**, 8: 3184-92.

(40) Marchandt E, Prichard AD, Casanegra P, Lindsay L. *Am. J. Cardiol.* **1984**, 53: 718.

(41) Shalinsky DR, Jekunen AP, Alcaraz JE, Christen RD, Kim S, Khatibi S, Howell SB. *Brit J Cancer* **1993,** 67(1): 30.

(42) Hejna M, Raderer M, Zielinski CC. *J. Natl. Cancer Inst.* **1999,** 91:22.

(43) Siepmann J, Peppas NA. *Adv Drug Delivery Rev.* **2001,** 48: 139.

(44) Giacomelli C, Schmidt V, Borsali R. *Langmuir* **2007**, 23: 6947-55.

(45) Avdeef A, Berger CM, Brownell C. *Pharm. Res.* **2000,** 17: 85-9.

Chapter 4

Semi-Interpenetrated Microgels for pH and Temperature Dual-Triggered Drug Release

4. 1 Introduction

Delivery vehicles that allow remote, repeatable, and reliable regulating of drug release could have a marked impact on the treatment of a variety of medical conditions.[1,2] An ideal vehicle for on-demand drug delivery should safely contain a large amount of drug, and be triggered noninvasively to release a consistent dosage. Responsive nanogels have attracted increasing attention due to their unique properties, including porous network structure, reversibly tunable dimensions from several nanometers to micrometers, and a very short response time.[3-6] Depending on the constructed constituents, the nanogels can respond to the change in pH value,[7] temperature,[3,8] or glucose level,[9,10] which occur commonly in many biological events. Thus, in principle, the nanogels can enhance our ability to address the complexity of biological systems by generating delivery vehicles with multi-responsive characteristics. Many pathological processes in various tissues and organs are accompanied with local pH decrease by 1–2.5 units (acidosis) and/or temperature increase by 1–5 ^{o}C.[2,11,12] Efforts for the preparation of pH and

temperature dual-responsive nanogels have been made recently. However, although the majority of the proposed applications of those dual-responsive nanogels are concentrated on biomedical area, most of the generated vehicles are only demonstrated to display single-stimuli-triggered drug release; even few of them described up to now can be effectively triggered by the pH or temperature changes over the physiologically narrow ranges.[2,5,13-18]

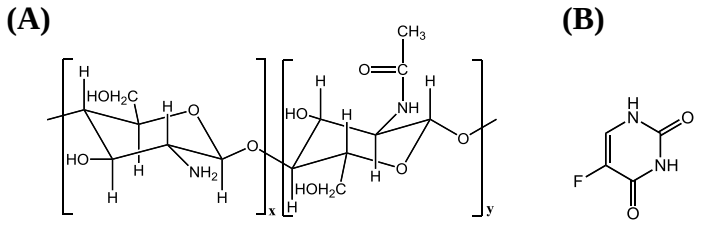

Scheme 4-1 Chemical structures of (A) chitosan and (B) 5-Fluorouracil.

To meet the clear clinical need, we report a first step in the research aimed at developing chitosan-based nanogels with semi-interpenetrating polymer networks (semi-IPN) structure, and with appropriate response to pathological pH and temperature microenvironment. Natural biopolymers have been widely used to prepare responsive hydrogels for biomedical application due to their biocompatibility, low toxicity, and a high content of functional groups.[4, 19] Chitosan, an important type of natural biopolymer, is a linear polysaccharide composed of randomly distributed β-(1-4)-linked D-glucosamine and N-acetyl-D-glucosamine units (Scheme 4-1). Chitosan is distinct from other commonly available polysaccharides due to the presence of nitrogen in its molecular structure. Its capacity to form polyelectrolyte complexes, making chitosan a pH-responsive biopolymer. To achieve pH and temperature dual-responsive characteristics, both "graft from" and "graft to" methods have been employed. For example,

while temperature-responsive PNIPAM brushes were covalently grafted from the chitosan chains,[20-22] linear poly(ethylene glycol)-poly(alanine) (PEG-PA) chains were covalently grafted to the chitosan backbone[23] to develop novel chitosan-based polymers. Those chitosan-based polymer chains can undergo coil-to-globule transition[24] to form gel or cluster particles under some certain conditions. Nah's group grafted chitosan chains onto the P(NIPAM-*co*-AA) nanoparticles by the carbodiimide-catalyzed carboxyl-amine reaction.[25] All of these methods require multistep fabricating processes. Our group and other groups have developed a simple and facile method to synthesize chitosan-based semi-IPN nanogel particles by in situ polymerization of the acrylic acid, methacrylic acid, and other monomers in the solutions containing chitosan chains.[4,16,26,27] However, few studies have been reported for synthesizing pH and temperature dual-responsive chitosan-based semi-IPN nanogels. Hua's group synthesized a pH and temperature dual-responsive nanoparticle by polymerization of acrylic acid with PNIPAM macro-RAFT agent in chitosan solution.[28] Wu's group developed PNIPAM-chitosan semi-IPN nanogels for delivery of camptothecin.[29] They found that the release rate of camptothecin was optimal at 37 ^{o}C and pH = 6.8 with the cumulative release amount ≈ 86.71%, which decreased to ~54–58% either at pH = 5.0–6.5 or 6.9–8.0 ranges; as the experimental temperature of release media (phosphate buffer of pH = 6.5) increases from 25/30 to 35/38 ^{o}C, the release rate increases rapidly, but the release behavior measured at 35 ^{o}C was nearly the same as that measured at 38 ^{o}C, likely due to the fact that PNIPAM exhibits a low LCST at ~32 ^{o}C.[24] These authors have applied the same PNIPAM-chitosan semi-IPN nanogels for the drug paclitaxel studies.[30] The results showed that the loaded nanogels exhibited a quite different pH-triggered release behavior: while pH value would not significantly affect the release behavior at pH = 5.0–6.9 or 7.5–8.0 ranges,

respectively, the cumulative release amount measured at pH = 5.0–6.9 was generally 4-fold larger than that measured at pH = 7.5–8.0. Moreover, the results also confirmed that their PNIPAM-chitosan nanogels did not exhibit a temperature response to the fluctuation of temperature around physiological values. Clearly, although some light has been shed on the development of pH and temperature dual-responsive nanogels for drug delivery, a chitosan-based semi-IPN nanogel that combines appropriate responsiveness to pathological microenvironment, good controllability, and biocompatibility is still lacking and remains highly desirable.

Herein, we design a novel class of chitosan-based nanogels comprising the nonlinear PEG based networks semi-interpenetrated with chitosan chains, denoted as PEG-chitosan (semi-IPN) nanogels. Concerning the fact that PNIPAM-based polymers have not been translated into biomedical breakthrough so far, PEG are believed to be more versatile for bio-applications.[8,31] Fang's group prepared PEG-chitosan semi-IPN membrane by interpenetrating linear PEG chains with crosslinked chitosan networks.[32] Recent work has crosslinked chitosan by poly(ethylene glycol)bis(carboxymethyl)ether (M_n = 600) and has shown that the resulting polymers can associate to form stable particles of 50-120 nm.[33] In a different way, the nonlinear PEG based networks in our PEG-chitosan nanogels were prepared by copolymerization and crosslinking of the monomers containing short oligo(ethylene glycol) side chains. More importantly, unlike conventional linear PEG chains that are mainly emphasized on the biocompatibility, these nonlinear PEG network chains are temperature-sensitive.[8,34-36] Both the pH- and temperature-responsive behaviors of the present PEG-chitosan nanogels can be well-tuned by engineering the composition, with the optimized ones exhibiting a continuous volume phase transition in response to the change in pH value and temperature over the physiologically relevant range. We

also demonstrated that the PEG-chitosan semi-IPN nanogels can regulate the delivery of preloaded model anti-cancer drug, 5-fluorouracil (5-FU, Scheme 4-1), as a function of pH value and temperature. In vitro cytotoxicity tests of the drug-loaded nanogels were also conducted. The PEG-chitosan nanogels should be a potential candidate for the drug delivery vehicles.

4. 2 Experimental

4. 2. 1 Materials

All reagents were purchased from Sigma-Aldrich. 2-(2-methoxyethoxy)ethyl methacrylate (MEO_2MA, 95%), oligo(ethylene glycol)methyl ether methacrylate (M_n = 300 g/mol, MEO_5MA), and poly(ethylene glycol) dimethacrylate (PEGDMA, $M_n \approx$ 550 g/mol, crosslinker) were purified with neutral Al_2O_3. Chitosan was dissolved in acetic acid, then pass through a filer and dialysis against distilled water for three days to remove free acetic acid. 5-Fluorouracil (5-FU), 0.1 N HCl standard solution, and ammonium persulfate (APS) were used as received. The water used in all experiments was of Millipore Milli-Q grade.

4. 2. 2 Surfactant-Free Synthesis of PEG-Chitosan Semi-IPN Nanogels

Table 4-1 Feeding Compositions for Synthesis of Nanogels

Sample Code	MEO_2MA ($\times 10^{-3}$ mol)	MEO_5MA ($\times 10^{-4}$ mol)	Chitosan* ($\times 10^{-3}$ mol)	Feeding mol ratio* $f_{PEG/chitosan}$
MG1	1.34	6.60	1.00	2:1
MG2	1.34	6.60	0.66	3:1
MG3	1.34	6.60	0.50	4:1

* The mol amount of chitosan is calculated by dividing the weight of chitosan by the mol weight of the structural units shown in Scheme 1.

Three PEG-chitosan nanogel samples were respectively synthesized according to the compositions listed in Table 4-1. Typically, the monomers, chitosan, and PEGDMA crosslinker (3 %) were dissolved in 200 mL deionized water (pH ≈ 5.8). The mixture was heated to 65 ℃ under a N_2 purge. After 1h, APS (3.0×10^{-4} mol) was added to the mixture to initiate the polymerization. The reaction was allowed to proceed for 5 h. The obtained nanogels were purified by 3 days of dialysis (Spectra/Por® molecularporous membrane tubing, cutoff 12000-14000) against very frequently changed water at room temperature (~ 22 °C).

2. 2. 3 Drug Uptake Experiments

20.0 mL nanogel dispersion was stirred under ice-water bath for 30 min, then 2.0 ml 5-FU solution (1.0 mg/mL, pH = 12.0) was added into the dispersion. After being stirred for 30 min, the pH of the mixture was adjusted to 7.0 by an addition of HCl solution and the mixture was continuously stirred overnight under ice-water bath. The 5-FU-nanogel complexes were then removed from dispersion by ultracentrifugation (Thermo Electron Co. SORVALL® RC-6 PLUS superspeed centrifuge, 20,000 rpm) at 22 ℃ for 60 min and washed by distilled water for six times. The complexes were redispersed in 5.0 mL distilled water for in vitro drug release test. The supernatant solution of residual 5-FU was collected and dissolved with adequate NaOH to form uniform solution (pH ≈ 12); the concentrations of the residual 5-FU were determined by UV-Vis absorbance at 270 nm, based on the linear calibration curve ($R^2 > 0.99$) measured using the 5-FU solutions with known concentrations under the same conditions. The amount of 5-FU

loaded into the nanogels was calculated from the decrease in 5-FU concentration. The loading content is expressed as the mass of loaded drug per unit weight of the dried nanogels.

4. 2. 4 In Vitro Drug Release

The release of model drug from the nanogels was evaluated by the dialysis method. 5.0 mL of the purified 5-FU-loaded nanogel dispersions were transferred into the dialysis bags and then immersed into 50.0 mL 0.005 M phosphate buffer solutions at different pH values and temperatures, respectively. The released 5-FU outside of the dialysis bag was sampled at defined time period and assayed by UV-Vis absorption at 270 nm. Cumulative release is expressed as the total percentage of drug released through the dialysis membrane over time.

4. 2. 5 In Vitro Cytotoxicity

B16F10 cells (2000 cell/well) were cultured in DMEM containing 10% FBS and 1% penicillin-streptomycin in two 96-well plates, and exposed to free 5-FU, drug-free PEG-chitosan nanogels, and 5-FU loaded PEG-chitosan nanogels. To cover the high concentrations, the nanogels were concentrated and adjusted to an appropriate concentration in DMEM right before feeding into the well. One plate was incubated at 37 ℃ for 2 h and another plate was incubated for 24 h. The medium was then aspirated, and these wells were washed using fresh serum-free DMEM. After that, 25.0 mL of 3-(4,5-dimethyl-2-thiazolyl)-2,5-diphenyltetrazolium bromide (MTT) solution (5.0 mg/mL in PBS) were added to the wells. After incubation for 2 h, the solution was aspirated. 100.0 mL of dimethyl sulfoxide was then added to each well and the plate was sealed and incubated for 30 min at 37 ℃ with gentle mixing. Three portions of the solution

obtained from each well were transferred to three respective wells of a 96-well plate. Cell viability was measured using a microplate reader at 570 nm. Positive controls contained no 5-FU or nanogels, and negative controls contained MTT.

4. 2. 6 Characterization

The morphology of nanogels was observed with transmission electron microscopy (TEM) on a FEI TECNAI transmission electron microscope at an accelerating voltage of 120 kV. Approximately 20 μL of the diluted nanogel dispersions (pH = 7.4) were dropped on a Formvar-covered copper grid (300 meshes) and then air-dried at room temperature for the TEM measurements. The UV-Vis absorption at 270 nm was recorded on a Thermo Electron Co. Helios β UV-Vis Spectrometer. The pH values were obtained on a METTLER TOLEDO SevenEasy pH meter. The size and size distribution of the nanogels under different conditions were measured using a standard light scattering spectrometer (BI-200SM) equipped with a BI-9000 AT digital time correlator (Brookhaven Instrument, Inc.). A Nd:YAG laser (150 mW, 532 nm) was used as the light source. The diluted nanogel dispersions were passed through 0.8 μm Millipore Millex-HV filters to remove dust.

4. 3 Results and Discussion

4. 3. 1 Surfactant-Free Synthesis of Semi-IPN PEG-Chitosan Nanogels

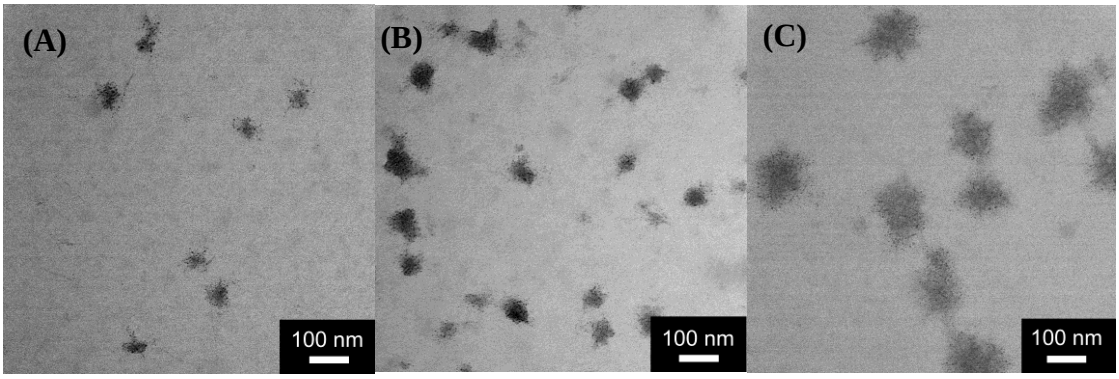

Figure 4-1 TEM images of semi-IPN PEG-chitosan nanogels: A) MG1, B) MG2 and C) MG3. All samples were dried from the dispersions of pH = 7.4.

In our proposal, the PEG-chitosan nanogels were prepared by direct polymerization of oligo(ethylene glycol) monomers, MEO_2MA and MEO_5MA, in chitosan aqueous solution (pH ≈ 5.8) containing crosslinker PEGDMA at 65 °C. Previously we have found that the polymerization and crosslinking of acrylic acid (AA) monomers that are complexed with hydroxypropylcellulose (HPC) chains can result in stable semi-IPN-structured PAA-HPC nanogels.[26] In the present case, the formation of PEG-chitosan nanogels can be attributed to the first complexation through the hydrogen bonding interaction between the ether oxygens of the oligo(ethylene glycol) monomers and the hydroxyl groups and the amino groups of the chitosan chains, and then precipitation polymerization and crosslinking of oligo(ethylene glycol) monomers. Different from the surfactant-assisted approach to PAA-HPC nanogels,[26] no surfactant was added in the present procedure, during which the slightly positive-charged chitosan (see below) may act as stabilizer to favor the formation of PEG-chitosan nanogel particles. As shown in Figure 4-1, the dried PEG-chitosan nanogel particles have a irregular morphology with a narrow size distribution. The DLS characterization further confirmed that the PEG-chitosan nanogels are nearly monodispersed with the polydispersity index $\mu_2/\langle\Gamma\rangle^2 < 0.1$

under all measurement conditions (see below). All PEG-chitosan nanogel dispersions are very stable with neglectable change in polydispersity index after setting for several months under room temperature, due to the formation of stable semi-IPN structure in the nanogel. The size of such semi-IPN-structured gel particles is tunable by simply varying the feeding mol ratio $f_{PEG/chitosan}$ of oligo(ethylene glycol) monomers and chitosan (use the mol amount of the structural units as shown in Scheme 1) in the synthesis. TEM images (Figure 4-1; the samples were dried from the dispersions of pH = 7.40) indicated that the PEG-chitosan nanogels MG1 ($f_{PEG/chitosan}$ = 2:1), MG2 ($f_{PEG/chitosan}$ = 3:1), and MG3 ($f_{PEG/chitosan}$ = 4:1) synthesized with increased $f_{PEG/chitosan}$ values revealed increased size of about 60 nm, 72 nm, and 120 nm, respectively. It should be noted that the size of colloidal drug carriers is very important to their fate in blood circulation and their biodistribution since the recognition by the reticuloendothelial system (RES) is known to be the principal reason for the removal of many colloidal drug carriers from the blood compartment. The sub-200 nm size has an actual advantage for the particles to extend their blood circulation time.[38] The small sized PEG-chitosan nanogels presented in this paper should have advantages to extend their circulation time and penetrate into cells.[27,35]

4.3.2 pH-Induced Volume Phase Transition

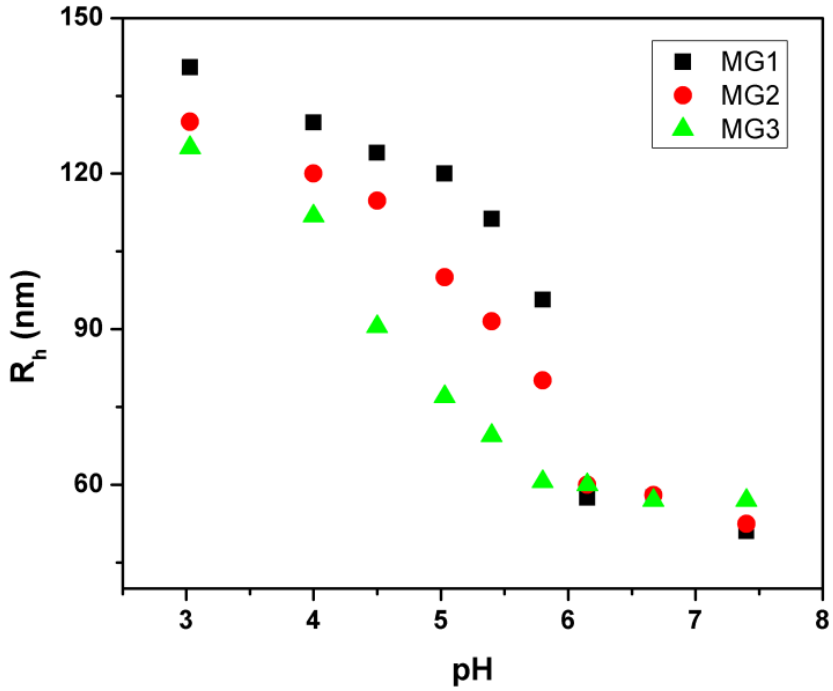

Figure 4-2 pH-dependent average R_h values of PEG-chitosan nanogels, measured at a scattering angle $\theta = 45^o$ and 37 ºC.

The primary aliphatic amine of chitosan is a pH-responsive moiety and the pH value of dispersion medium can significantly influence the size of the PEG-chitosan nanogels. Figure 4-2 shows the pH-induced swelling curves of the PEG-chitosan nanogels, in terms of the R_h change measured at physiological temperature of 37 ^oC and a scattering angels of $\theta = 45^o$. A well-defined volume transition is observed for all the studied nanogels. At high pH values, the size of nanogels remains nearly a constant due to the strong hydrogen bonding between PEG chains and the uncharged chitosan chains. When the pH value is below the pK_b (≈ 6.5) of chitosan, the $–NH_2$ groups of chitosan chains are gradually protonated, which can not only weaken the hydrogen bonding between the PEG and chitosan chains, but also induce the Coulombic repulsion among the ionized $–NH_3^+$ groups, resulting in the gradual increase in the size of the nanogels. Typically, the $–NH_2$ groups were slightly ionized in the synthesis medium of pH ≈ 5.8 and still not

completely ionized at pH = 3.0, i.e., a much lower pH (< 3.0) is needed to make the full swelling of all the studied nanogels.

Interestingly, the PEG-chitosan nanogels MG1 ($f_{PEG/chitosan}$ = 2:1), MG2 ($f_{PEG/chitosan}$ = 3:1), and MG3 ($f_{PEG/chitosan}$ = 4:1) synthesized with increased $f_{PEG/chitosan}$ values exhibited different phase behaviors as a function of pH value. Some very important studies have focused on the differences between macro- and nanogels with respect to their phase behavior.[39,40] For example, our previous work has shown that the temperature-induced phase transition region of PNIPAM nanogels is less sharp than that of bulk gels, due to a greater heterogeneity in the subchain lengths of the nanogels than in the traditionally prepared macrogels.[39] We have also observed this phenomenon among the nonlinear PEG nanogels, whose temperature-responsive phase behaviors can be tailored by tuning the feeding mol ratio of MEO_2MA and MEO_5MA and thus varying the balance of overall hydrophilicity/hydrophobicity of the nanogel network segments.[35, 36] The observed phase transition for a nanogel can be thought of as being the summation of the phase transitions of the different sub-networks in the particle. However, to the best of our knowledge, no literature referring to similar phenomenon has been reported on a pH-responsive polymeric material, especially on a micro-/nanogel. We speculate that when the PEG-chitosan nanogels are subjected to pH < pK_b (≈ 6.5) of chitosan, the physical interactions between ether oxygens of the PEG chains and the $–NH_2$ groups of the chitosan chains could hinder the ionization of the $–NH_2$ groups, and the regions of the particle with dense PEG/$–NH_2$ associations (shorter chitosan "subchain" lengths) swell less at a lower pH than the regions with dumb associations (longer "subchains"). Consequently, the swelling onset of the PEG-chitosan nanogels slightly shifted to ~5.8−6.2, whilst the MG1, MG2, and MG3 synthesized with

increased $f_{PEG/chitosan}$ correspondingly have a significantly degressive sharp pH-induced volume change. Typically, when the environmental pH value was varied from 7.4 to 5.0 at physiological temperature of 37 ^{o}C, the MG1, MG2, and MG3 also displayed a decreased swelling ratio, $SR_{pH} = R_{h,pH5.0} / R_{h,pH7.4}$, of 2.8, 2.6 and 2.2, respectively.

4. 3. 3 Temperature-Induced Volume Phase Transitions

Figure 4-3 shows the temperature-induced volume phase transitions of the PEG-chitosan nanogels, in terms of the change of R_h measured at a scattering angles of $\theta = 45^{o}$. It is clear that the increase in temperature can also induce shrinkage of the PEG-chitosan nanogels, demonstrating pH and temperature dual-responsive abilities of the PEG-chitosan nanogels. Under a fixed pH environment, the chitosan chains will not undergo conformational and chemical changes in water when giving external stimuli of temperature change. The observed temperature-induced volume phase transitions of the nanogels should be contributed from the gel networks containing short oligo(ethylene glycol) side chains. The formation of hydrogen bonds between the ether oxygens of the side PEG chains and the hydrogens of water is thought to be one of the key factors responsible for the unusual water solubility of this type of nonlinear PEG polymers. This conformationally favorable effect in water is counterbalanced by the hydrophobicity of the apolar backbone, and the physical association between PEG and chitosan chains.[34-36]

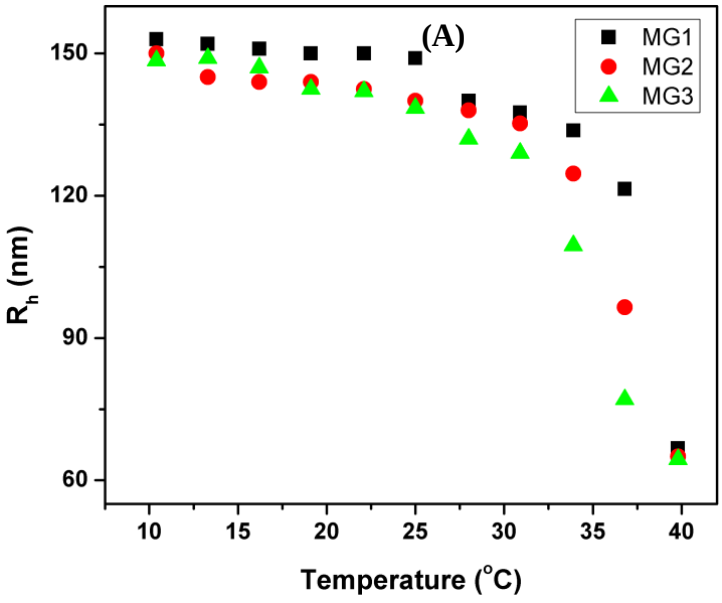
(A)
MG1
MG2
MG3
150
120
90
60
R_h (nm)
10
15
20
25
30
35
40
Temperature (°C)

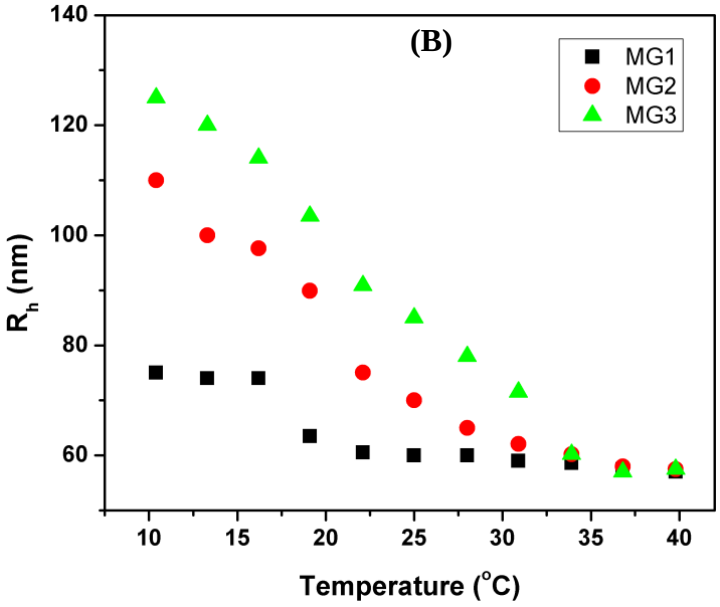
(B)
MG1
MG2
MG3
140
120
100
80
60
R_h (nm)
10
15
20
25
30
35
40
Temperature (°C)

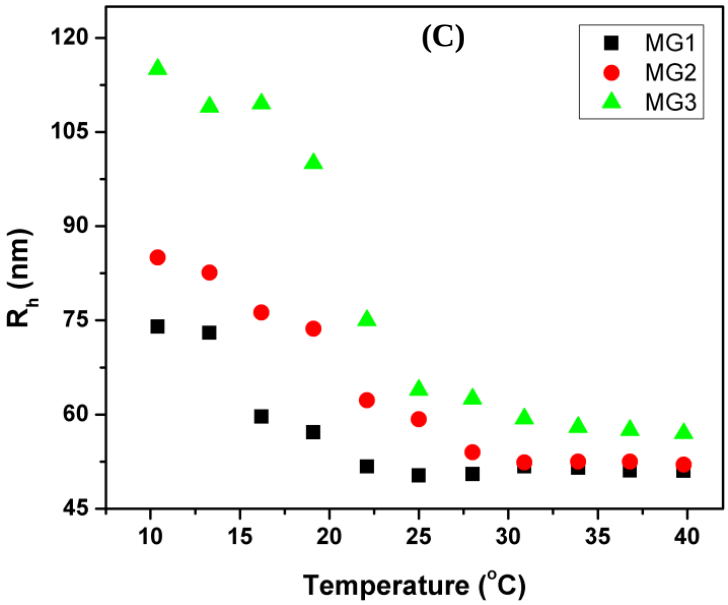

Figure 4-3 Temperature-dependent average R_h of PEG-chitosan nanogels, measured at a scattering angle $\theta = 45^o$ and different pH values: A) pH 5.03; B) pH 6.67; C) pH7.40, respectively.

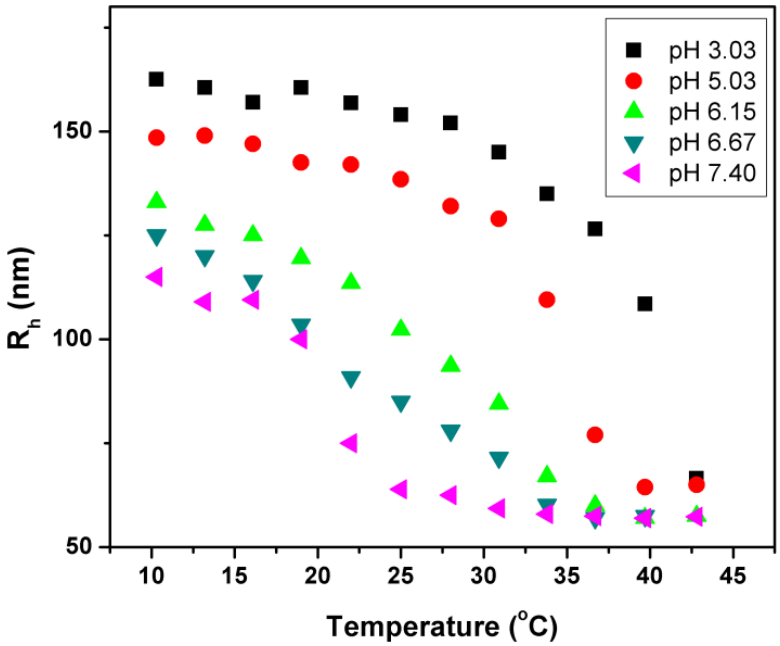

Figure 4-4 Temperature-dependent average R_h values of PEG-chitosan nanogels MG3, measured at a scattering angle $\theta = 45^o$ and different pH values.

Tunable temperature-induced phase behavior can be readily achieved in the PEG-chitosan nanogels. First, at the same pH of 7.40, MG1 ($f_{PEG/chitosan}$ = 2:1), MG2 ($f_{PEG/chitosan}$ = 3:1), and MG3 ($f_{PEG/chitosan}$ = 4:1) synthesized with increased $f_{PEG/chitosan}$ displayed a increased swelling ratio, $SR_T = R_h(10\ ^oC) / R_h(40\ ^oC)$, of 1.43, 1.66, and 2.09, respectively. The temperature-induced volume changes of the three nanogels is possibly varied by the shift in the counterbalance between attractive PEG-water interactions and PEG-PEG/PEG-chitosan segment-segment interactions, in good agreement with its influence in the pH-induced phase behaviors (Figure 4-2).[34-36] Second, since the $–NH_2$ groups of the chitosan chains is ionizable, it is possible that at a lower pH the gradual ionization of chitosan segments could weaken their hydrogen bonding and other physical interactions with neutral PEG segments, leading to a weakening retracting forces that hinder the expanding of the gel networks. Indeed, a decrease of the pH value from 7.40 to 6.67 or 5.03 has resulted in a increase in the swelling ratio of all studied nanogels. Moreover, to induce the PEG network chains to collapse, a higher temperature also needs to be provided. At pH = 5.03, MG1 and MG2 still not reached fully collapse in our maximum experimental temperature of 40 ^{o}C. To further visualize the effect of pH value on the temperature-induced phase behavior (including both SR_T and LCST), we plotted in Figure 4 the temperature-induced volume phase transitions of the PEG-chitosan nanogels MG3, which were measured at different pH values. While the environmental pH/temperature change can induce reversible volume changes of the PEG-chitosan nanogels, it should be mentioned that both the morphology and composition of the nanogels are stable in the different environments. Therefore, the PEG-

chitosan nanogels presented in this work could offer two main advantages for the potential biomedical applications. The small size of the nanogels allows the deep penetration into cell/tissue such as poorly permeable tumors for therapy,[38] while the responsive nanogels can serve as excellent drug carriers with a pH and temperature dual-controllable drug releasing behavior.

4. 3. 4 In Vitro Drug Release

Two PEG-chitosan nanogels of MG1 and MG2 with high pH/temperature-sensitivity over the physiological pH/temperature range were selected for further *in vitro* experiments. 5-FU is widely used in the treatment of a range of cancers, including colorectal and breast cancers, and cancers of the aerodigestive tract. The chemotherapy agent 5-FU acts in several ways, but principally as a thymidylate synthase (TS) inhibitor.[41,42] TS catalyzes the reductive methylation of deoxyuridine monophosphate (dUMP) into deoxythymidine monophosphate (dTMP). Interrupting the action of TS can blocks synthesis of the pyrimidine thymidine, which is a nucleotide required for DNA replication. Facing a scarcity of dTMP, rapidly dividing cancerous cells undergo cell death via thymineless death. Side effects of 5-FU administration include myelosuppression, CNS (central nervous system) damage and cardiac toxicity.[43,44] As such, 5-FU was chosen as a model drug for demonstrating the pH/temperature-regulated drug release. Due to the porous structure of the gel networks and the complex interaction between the nanogel network chains and 5-FU, the drug-loading content in the nanogels MG1 and MG2 was as high as 167 and 227 w/w%, respectively.

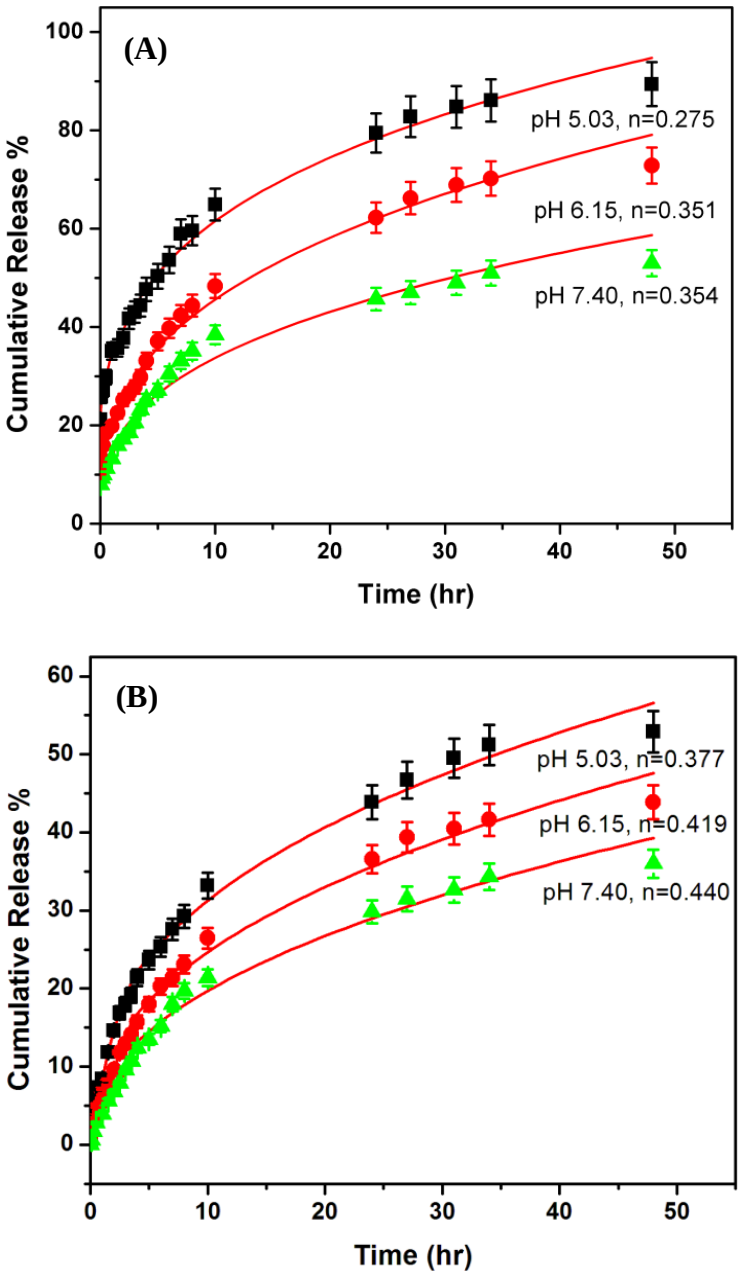

Figure 4-5 Cumulative release of 5-FU from PEG-chitosan nanogels MG1 (A) and MG2 (B) at 37 ^{o}C, measured at buffer solutions of different pH values: ■: 5.03; ●: 6.15; ▲: 7.40.

Figure 4-5 shows the cumulative release profiles of 5-FU from the PEG-chitosan nanogels of MG1 and MG2 into buffer solutions measured by a conventional dialysis bag

method at a physiological temperature of 37 ℃ and three different pH values of 5.03, 6.15 and 7.40, respectively. Two features should be noted from the controlled release of 5-FU from the nanogels. First, the pH of the external buffer solution can trigger the 5-FU release. The decrease in pH increases the 5-FU releasing rate from both nanogels. When the 5-FU-loaded nanogels were placed in a pH 7.40 buffer, only ~51% (MG1) and ~36% (MG2) of the loaded 5-FU could be released even after 48 h. When the pH of the external buffer solution was decreased to 6.15, about 70% (MG1) and 44% (MG2) of the loaded 5-FU could be released within 48 h. When the pH was further decreased to 5.03, about 89% (MG1) and 52% (MG2) of the loaded 5-FU could be released in 48 h. Second, the tailoring of the PEG-chitosan nanogels by varying the feeding mol ratio $f_{PEG/chitosan}$ can also modify the 5-FU releasing profiles to a certain extent. In comparison with MG2, MG1 synthesized with a smaller $f_{PEG/chitosan}$ exhibited a larger pH-induced swelling ratio, and thus a higher 5-FU releasing rate.

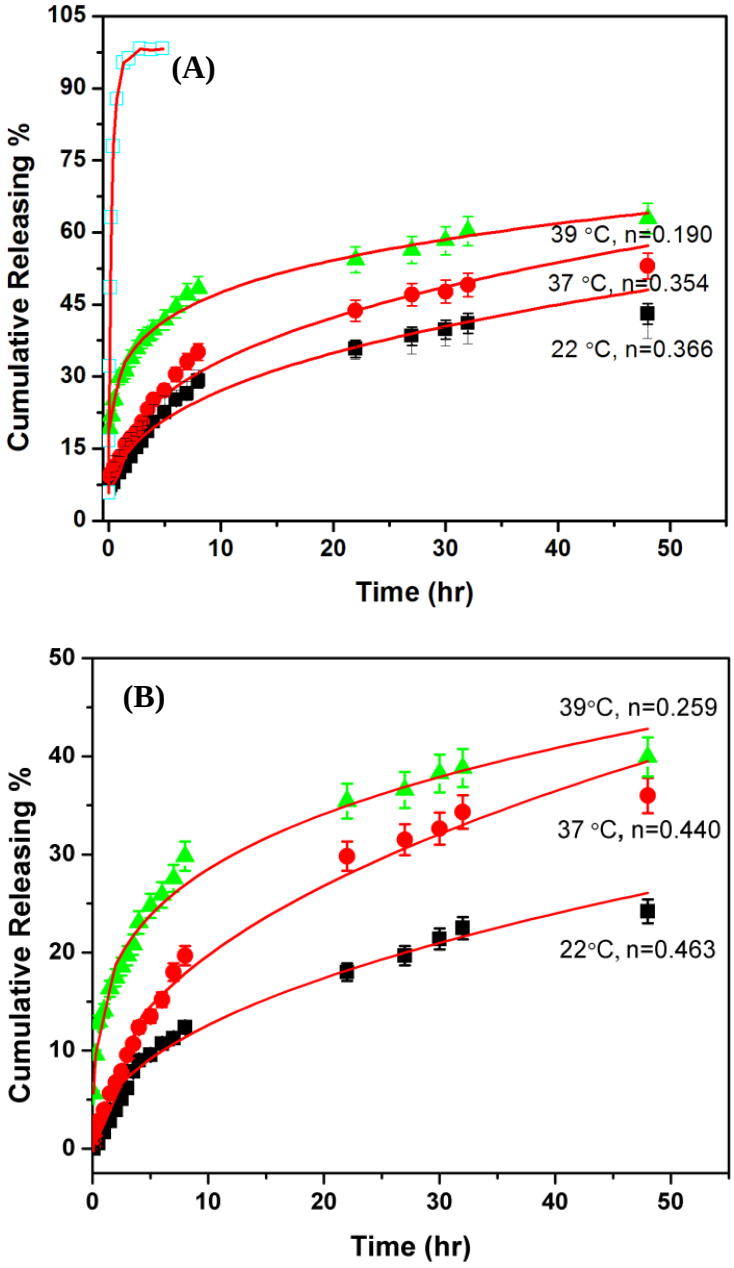

Figure 4-6 Cumulative release of 5-FU from PEG-chitosan nanogels MG1 (A) and MG2 (B), measured at pH 7.40 buffer solutions of different temperatures: ■: 22 ^{o}C; ●: 37 ^{o}C; ▲: 39 ^{o}C. In the blank (□), 1 mL diluted solution of free 5-FU with an equivalent amount of drug to that trapped in MG1 was performed at pH = 5.03 and 39 ^{o}C.

To further understand the release mechanism, the results were further analyzed on the basis of the empirical equation proposed by Peppas *et al.*:[45]

$$M_t / M_\infty = kt^n \qquad (1)$$

where M_t and M_∞ is the amount of drug released up to any time t and the infinite time; k is a structural/geometric constant and n is a release exponent related to the intimate mechanism of release. Eq. (1) has two distinct physical realistic meanings in the two special cases of n = ~0.43 (indicating diffusion-controlled drug release) and n = ~0.85 (indicating swelling-controlled drug release). Values of n = ~0.43−0.85 can be regarded as indicator for the superposition of both phenomena (anomalous transport), while n < ~0.43 indicate another transportation process in addition to the diffusion process.[45] While n = 0.44 is found for the drug release from MG2 at pH = 7.40, the n values for other cases are all below 0.43, which indicate that the releasing mechanism involves two processes: one is simple diffusion step; another is related to the breakage of hydrogen bonding between the 5-FU and polymer chains.

Note that the temperature of the external buffer solution also can be used to trigger the release of 5-FU from drug-loaded PEG-chitosan nanogels. Figure 4-6 shows the cumulative drug release profile of MG1 and MG2 in the same PBS buffer of pH = 7.40 but at different temperatures. The increase in temperature increases the 5-FU releasing rate from both nanogels. At 22 ℃, about 42% and 23% of 5-FU was released from MG1 and MG2 within 48 h, respectively; when the temperature was increased to 39 ℃, the release of 5-FU was increased to 65% and 40% correspondingly. The releasing profiles fit well to the empirical equation proposed by Peppas *et al*. The increase in temperature from 22 ºC to 39 ºC decreased the n value. While n > 0.43 is found for the drug release from MG2 at 22 ℃ and 37 ℃, the n values for other cases are

all below 0.43. Clearly, both the increase in temperature and the decrease in pH value can speed up the releasing rate of 5-FU from the PEG-chitosan nanogels. The pH and temperature dual-responsive nanogels developed in this work, being able to regulate the transport of therapeutics when necessary under the local stimuli of the target pathological zone such as cancer and cystic fibrosis that are associated with disruptions in acid/base and temperature homeostasis,[2,11,12] could be extremely important in the treatment of diseases.

4. 3. 5 In Vitro Cytotoxicity

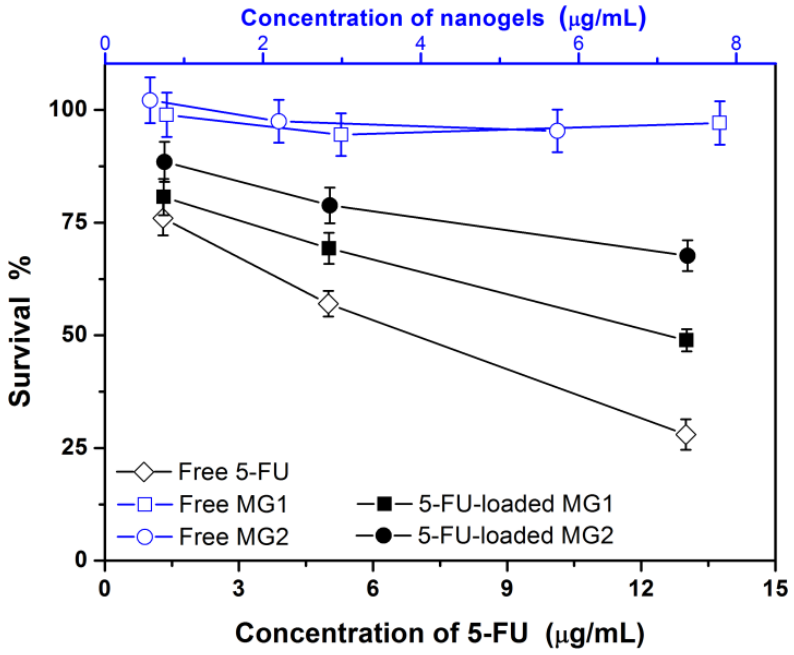

Figure 4-7 Comparison of B16F10 cell survivability following treatments with MG1 and MG2 nanogels as drug carriers, respectively (■: 5-FU-loaded MG1; ●: 5-FU-loaded MG2). B16F10 cell survivability after treated with free nanogels (□: MG1; ○: MG2) and free 5-FU solutions (◊).

A beautiful characteristic of the PEG-chitosan nanogels for future biological applications, especially for clinical applications, is non-cytotoxicity of each component. More than 98% of

B16F10 cells can survive upon treatment with the nanogels with concentrations up to 7.79 μg/mL and 5.73 μg/mL for MG1 and MG2, respectively (Figure 4-7). In contrast, the cell viability drastically decreased when the cells were treated with 5-FU-loaded MG1 and MG2 even at a concentration as low as 0.78 μg/mL and 0.57 μg/mL, respectively (equivalent to 1.3 μg/mL free 5-FU). These results indicate that the 5-FU-loaded nanogels provide high anticancer activity. The cytotoxicity of 5-FU-loaded nanogels is lower than that of free 5-FU solution at all the correspondingly studied concentrations. This can be attributed to the sustained-release property of the 5-FU-loaded hybrid nanogels. Considering that less than 45% of the loaded 5-FU was released in 24 h under physiological conditions (Figure 5 and 6), the slightly lower cytotoxicity of the 5-FU-loaded hybrid nanogels than the free 5-FU solutions is understandable.

4. 4 Conclusion

PEG-chitosan gel nanoparticles with semi-IPN structure and tunable diameter were successfully prepared by in-situ free radical polymerization and crosslinking of the monomers containing short oligo(ethylene glycol) side chains in the solution of natural biopolymer chitosan. The PEG-chitosan semi-IPN nanogels can adapt with high-sensitivity to a surrounding medium of different pH values and temperatures over the physiologically relevant ranges of 5.0-7.4 and 36-40 ^{o}C, respectively. The PEG-chitosan nanogels can also provide excellent stability as a drug carrier, which cannot only provide a high drug loading capacity of the model anticancer drug 5-FU, but also offer pH and temperature dual-triggered drug delivery possibilities. The drug release kinetics studies demonstrate that the multifunctional nanogels show drug sustained properties and the release could be triggered by the pH and temperature dual-responsive volume

phase transition of the gel. In vitro cytotoxicity tests indicate that the empty nanogels have very low cytotoxicity, while the 5-FU-loaded nanogels have high anticancer activity. These characteristics are important in both fundamental research and practical applications. The properly designed dual-responsive nanogels as delivery vehicles should enhance our ability to address the complexity of biological systems, and thus offer broad opportunities for biomedical applications.

4. 5 References

(1) Shi, J.; Votruba, A.R.; Farokhzad, O.C.; Langer, R. *Nano Lett.* **2010**, *10*, 3223.

(2) Torchilin, V.P. *Pharm. Res.* **2007**, *24*, 1.

(3) Reese, C.E.; Mikhonin, A.V.; Kamenjicki, M.; Tikhonov, A.; Asher, S.A. *J. Am. Chem. Soc.* **2004**, *126*, 1493.

(4) Oh, J.K.; Lee, D.I.; Park, J.M. *Prog. Polym. Sci.* **2009**, *34*, 1361.

(5) Stuart, M.A.C.; Huck, W.T.S.; Genzer, J.; Muller, M.; Ober, C.; Stamm, M.; Sukhorukov, G.B.; Szleifer, I.; Tsukruk, V.V.; Urban, M.; Winnik, F.; Zauscher, S.; Luzinov, I.; Minko, S. *Nature Mater.* **2010**, *9*, 101.

(6) Wu, W.; Zhou, S. *Nano Review* **2010**, *1*, 5730-DOI:10.3402/nano.v1io.5730.

(7) Tan, B.H.; Tam, K.C. *Adv. Colloid Interface Sci.* **2008**, *136*, 25.

(8) Hu, Z.B.; Cai, T.; Chi, C.L. *Soft Matter* **2010**, *6*, 2115.

(9) Wu, W.; Zhou, T.; Shen, J.; Zhou, S. *Chem. Commun.* **2009**, 4390.

(10) Wu, W.; Mitra, N.; Yan, E.C.Y.; Zhou, S. *ACS Nano* **2010**, *4*, 4831.

(11) Gerweck, L.; Seetharaman, K. *Cancer Res.* **1996**, *56*, 1194.

(12) Stefanadis, C.; Chrysochoou, C.; Markou, D.; Petraki, K.; Panagiotakos, D.; Fasoulakis, C.; Kyriakidis, A.; Papadimitriou, C.; Toutouzas, P. *J. Clin. Oncol.* **2001**, *19*, 676.

(13) Soppimath, K.; Tan, D.; Yang, Y. *Adv. Mater.* **2005**, *17*, 318.

(14) Lo, C.; Lin, K.; Hsiue, G. *J. Control. Release* **2005**, *104*, 477.

(15) Zhang, L.; Guo, R.; Yang, M.; Jiang, X.; Liu, B. *Adv. Mater.* **2007**, *19*, 2988.

(16) Chen, Y.; Ding, D.; Mao, Z.; He, Y.; Hu, Y.; Wu, W.; Jiang, X. *Biomacromolecules* **2008**, *9*, 2609.

(17) Yang, L.; Guo, C.; Jia, L.; Liang, X.; Liu, C.; Liu, H. *J. Colloid Interface Sci.* **2010**, *350*, 22.

(18) Huynh, C.T.; Nguyen, M.K.; Kim, J.H.; Kang, S.W.; Kim, B.S.; Lee, D.S. *Soft Matter* **2011**, *7*, 4974.

(19) Carreira, A.S.; Goncalves, F.A.M.M.; Mendonca, P.V.; Gil, M.H.; Coelho, J.F.J. *Carbohydr. Polym.* **2010**, *80*, 618.

(20) Liu, W.; Huang, Y.; Liu, H.; Hu, Y. *J. Colloid Interface Sci.* **2007**, *313*, 117.

(21) Cao, Y.; Zhang, C.; Shen, W.; Cheng, Z.; Yu, L.; Ping, Q. *J. Control. Release* **2007**, *120*, 186.

(22) Duan, C.; Zhang, D.; Wang, F.; Zheng, D.; Jia, L.; Feng, F.; Liu, Y.; Wang, Y.; Tian, K.; Wang, F.; Zhang, Q. *Int. J. Pharm.* **2011**, *409*, 252.

(23) Jang, J.H.; Choi, Y.M.; Choi, Y.Y.; Joo, M.K.; Park, M.H.; Choi, B.G.; Kang, E.Y.; Jeong, B. *J. Mater. Chem.* **2011**, *21*, 5484.

(24) Zhang, G.Z.; Winnik, F.M.; Wu, C. *Phys. Rev. Lett.* **2003**, *90*, 035506.

(25) Jung, H.; Jang, M.K.; Nah. J.W. *Macromol. Res.* **2009**, *17*, 265.

(26) Wu, W.; Aiello, M.; Zhou, T.; Berliner, A.; Banerjee, P.; Zhou, Q. *Biomaterials* **2010**, *31*, 3023.

(27) Wu, W.; Shen, J.; Banerjee, P.; Zhou, S. *Biomaterials* **2010**, *31*, 8371.

(28) Jiang, J.; Hua, D.; Tang, J. *Int. J. Biol. Macromol.* **2010**, *46*, 126.

(29) Fan, L.; Wu, H.; Zhang, H.; Li, F.; Yang, T.; Gu, C.; Yang, Q. *Carbohydr. Polym.* **2008**, *73*, 390.

(30) Li, F.; Wu, H.; Zhang, H.; Li, F.; Gu, C.; Yang, Q. *Carbohydr. Polym.* **2009**, *77*, 773.

(31) van Vlerken, L.E.; Vyas, T.K.; Amiji, M.M. *Pharm. Res.* **2007**, *24*, 1405.

(32) Zeng, M.; Fang, Z. *J. Membr. Sci.* **2004**, *245*, 95.

(33) Wu, J.; Wei, W.; Wang, L.; Su, Z.; Ma, G. *Biomaterials* **2007**, *28*, 2220.

(34) Lutz, J.F.; Akdemir, O.; Hoth, A. *J. Am. Chem. Soc.* **2006**, *128*, 13046.

(35) Wu, W.; hen, J.; Banerjee, P.; Zhou, S. *Biomaterials* **2010**, *31*, 7555.

(36) Zhou, T.; Wu, W.; Zhou, S. *Polymer* **2010**, *51*, 3926.

(37) Chu, B. *Laser Light Scattering, 2nd ed, Academic Press: New York,* **1991**.

(38) Alexis, F.; Pridgen, E.; Molnar, L.K.; Farokhzad, O.C. *Mol. Pharm.* **2008**, *5*, 505.

(39) Wu, C.; Zhou, S. *Macromolecules* **1997**, *30*, 574.

(40) Nayak, S.; Lyon, L.A. *Angew. Chem. Int. Ed.* **2005**, *44*, 7686.

(41) Longley, D.B.; Harkin, D.P.; Johnston, P.G. *Nature Rev. Cancer* **2003**, *3*, 330.

(42) Parker, J.B.; Stivers, J.T. *Biochemistry* **2011**, *50*, 612.

(43) Duffner, P.K. *J. Biol.* **2006**, *5*, 21.

(44) Han, R.; Yang, Y.M.; Dietrich, J.; Luebke, A.E.; Mayer-Proschel, M.; Noble, M. *J. Biol.* **2008**, *7*, e12.

(45) Siepmann, J.; Peppas, N.A. *Adv. Drug Delivery Rev.* **2001**, *48*, 139.

Chapter 5

ZnO QDs Encapsulated Semi-Interpenetrated PEG-Chitosan Microgels for Multifunctional Drug Delivery Vehicles

5. 1 Introduction

Multifunctional biomaterials that can combine imaging, sensing, and intelligent dose of therapeutic agents hold great promise for the investigation and treatment of various diseases because they can potentially provide simultaneous diagnosis, therapy, and monitoring on the response to treatments. However, the ability to rationally design such multifunctional drug delivery carriers is still one the most important and challenging tasks in biomedical technology. So far, cadmium-based semiconductors are the most studied materials for bioimaging and biosensor applications.[1,2,3] Considering the utmost biological exploitation purpose, developments of biologically- and eco-friendly light-emitting semiconductor quantum dots (QDs) nanoparticles are preferred.[4, 5] ZnO is an environmentally friendly semiconductor and displays luminescent properties in the near UV and visible regions of the spectrum. Meanwhile, it is

inexpensive and has been reported to be nontoxic to living cells and possesses antimicrobial properties.[6-10] Therefore, we can consider ZnO as an ideal biofriendly substitute for Cd-based semiconductors in biological labeling. To make the QDs more useful for bioapplications, new strategies are required to design and develop multifunctional hybrid nanomaterials that can combine the unique optical property of QDs with the biopolymer-based drug carriers. Responsive microgels are idea candidates for drug delivery carriers due to their unique properties, including porous network structure, reversibly tunable dimensions from several nanometers to micrometers, and a very short response time.[11,12,13] According to the incorporated components, the microgels can respond to the environmental changes, such as, pH value,[14,15] temperature,[16,17] or glucose level,[3,18] which occur commonly in many biological events. Hence, microgels delivery vehicles with multi-responsive characteristics based on application requirements could be generated. Since pathological processes in various tissues and organs are accompanied with local pH decrease by 1–2.5 units (acidosis) and/or temperature increase by 1–5 °C,[19-21] the preparation of pH and temperature dual-responsive microgels will enable the biological control to intelligently dose the drugs at the pathological sites.

Chitosan is a natural biopolymer which has been widely used to prepare responsive hydrogels for biomedical application due to their biocompatibility, low toxicity, and a high content of functional groups.[22-24] It is a linear polysaccharide composed of randomly distributed β-(1-4)-linked D-glucosamine and N-acetyl-D-glucosamine units. Due to the presence of nitrogen in its molecular structure, it is able to form polyelectrolyte complexes. Therefore, chitosan has been widely selected as a pH-responsive component in hydrogels. On the other hand, since PNIPAM-based polymers have not been translated into biomedical breakthrough so far,

PEG is believed to be a more versatile alternative for bio-applications.[25-29] Unlike conventional linear PEG chains, the nonlinear PEG-based networks prepared by copolymerization and crosslinking of the monomers containing short oligo(ethylene glycol) side chains are temperature-sensitive.[25, 28] Our group and other groups have developed a simple and facile method to synthesize chitosan-based semi-IPN microgel particles by in situ polymerization of the acrylic acid, methacrylic acid, and other monomers in the solutions containing chitosan chains.[30-32]

In this work, we aim to develop a class of pH and temperature dual-responsive core-shell structure microgels embedded with ZnO QDs in the core, which should display the properties from each component and demonstrate the ability for simultaneous diagnosis, therapy, and monitoring of various diseases. The stabilized fluorescent ZnO QDs core can act as an optical identification code for sensing and imaging the surroundings. The PEG-chitosan semi-IPN microgels comprising the crosslinked nonlinear PEG based networks semi-interpenetrated with chitosan will act as shell and can serve as pH and temperature regulated drug delivery vehicles via its reversible swelling/shrinking transitions. Such designed stimulus responsive hybrid microgels, denoted as ZnO@PEG-chitosan, should be able to integrate the optical pH-sensing, cell imaging, and drug delivery functions into a single particle, which can further switch on and off certain functions when necessary, under the local environmental stimuli of the targeted pathological zone such as cancer and cystic fibrosis that are associated with disruptions in acid/base homeostasis. Specifically, we have demonstrated that the ZnO@PEG-chitosan hybrid microgels can regulate the delivery of preloaded model anti-cancer drug, 5-fluorouracil (5-FU), in response to a local pH value and temperature change, enter into and light up the B16F10

cancer cells, and optically sense the pH and temperature change in the surroundings. In vitro cytotoxicity tests of the drug-loaded microgels were also conducted.

5. 2 Experimental

5. 2. 1 Materials

All reagents were purchased from Sigma-Aldrich. 2-(2-methoxyethoxy)ethyl methacrylate (MEO_2MA, 95%), oligo(ethylene glycol)methyl ether methacrylate (M_n = 300 g/mol, MEO_5MA), and poly(ethylene glycol) dimethacrylate (PEGDMA, $M_n \approx 550$ g/mol, crosslinker) were purified with neutral Al_2O_3. Chitosan was dissolved in acetic acid, then pass through a filer and dialysis against distilled water for three days to remove free acetic acid. 2,2′-azobisisobutyronitrile (AIBN), zinc methacrylate, NaOH, 5-Fluorouracil (5-FU), 0.1 N HCl standard solution, and ammonium persulfate (APS) were used as received. The water used in all experiments was of Millipore Milli-Q grade.

5. 5. 2 Synthesis of Nonlinear PEG Protected ZnO Nanoparticles

0.04 g of 2,2′-azobisisobutyronitrile (AIBN), 0.30g zinc methacrylate and 6 mL of poly(ethylene glycol) methyl ether methacrylate PEGMEMA (M_n=300) were dissolved in 30 mL absolute ethanol. The solution was stirred and heated at 80 ℃ for 30 min under purge of nitrogen. Then 0.06 g of AIBN and 500 μL of 10 M NaOH aqueous solution were added into the reaction system and refluxed for 1 h. After cooling to room temperature, the solution was dialyzed against deionized water for 3 days. [6]

5. 2. 3 Synthesis of ZnO@PEG-Chitosan core-shell microgels

Table 5-1 Feeding Compositions for Synthesis of core-shell microgels

Sample Code	ZnO core dispersion (ml)	MEO_2MA ($\times10^{-3}$ mol)	MEO_5MA ($\times10^{-3}$ mol)	Chitosan ($\times10^{-3}$ g)
CSM1	10	2	2	8
CSM2	10	1	3	8
CSM3	10	0	4	8

.

Three ZnO@PEG-chitosan core-shell hybrid microgel samples were respectively synthesized according to the compositions listed in Table 5-1. Typically, the nonlinear PEG-stabilized parent ZnO core, monomers, chitosan, and PEGDMA crosslinker (3 %) were dissolved in 180 mL deionized water (pH ≈ 5.8). The mixture was heated to 65 ℃ under a N_2 purge. After 1h, APS (3.0×10^{-4} mol) was added to the mixture to initiate the polymerization. The reaction was allowed to proceed for 5 h. The obtained microgels were purified by 3 days of dialysis (Spectra/Por® molecularporous membrane tubing, cutoff 12000-14000) against very frequently changed water at room temperature (~ 22 °C) and then diluted to 200 ml.

5. 2. 4 Drug Uptake Experiments

20.0 mL microgel dispersion was stirred under ice-water bath for 30 min, then 2.0 ml 5-FU solution (1.0 mg/mL, pH = 12.0) was added into the dispersion. After being stirred for 30 min, the pH of the mixture was adjusted to 7.0 by an addition of HCl solution and the mixture was continuously stirred overnight under ice-water bath. The 5-FU-nanogel complexes were then

removed from the dispersion by ultracentrifugation (Thermo Electron Co. SORVALL® RC-6 PLUS superspeed centrifuge, 20,000 rpm) at 22 ℃ for 60 min and washed by distilled water for six times. The complexes were redispersed in 5.0 mL distilled water for in vitro drug release test. The supernatant solution of residual 5-FU was collected and dissolved with adequate NaOH to form uniform solution (pH ≈ 12). The concentrations of the residual 5-FU were determined by UV-Vis absorbance at 270 nm, based on the linear calibration curve ($R^2 > 0.99$) measured using the 5-FU solutions with known concentrations under the same conditions. The amount of 5-FU loaded into the microgels was calculated from the decrease in 5-FU concentration. The loading content is expressed as the mass of loaded drug per unit weight of the dried microgels.

5. 2. 5 In Vitro Drug Release

The release of model drug from the microgels was evaluated by the dialysis method. 5.0 mL of the purified 5-FU-loaded microgel dispersions were transferred into the dialysis bags and then immersed into 50.0 mL 0.005 M phosphate buffer solutions at different pH values and temperatures, respectively. The released 5-FU outside of the dialysis bag was sampled at defined time period and assayed by UV-Vis absorption at 270 nm. Cumulative release is expressed as the total percentage of drug released through the dialysis membrane over time.

5. 2. 6 In Vitro Cytotoxicity

B16F10 cells (2000 cell/well) were cultured in DMEM containing 10% FBS and 1% penicillin-streptomycin in two 96-well plates, and exposed to free 5-FU, drug-free ZnO@PEG-chitosan microgels, and 5-FU loaded ZnO@PEG-chitosan microgels. To cover the high

concentrations, the microgels were concentrated and adjusted to an appropriate concentration in DMEM right before feeding into the well. The plate was incubated at 37 ℃ for 24 h. The medium was then aspirated, and these wells were washed using fresh serum-free DMEM. After that, 25.0 mL of 3-(4,5-dimethyl-2-thiazolyl)-2,5-diphenyltetrazolium bromide (MTT) solution (5.0 mg/mL in PBS) were added to the wells. After incubation for 24 h, the solution was aspirated. 100.0 mL of dimethyl sulfoxide was then added to each well and the plate was sealed and incubated for 30 min at 37 ℃ with gentle mixing. Three portions of the solution obtained from each well were transferred to three respective wells of a 96-well plate. Cell viability was measured using a microplate reader at 570 nm. Positive controls contained no 5-FU or microgels, and negative controls contained MTT.

5. 2. 7 Characterization

The morphology of ZnO QDs and ZnO@PEG-chitosan core-shell microgels were observed with transmission electron microscopy (TEM) on a FEI TECNAI transmission electron microscope at an accelerating voltage of 120 kV. Approximately 20 μL of the diluted microgel dispersions (pH = 7.4) were dropped on a Formvar-covered copper grid (300 meshes) and then air-dried at room temperature for the TEM measurements. The PL spectra of the hybrid nanogel dispersions at different pH values were respectively obtained on a JOBIN YVON Co. FluoroMax-3 Spectrofluorometer equipped with a Hamamatsu R928P photomultiplier tube, calibrated photodiode for excitation reference correction from 200 to 980 nm, and an integration time of 1 s. The UV-Vis absorption at 270 nm was recorded on a Thermo Electron Co. Helios β UV-Vis Spectrometer. The B16F10 cells incorporated with the hybrid microgels were imaged

using a confocal laser scanning microscopy (LEICA TCS SP2 AOBS^{TM}) equipped with an HC PL APO CS×20 0.7 DRY len. A Argon laser (405 nm) was used as the light source. The pH values were obtained on a METTLER TOLEDO SevenEasy pH meter. The size and size distribution of the microgels under different conditions were measured using a standard light scattering spectrometer (BI-200SM) equipped with a BI-9000 AT digital time correlator (Brookhaven Instrument, Inc.). A Nd:YAG laser (150 mW, 532 nm) was used as the light source. The diluted microgel dispersions were passed through 0.8 μm Millipore Millex-HV filters to remove dust.

5. 3 Results and Discussion

5. 3. 1 Synthesis of ZnO@PEG-chitosan core-shell microgels

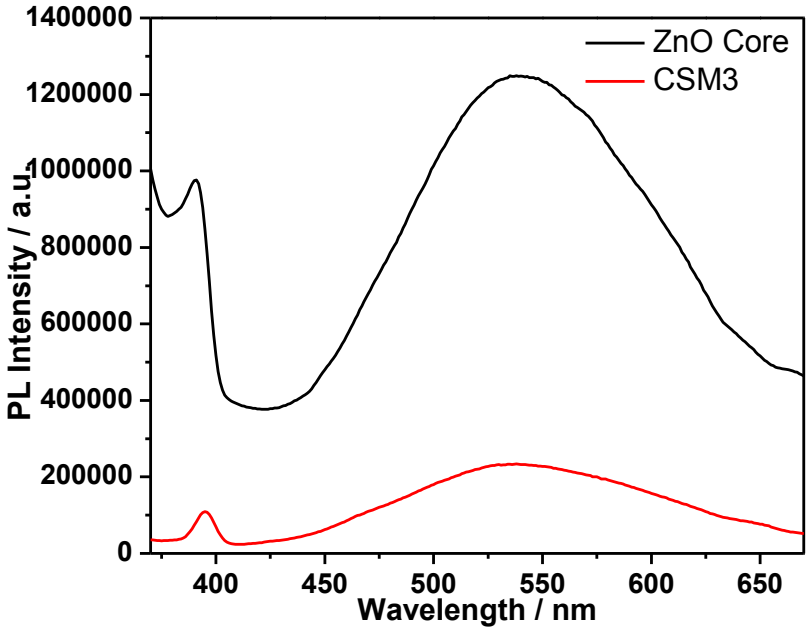

Figure 5-1 PL spectra of the ZnO core and CSM3 suspension in water at room temperature.

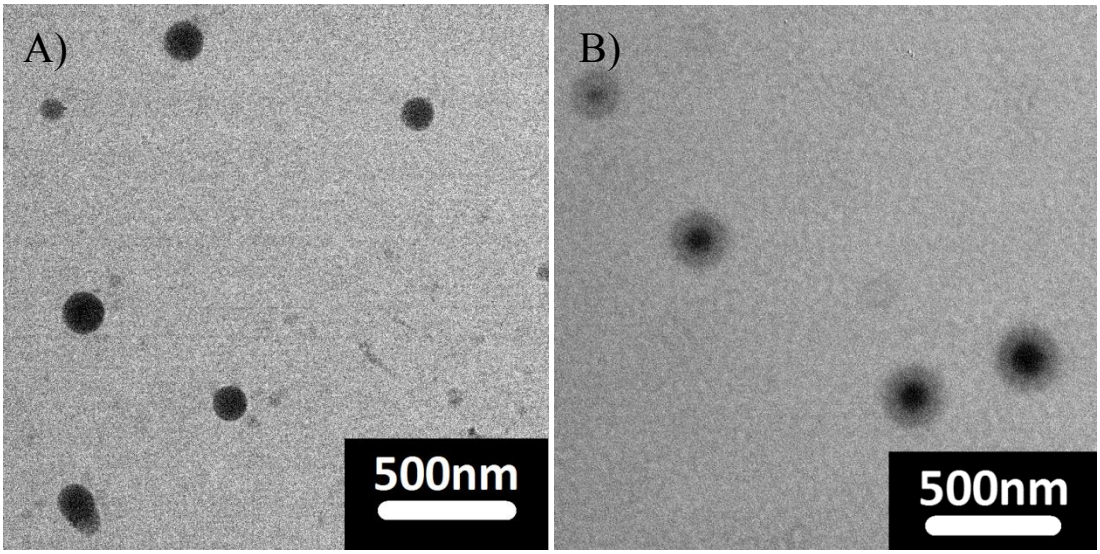

Figure 5-2 TEM images of A) ZnO QDs core and B) CSM3 hybrid microgel particles, dried at room temperature.

The conventional ZnO QDs are not stable in aqueous solution. Our strategy involves the copolymerization of PEGMEMA macromonomer with the ZnO precursor of Zinc methacrylate and the simultaneous formation of ZnO QDs in the basic solution. This synthetic process enables the hydrophilic side PEG chains to segregate and cap the newly formed ZnO QDs, thus increases the hydrophicility of ZnO QDs, which can be stably dispersed in aqueous phase. The addition of the PEG-chitosan semi-IPN shell were prepared by the direct polymerization and crosslinking of the MEO_2MA and MEO_5MA comonomers in chitosan solution in the presence of the nonlinear PEG stabilized ZnO QDs at 65 °C. No surfactant was added since the slightly positive-charged chitosan can act as stabilizer to favor the formation of ZnO@PEG-chitosan core-shell structured microgel particles. The formation of PEG-chitosan semi-IPN network can be attributed to the first complexation through the hydrogen bonding interaction between the ether oxygens of the

oligo(ethylene glycol) monomers and the hydroxyl and amine groups of the chitosan chains, and then followed by precipitation polymerization of the chitosan-complexed monomers.

Figure 5-1 shows the PL spectra of the nonlinear PEG stabilized ZnO QDs core and the ZnO@PEG-chitosan core-shell hybrid microgels. Both of them show an emission at about 540 nm which is typical ZnO vacancy luminescence. Their absorption onsets locate around 3.4 eV, which is also typical for ZnO band gap. Hence, ZnO@PEG-chitosan core-shell hybrid microgels maintained the optical property of ZnO QDs in the core. Figure 5-2 shows a typical TEM image of PEG stabilized ZnO QDs core and ZnO@PEG-chitosan hybrid microgel CSM3. Obviously, the core-shell structured ZnO@PEG-chitosan hybrid microgels have been prepared successfully, which have a spherical morphology with a very narrow size distribution and a clear core-shell structure with a dark inorganic ZnO core and less contrasted PEG-chitosan polymer shell. The DLS characterization further confirmed that the ZnO@PEG-chitosan microgels are nearly monodispersed with the polydispersity index $\mu_2/<\Gamma>^2 < 0.1$ under all the measurement conditions. All the ZnO@PEG-chitosan microgel dispersions are very stable with neglectable change in the polydispersity index after setting for several months under room temperature, due to the formation of stable semi-IPN structure of the PEG-chitosan gel shell.

5. 3. 2 pH-Induced Volume Phase Transition

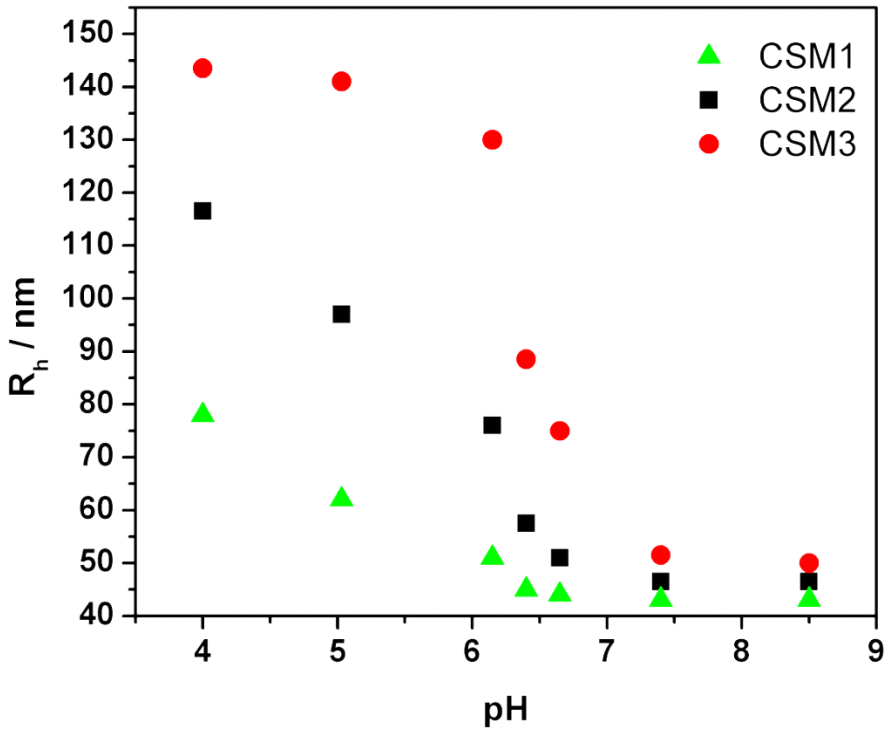

Figure 5-3 pH-dependent average R_h values of the ZnO@PEG-chitosan microgels, measured at a scattering angle θ = 45° and 37 ºC

The primary aliphatic amine of chitosan is a pH-responsive moiety and the pH value of dispersion medium can significantly influence the size of the ZnO@PEG-chitosan core-shell microgels. Figure 5-3 shows the pH-dependent swelling curves of the ZnO@PEG-chitosan hybrid microgels, in terms of the R_h change measured at a scattering angels of θ = 45° and physiological temperature of 37 °C. A well-defined volume phase transition is observed for all the studied core-shell microgels. When the pH value is below the pK_b (≈ 6.5) of chitosan, the –NH_2 groups of chitosan chains are gradually protonated. The generation of ionized –NH_3^+ can weaken the hydrogen bonding between the PEG and chitosan chains and induce the coulombic

repulsion among these $–NH_3^+$ groups, resulting in the gradual increase in the size of the microgels. The $–NH_2$ groups were slightly ionized in the synthetic medium of pH ≈ 6.2 and still not completely ionized at pH = 4.0, therefore, a much lower pH (< 4.0) is needed to let the studied microgels swell completely. At high pH values (pH>7.0), the size of microgels remains nearly a constant due to the strong hydrogen bonding between PEG chains and the uncharged chitosan chains. Interestingly, the volume phase transition pH values and sharpness as well as the swelling ratios of the hybrid microgels can be easily controlled through the comonomer MEO_2MA/MEO_5MA feeding ratio ($f_{PEG2/PEG5}$) in the synthesis of PEG-chitosan gel shell. For example, the CSM1, CSM2, and CSM3 synthesized with a gradually decreased $f_{PEG2/PEG5}$ exhibited a corresponding progressively sharper pH-induced volume change and larger swelling ratio. These results are understandable. We had fixed the total mole number of the comonomers of MEO_2MA and MEO_5MA, but varied their ratio of $f_{PEG2/PEG5}$ in the synthesis. At a higher $f_{PEG2/PEG5}$, the MEO_2MA monomers are dominant. The short EO_2 segments in the MEO_2MA monomers will complex less chitosan chains from the solution, resulting a lower content of chitosan to be semi-interpenetrated into the nonlinear PEG chain network. In contrast, the lower $f_{PEG2/PEG5}$ could provide more MEO_5MA comonomers with a longer EO_5 side chain, which can complex more chitosan chains into the final PEG-chitosan semi-IPN gel shell. The higher content of chitosan in the gel shell should enable the ZnO@PEG-chitosan hybrid microgels more sensitive to the pH change. Nevertheless, when the pH value was varied from 7.4 to 5.0 at physiological temperature of 37 ^oC, all the hybrid microgels demonstrated a significant swelling, which should be very important for the on-site pH-triggable drug release.

5. 3. 3 Temperature-Induced Volume Phase Transitions

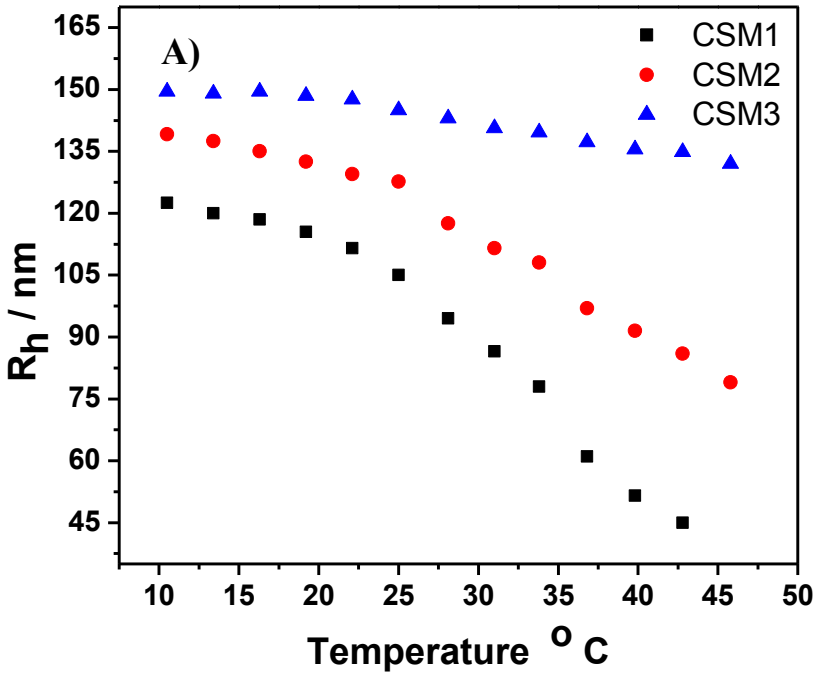

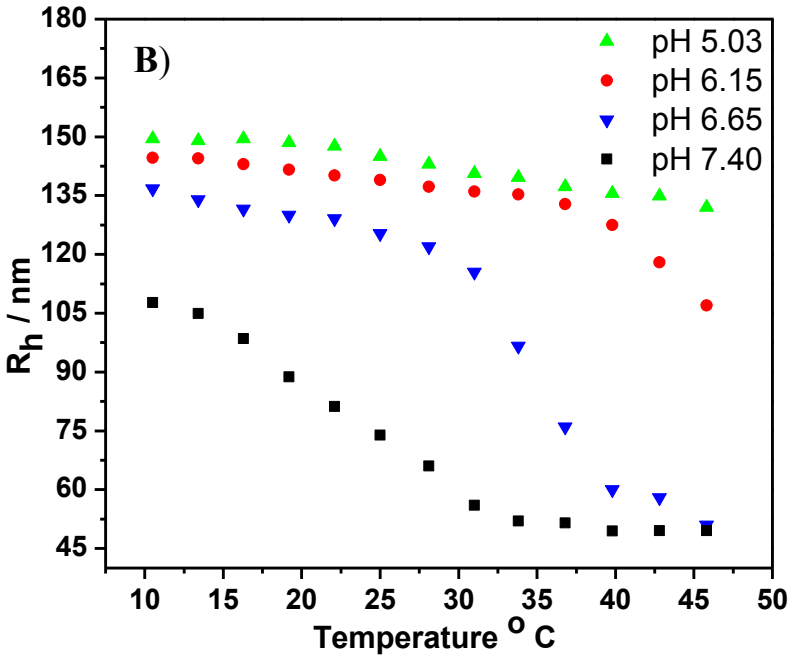

Figure 5-4 A) Temperature-dependent average R_h of CSM1, CSM2 and CSM3 microgels at pH 5.03, measured at a scattering angle θ = 45°; B) Temperature-dependent average R_h of CSM3 microgels, measured at a scattering angle θ = 45° and different pH values.

Figure 5-4 shows the temperature-induced volume phase transitions of the ZnO@PEG-chitosan hybrid microgels, in terms of the change of R_h measured at a scattering angles of $\theta = 45^{o}$. It is clear that as the increasing in temperature, the particle size of ZnO@PEG-chitosan hybrid microgels start to decrease. Combining the pH-responsive volume phase transitions as shown in figure 5-3, it is clear that our ZnO@PEG-chitosan microgels are pH and temperature dual-responsive. At a certain pH value but different temperature, all $–NH_2$ groups in chitosan will remain their status and no more $–NH_3^+$ ions will be formed to induce conformational and chemical changes of chitosan chains in water. Therefore, the observed temperature-induced

volume phase transitions of the microgels should be attributed to the thermo-responsive nonlinear PEG gel networks. The unusual water solubility of this type of nonlinear PEG polymers is arises from the strong hydrogen bonds between the side PEG chains and water molecules. This conformationally favorable effect in water is counterbalanced by the hydrophobicity of the apolar backbone, and the physical association between PEG and chitosan chains.[34] Tunable temperature-induced phase behavior can be readily achieved in the ZnO@PEG-chitosan hybrid microgels by adjusting the comonomer feeding ratio $f_{PEG2/PEG5}$. It has been well studied that the LCST of the nonlinear PEG polymers can be adjusted by the side PEG chain length.[27,34] The $PMEO_2MA$ polymer with short side PEG segments (2 EO units) has a LCST around 22 ^oC, while the $PMEO_5MA$ polymer with relatively longer side PEG segments (5 EO units) has a LCST above 60 ^oC. At a fixed pH of 5.03, CSM1, CSM2, and CSM3 synthesized with the decreased $f_{PEG2/PEG5}$ displayed a clear shift of VPTT to higher temperatures. For example, the CSM1 with the highest $f_{PEG2/PEG5}$ value had a lowest VPTT and reached nearly a full collapsing degree at 43 ^oC. In contrast, the CSM2 still did not reach a full collapse at 46 ^oC and the CSM3 demonstrated a very small shrinking degree when temperature was increased from 15 to 46 ^oC. Clearly, to induce the hydrophilic nonlinear PEG network with longer side PEG chains to collapse, a higher temperature needs to be provided. Furthermore, the temperature-induced phase behavior in terms of both the swelling ratio and VPTT of the ZnO@PEG-chitosan hybrid microgels can be tuned through the pH adjustment of the dispersion medium of microgels. Figure 5-4B shows the temperature-induced volume phase transitions of the CSM3 hybrid microgels measured at different pH values. A gradual decrease in the pH value from 7.40 to 5.03 has resulted in a gradual increase in the volume phase transition temperature. It should be

mentioned that both the morphology and composition of the ZnO@PEG-chitosan hybrid microgels are stable in the different environments and the pH- or temperature-induced volume phase transition is reversible. Therefore, the ZnO@PEG-chitosan hybrid microgels presented in this work can serve as excellent drug carriers with a pH and temperature dual-controllable drug releasing behavior.

5. 3. 4 In Vitro Drug Release

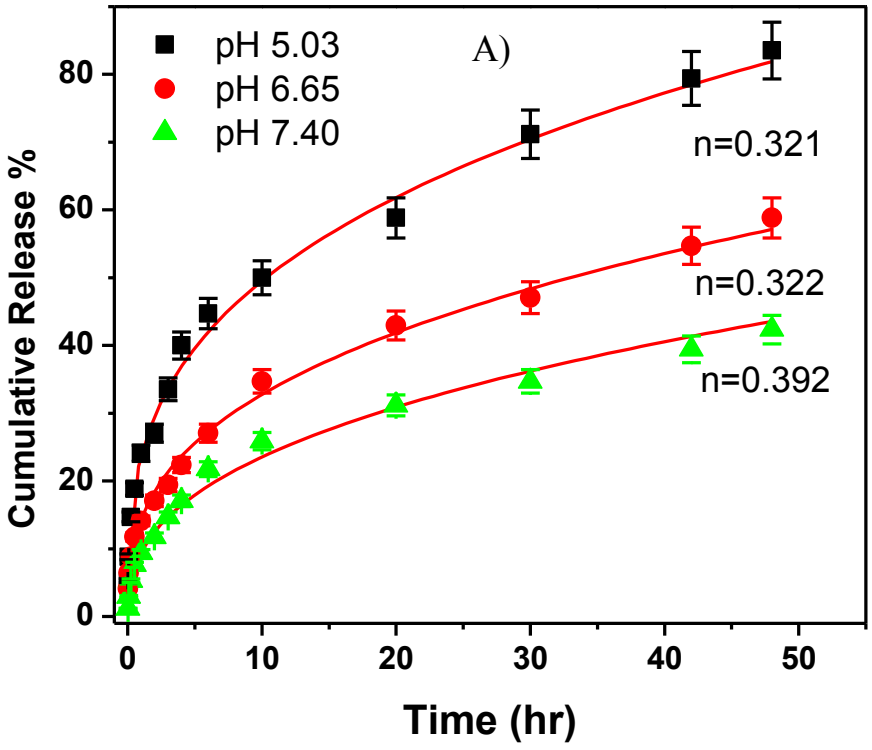

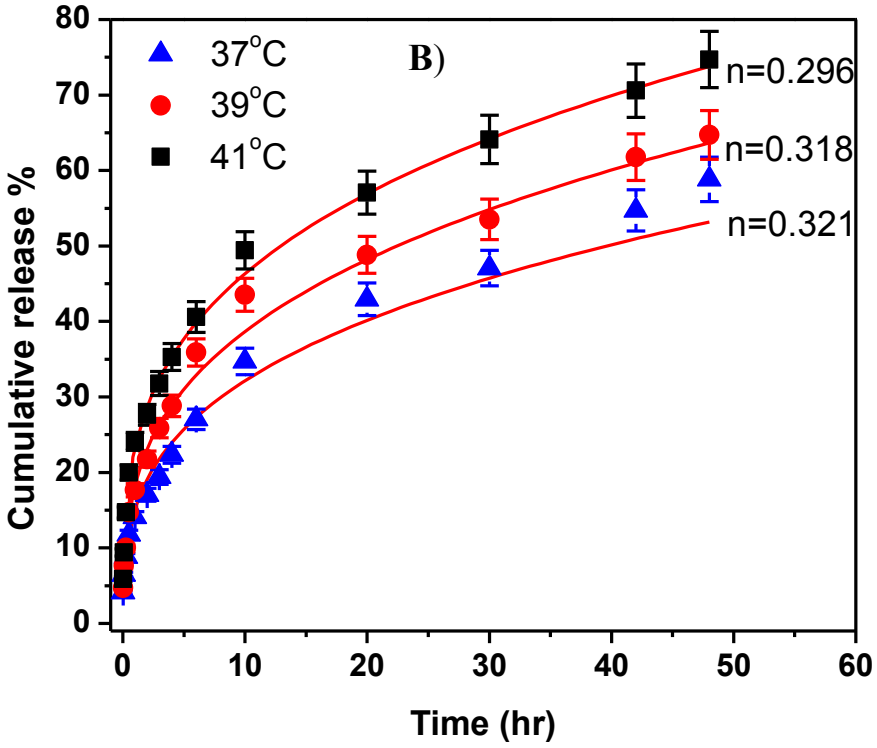

.

Figure 5-5 Cumulative release of 5-FU from CSM3: A), measured at buffer solutions of different pH values at 37 °C; B) measured at pH 6.65 buffer solutions of different temperatures.

The CSM3 ZnO@PEG-chitosan hybrid microgels with high pH and temperature-sensitivity over the physiologically important pH/temperature range were chosen for further *in vitro* experiments. 5-FU was selected as a model drug for demonstrating the pH/temperature-regulated drug release due to the widely use of 5-FU in the treatment of a range of cancers, such as colorectal and breast cancers and cancers of the aerodigestive tract. The chemotherapy agent 5-FU acts in several ways, but principally as a thymidylate synthase (TS) inhibitor.[35, 36, 37] TS catalyses the reductive methylation of deoxyuridine monophosphate (dUMP) into

deoxythymidine monophosphate (dTMP). The presence of 5-FU can interrupt the action of TS and then block the synthesis of the pyrimidine thymidine, which is a nucleotide required for DNA replication. Hence, under a scarcity of dTMP, cancerous cells will undergo cell death via thymineless death quickly. Side effects of 5-FU administration include myelosuppression, CNS (central nervous system) damage and cardiac toxicity.[38, 39]

Figure 5-5A shows the cumulative release profiles of 5-FU from the CSM3 into buffer solutions measured by a conventional dialysis bag method at a physiological temperature of 37 ℃ and three different pH values of 5.03, 6.65 and 7.40, respectively. Clearly, the pH of the external buffer solution can trigger the 5-FU release. The decrease in pH increases the 5-FU releasing rate from microgels. When the 5-FU-loaded microgels were placed in a pH 7.40 buffer, only ~40% of the loaded 5-FU could be released even after 48 h. When the pH of the external buffer solution was decreased to 6.65, about 56% of the loaded 5-FU could be released within 48 h. When the pH was further decreased to 5.03, about 85% of the loaded 5-FU could be released in 48 h.

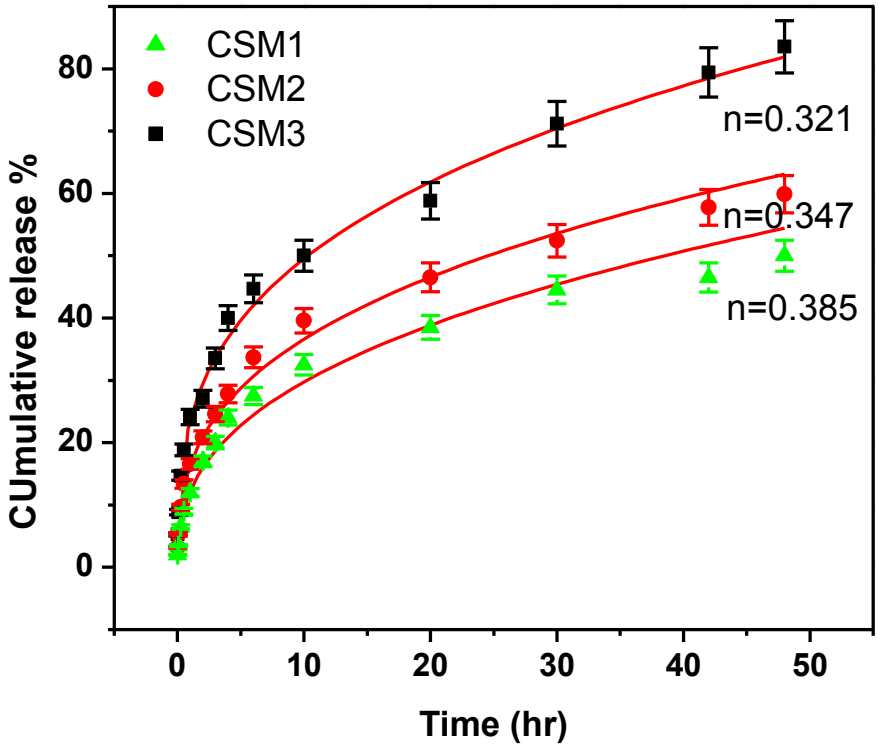

Figure 5-6 Cumulative releases of 5-FU from CSM1, CSM2 and CSM3 at 37 ^{o}C and pH 5.03, respectively.

On the other hand, the temperature of the external buffer solution can also trigger the release of 5-FU from drug-loaded ZnO@PEG-chitosan hybrid microgels. Figure 5-5B shows the cumulative drug release profile of CSM3 in the same PBS buffer of pH = 6.65 but at different temperatures. The increase in temperature increases the 5-FU releasing rate from the microgels. At 37 ℃, about 56% of 5-FU was released from the CSM3 within 48 h. When the temperature was increased to 41 ℃, the release amount of 5-FU was increased to 75%. Clearly, both the increase in temperature and the decrease in pH of the releasing medium can speed up the

releasing rate of 5-FU from the ZnO@PEG-chitosan hybrid microgels. The pH-regulated drug releasing process is mainly diffusion controlled because the decrease in pH induces the semi-IPN gel networks to swell. The large mesh size of the swollen gel network allows the entrapped drug molecules to diffuse out more easily. The temperature-regulated drug releasing process should be based on the squeezing mechanism because the increase in temperature can shrink the gel networks (or reduce the mesh size), which will squeeze out the entrapped drug molecules. In addition, the tailoring of the PEG-chitosan semi-IPN gel shell by varying the synthetic feeding mol ratio $f_{PEG2/PEG5}$ can also modify the 5-FU releasing profiles to a certain extent. For example, at a fixed temperature of 37 °C and a fixed pH of 5.03, CSM1, CSM2 and CSM3 synthesized with a gradual decreased $f_{PEG2/PEG5}$ exhibited a gradually increased pH-induced swelling ratio, and demonstrated a corresponding faster 5-FU releasing rate (figure 5-6).

To further investigate the release mechanism, the cunmulative drug release curves were further analyzed according to the empirical equation proposed by Peppas *et al.*:[40]

$$M_t / M_\infty = kt^n \qquad (1)$$

where M_t and M_∞ standard for the amount of drug released up to any time t and the infinite time; k represent a structural/geometric constant and n is a release exponent related to the intimate mechanism of release. Eq. (1) has two distinct physical realistic meanings in the two special cases of n = ~0.43 (indicating diffusion-controlled drug release) and n = ~0.85 (indicating swelling-controlled drug release). When n = ~0.43−0.85, the release can be regarded as indicator for both phenomena (anomalous transport), while n < ~0.43 indicate another transportation process in addition to the diffusion-controlled process.[40] The n values for all release curves are all below 0.43, which indicate that the releasing mechanism of all cases involves two processes:

one is simple diffusion step; another is related to the breakage of hydrogen bonding between the 5-FU and polymer chains. The increase of temperature will weaken the hydrogen bonding between 5-FU and polymer chains, which will help the release of 5-FU.

The releasing profiles fit well to the empirical equation proposed by Peppas *et al*. Both increase in temperature from 37 ºC to 41 ºC and decrease in pH value from 7.40 to 5.03 decreased the n values, which indicate diffusion-controlled drug release mechanism will be dominant at lower temperature and higher pH value. Clearly, the pH and temperature dual-responsive hybrid microgels developed here could be promising potential materials for the treatment of various diseases since they are able to regulate the transport of therapeutics at targeted pathological zone such as cancer and cystic fibrosis that are associated with disruptions in acid/base and temperature homeostasis.

5. 3. 5 In Vitro Cytotoxicity

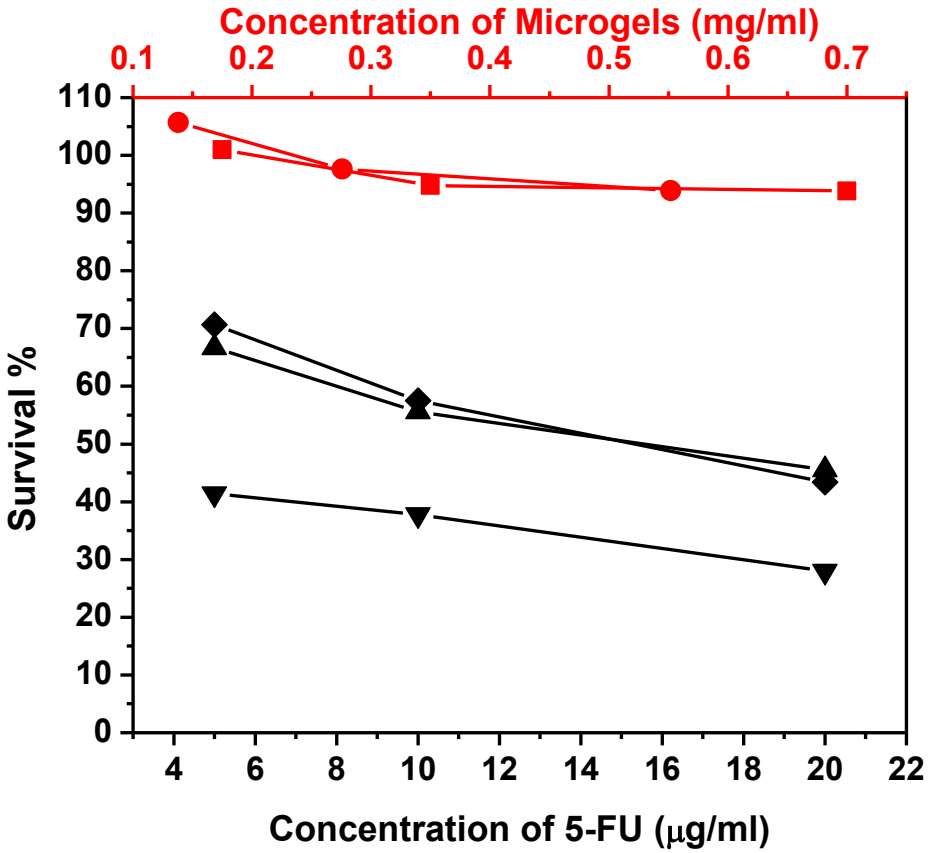

Figure 5-7 Comparison of B16F10 cell survivability following treatments with CSM1 and CSM2 hybrid microgels as drug carriers, respectively (■: 5-FU-loaded CSM1; ▲: 5-FU-loaded CSM2). B16F10 cell survivability after treated with free microgels (●: CSM1; ♦: CSM2) and free 5-FU solutions (▼) were also presented for a comparison.

For future biological applications, the cytotoxicity of ZnO@PEG-chitosan hybrid microgels has been investigated. More than 95% of B16F10 cells can survive upon treatment with the ZnO@PEG-chitosan microgels with concentrations up to 0.55 mg/mL and 0.70 mg/mL for CSM1 and CSM2, respectively (Figure 5-7). However, after the treatment of cell with 5-FU loaded CSM1 and CSM2, the cell viability decreased drastically even at a concentration as low

as 0.078 mg/mL and 0.12 mg/mL, respectively (equivalent to 5.0 μg/mL free 5-FU). These results indicate that the 5-FU-loaded microgels provide high anticancer activity. Besides, it is found that the cytotoxicity of 5-FU loaded hybrid microgels is lower than that of the free 5-FU solution at the correspondingly studied concentrations. This can be attributed to the sustained-release property of the 5-FU-loaded hybrid microgels.

5. 3. 6 Tumor Cell Image

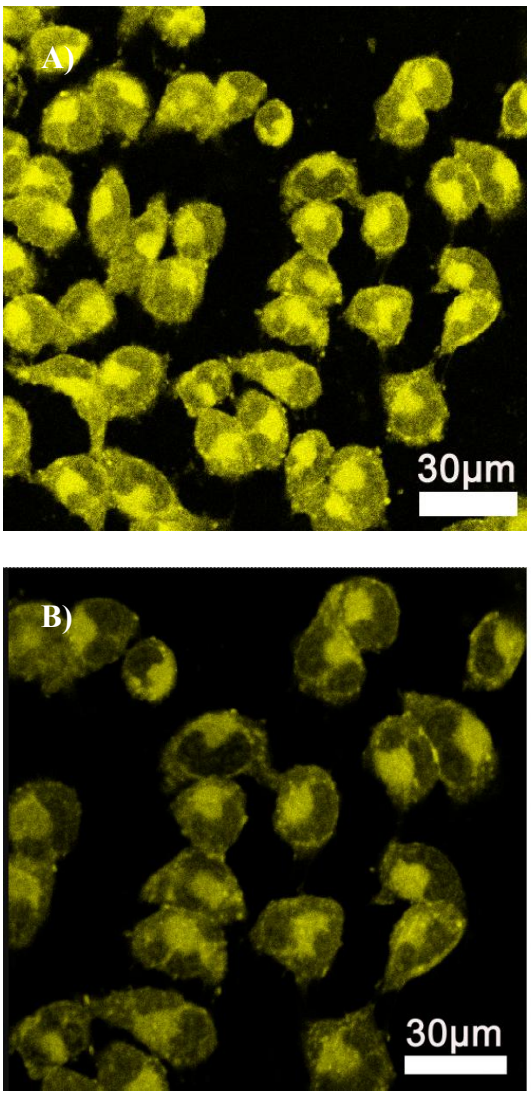

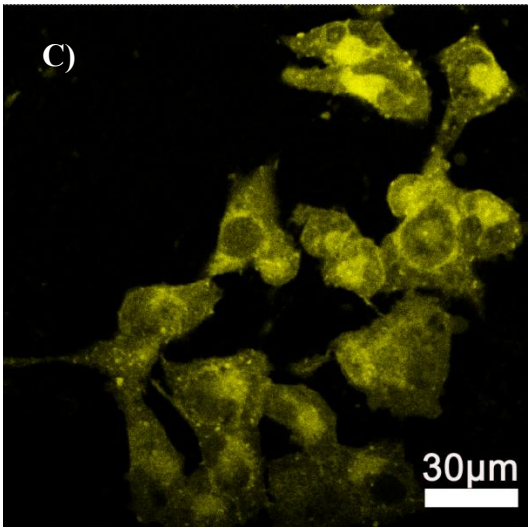

Figure 5-8 Scanning confocal fluorescence images of the mouse melanoma B16F10 cells after incubated with the A) CSM1; B)CSM2; C)CSM3 hybrid microgels. Excitation laser wavelength =405 nm.

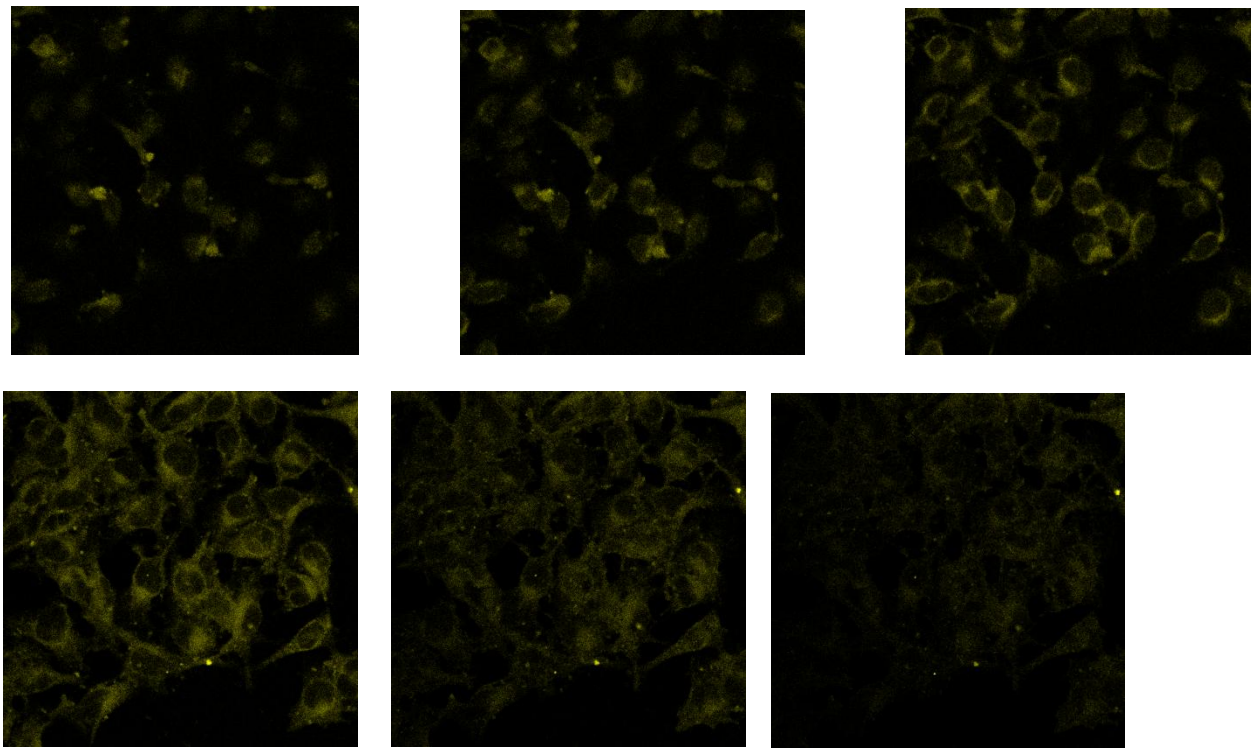

Figure 5-9 Z-scan of a selected sample area of CSM1 (top to bottom). Excitation laser wavelength =405 nm.

To examine whether the ZnO@PEG-chitosan hybrid microgels can enter into tumor cells and the ZnO QDs in the core preserved their luminescence property, laser confocal microscopy was used to evaluate the hybrid microgels as a fluorescence-labeling agent in tumor cell imaging application. Confocal micrographs reveal that all the three hybrid microgels of CSM1, CSM2, and CSM3 in different size and composition ratio were successfully endocytosed into the mouse melanoma B16F10 cells (Figure 5-8). Strong fluorescence was observed when irradiated by the laser of 405 nm, the QDs immobilized in the hybrid microgels produced a bright yellow color. It is thus obvious that these probes do not give dark regions in the cells and the areas where the hybrid microgels did not permeate are clear. To identify the distribution of the ZnO@PEG-chitosan core-shell microgels in the cells, Z-scan images of CSM1 were taken from top to bottom for selected sample area (Figure 5-9). These images indicate that our microgels can overcome cellular barriers to enter the intracellular region (even the nuclear regions).

5. 4 Conclusion

Multifunctional core-shell structured ZnO@PEG-chitosan hybrid microgels composed of PEG stabilized ZnO QDs as core and semi-IPN PEG-chitosan gel layer as shell were successfully prepared by free radical polymerization of shell components onto the colloidal ZnO particles. The presence of PEG-chitosan gel shell at appropriate ratios enables the hybrid microgels highly sensitive to a surrounding medium of different pH values and temperatures over the physiologically relevant ranges of 5.0-7.4 and 36-40 ^{o}C, respectively. Therefore, the pH

and temperature dual-triggerable drug delivery becomes possible. The drug releasing studies demonstrated that the hybrid microgels show drug sustained properties and the release could be triggered by the pH and temperature dual-responsive volume phase transition of the PEG-chitosan gel shell. Meanwhile, the encapsulated ZnO QDs in the core extend the application to cell imaging. The resultant hybrid microgels can enter intracellular region successfully. In vitro cytotoxicity tests indicate that the empty hybrid microgels have very low cytotoxicity, while the 5-FU-loaded microgels have high anticancer activity. These characteristics are important in both fundamental research and practical applications. The properly designed dual-responsive ZnO QDs encapsulated microgels as delivery vehicles should enhance our ability to address the complexity of biological systems, and thus offer broad opportunities for biomedical applications.

5. 5 References

(1) Wu, W.; Zhou, T.; Aiello, M.; Zhou, S. *Biosensors and Bioelectronics* **2010**, *25*, 2603-2610.

(2) Yildiz, I.; Deniz, E.; McCaughan, B.; Cruickshank, S. F.; Callan, J. F.; Raymo, F. M. *Langmuir* **2010**, *26*, 11503-11511.

(3) Wu, W.; Zhou, T.; Berliner, A.; Banerjee, P.; Zhou, S. *Angewandte Chemie International Edition* **2010**, *49*, 6554-6558.

(4) Obonyo, O.; Fisher, E.; Edwards, M.; Douroumis, D. *Crit. Rev. Biotechnol.* **2010**, *30*, 283-301.

(5) Vannoy, C. H.; Tavares, A. J.; Noor, M. O.; Uddayasankar, U.; Krull, U. J. *Sensors (Basel, Switzerland)* **2011**, *11*, 9732-9763.

(6) Xiong, H.-M.; Xu, Y.; Ren, Q.-G.; Xia, Y.-Y. *Journal of the American Chemical Society* **2008**, *130*, 7522-7523.

(7) Yuan, Q.; Hein, S.; Misra, R. D. K. *Acta Biomater* **2010**, *6*, 2732-2739.

(8) Fu, Y.-S.; Du, X.-W.; Kulinich, S. A.; Qiu, J.-S.; Qin, W.-J.; Li, R.; Sun, J.; Liu, J. *J. Am. Chem. Soc.* **2007**, *129*, 16029-16033.

(9) Tang, X.; Choo, E. S. G.; Li, L.; Ding, J.; Xue, J. *Chem. Mater.* **2010**, *22*, 3383-3388.

(10) Zhang, P.; Liu, W. *Biomaterials* **2010**, *31*, 3087-3094.

(11) Saunders, B. R.; Laajam, N.; Daly, E.; Teow, S.; Hu, X.; Stepto, R. *Adv Colloid Interface Sci* **2009**, *147-148*, 251-262.

(12) Das, M.; Zhang, H.; Kumacheva, E. *Annu. Rev. Mater. Res.* **2006**, *36*, 117-142.

(13) Baker, W. O. *Ind. Eng. Chem.* **1949**, *41*, 511-520.

(14) Shin, B. C.; Jhon, M. S.; Lee, H. B.; Yuk, S. H. *European Polymer Journal* **1998**, *34*, 1675-1681.

(15) Dalmont, H.; Pinprayoon, O.; Saunders, B. R. *Langmuir* **2008**, *24*, 2834-2840.

(16) Katono, H.; Maruyama, A.; Sanui, K.; Ogata, N.; Okano, T.; Sakurai, Y. *Journal of Controlled Release* **June**, *16*, 215-227.

(17) Okano, T.; Bae, Y. H.; Jacobs, H.; Kim, S. W. *Journal of Controlled Release* **1990**, *11*, 255-265.

(18) Lapeyre, V.; Ancla, C.; Catargi, B.; Ravaine, V. *Journal of Colloid and Interface Science* **2008**, *327*, 316-323.

(19) Torchilin, V. P. *Pharm. Res.* **2007**, *24*, 1-16.

(20) Stefanadis, C.; Chrysochoou, C.; Markou, D.; Petraki, K.; Panagiotakos, D. B.; Fasoulakis, C.; Kyriakidis, A.; Papadimitriou, C.; Toutouzas, P. K. *J. Clin. Oncol.* **2001**, *19*, 676-681.

(21) Gerweck, L. E.; Seetharaman, K. *Cancer Research* **1996**, *56*, 1194 -1198.

(22) Park, J. H.; Saravanakumar, G.; Kim, K.; Kwon, I. C. *Advanced Drug Delivery Reviews* **2010**, *62*, 28-41.

(23) Honarkar, H.; Barikani, M. *Monatshefte für Chemie Chemical Monthly* **2009**, *140*, 1403-1420.

(24) Polk, A.; Amsden, B.; De Yao, K.; Peng, T.; Goosen, M. F. A. *Journal of Pharmaceutical Sciences* **1994**, *83*, 178-185.

(25) Lutz, J.-F.; Hoth, A. *Macromolecules* **2006**, *39*, 893-896.

(26) Hu, Z.; Cai, T.; Chi, C. *Soft Matter* **2010**, *6*, 2115.

(27) Lutz, J. *Journal of Polymer Science Part A: Polymer Chemistry* **2008**, *46*, 3459-3470.

(28) Badi, N.; Lutz, J.-F. *J Control Release* **2009**, *140*, 224-229.

(29) Buyukserin, F.; Camli, S. T.; Yavuz, M. S.; Budak, G. G. *Journal of Colloid and Interface Science* **2011**, *355*, 76-80.

(30) Wu, W.; Aiello, M.; Zhou, T.; Berliner, A.; Banerjee, P.; Zhou, S. *Biomaterials* **2010**, *31*, 3023-3031.

(31) Chung, T.-W.; Lin, S.-Y.; Liu, D.-Z.; Tyan, Y.-C.; Yang, J.-S. *Int J Pharm* **2009**, *382*, 39-44.

(32) Dong, Y.; Hassan, W.; Zheng, Y.; Saeed, A. O.; Cao, H.; Tai, H.; Pandit, A.; Wang, W. *J Mater Sci Mater Med* **2011**.

(33) Chu, B. *Laser light scattering: basic principles and practice*; Academic Press, 1991.

(34) Lutz, J.-F.; Akdemir, Ö.; Hoth, A. *J. Am. Chem. Soc.* **2006**, *128*, 13046-13047.

(35) Scartozzi, M.; Maccaroni, E.; Giampieri, R.; Pistelli, M.; Bittoni, A.; Del Prete, M.; Berardi, R.; Cascinu, S. *Pharmacogenomics* **2011**, *12*, 251-265.

(36) Longley, D. B.; Harkin, D. P.; Johnston, P. G. *Nat. Rev. Cancer* **2003**, *3*, 330-338.

(37) Parker, J. B.; Stivers, J. T. *Biochemistry* **2011**, *50*, 612-617.

(38) Duffner, P. K. *J. Biol.* **2006**, *5*, 21.

(39) Han, R.; Yang, Y. M.; Dietrich, J.; Luebke, A.; Mayer-Pröschel, M.; Noble, M. *J. Biol.* **2008**, *7*, 12.

(40) Siepmann, J.; Peppas, N.A. *Adv. Drug Delivery Rev.* **2001**, *48*, 139.

Chapter 6

Optical Detection of Glucose by CdS Quantum Dots Embedded in Glucose-responsive Microgels

6. 1 Introduction

The in situ detection of saccharides, including D-glucose and D-fructose, has been of great interest for a long time due to the importance of saccharides in medical diagnostics and bioprocessing. Although enzyme-based detection approaches are highly selective and effective, many difficulties remain. For example, reliable continuous, non-invasive, or minimally invasive glucose monitoring systems are still a major challenge for optimal glycemic control in diabetic patients.[1–3] This has led to considerable research interest in developing synthetic chemical ligands for continuous monitoring of saccharides. So far, the best ligands identified for binding glucose in aqueous media are boronic acids.[4] These boronic acid-based ligands have been coupled with fluorescent moieties[1,5] or polymers[6–9] for continuous glucose sensing. The selectivity and significant reduction of lactate interference of the boronic acid-based glucose sensors have been investigated.[8] Novel triply-responsive boronic acid block copolymers have

been recently developed for potential applications as self-regulated drug delivery systems and sensors for sugars and glycoproteins.[10] On the other hand, there is a growing interest in using fluorescent quantum dots (QDs) as optical labels for biosensing events due to their size-controlled fluorescence properties, high quantum yield, and stability against photobleaching.[11–13] Singaram's group was the first one to utilize fluorescent QDs for glucose sensing.[14a] The fluorescence of CdTe/ZnS QDs can be quenched after their complexation with a viologen quencher.

The binding of glucose to the boronic acid-substituted quencher weakens the quencher–QD interactions and induces a robust fluorescence recovery. Tang et al.[14b] conjugated CdTe QDs with concanavalin A (Con A) that can be combined to the β-cyclodextrin-modified fluorescence quenchers. The binding of glucose with ConA breaks the quencher–QD interactions, leading to fluorescence recovery. Willner et al.[15] prepared H_2O_2-sensitive CdSe/ZnS QDs that can be further linked with glucose oxidase (GOx). The enzyme GOx catalyzes the oxidation of D-glucose and produces H_2O_2, resulting in the quenching of fluorescence of the QDs. However, these systems require very complicated functionalizations of both QDs and quenchers and are only good for homogeneous detection.

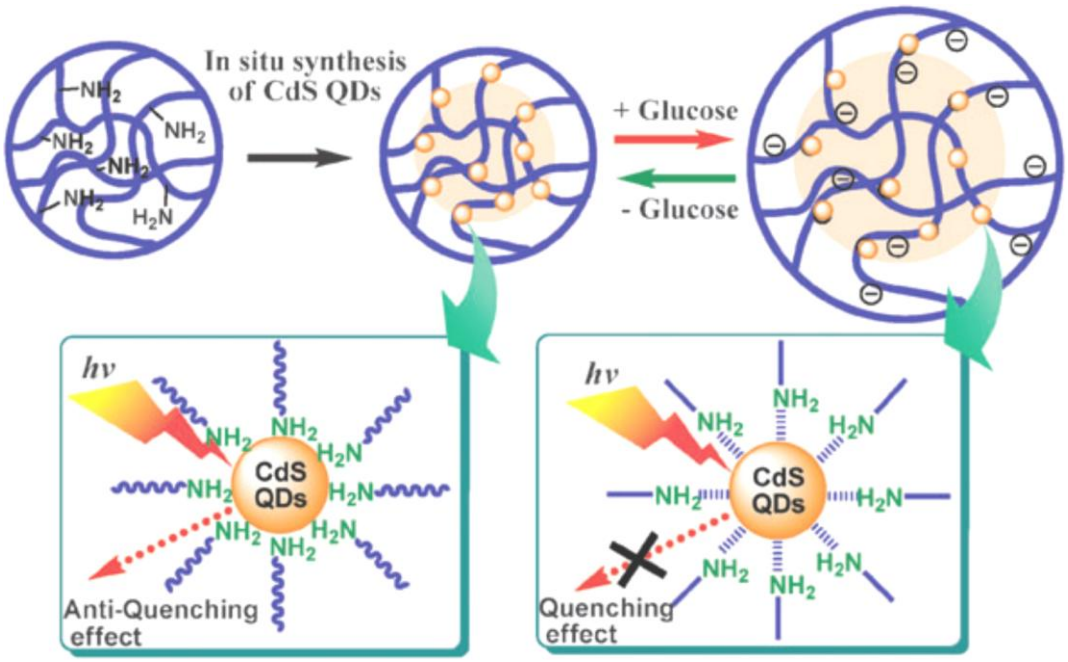

Scheme 6-1 Reversible fluorescence quenching and antiquenching of CdS QDs embedded in the interior of p(NIPAM-AAm-PBA) microgels in response to the change in glucose concentration.

Herein, we report a simple and reliable glucose sensing system based on the in situ immobilization of fluorescent CdS QDs in the interior of boronic acid based microgels for non-invasive continuous optical detection of saccharides. We demonstrate that the fluorescence of CdS QDs in the copolymer microgels of poly(N-isopropylacrylamide-acrylamide-phenylboronic acid) [p(NIPAM-AAm-PBA)] could be reversibly quenched and anti-quenched when the microgel undergoes swelling and deswelling in response to the glucose concentration change (Scheme 6-1). The hybrid materials with inorganic QDs embedded in smart microgels, combining the properties of both QDs and smart microgels, can offer the possibilities of external switching and manipulation for sensor devices. Microgels also offer several advantages over other polymer template systems: simple synthesis, easy functionalization, uniform size distribution, tunable dimension (tens of nm to a few mm), potential biocompatibility, and rapid response time.[16] The pAAm segments designed in the microgels are not only able to complex

with the Cd^{2+} precursors and stabilize the produced CdS QDs,[17] but also greatly improve the stability of the resulting p(NIPAM-AAm-PBA)–CdS hybrid microgels. The optical nanoscale glucose "meter" reported here is likely to be highly useful in a wide range of applications in biology and biomedicine for research, diagnosis, or monitoring.

6. 2 Experimental

6. 2. 1 Materials

D(+)-Glucose was purchased from ACROS, and all other chemicals were purchased from Aldrich. NIPAM was recrystallized from a hexane-toluene mixture. Acrylic acid (AA) was distilled under reduced pressure. Cadmium perchlorate hydrate ($Cd(ClO_4)_2 \cdot H_2O$), thioacetamide (CH_3CSNH_2), Acryamide (AAm), N,N'-methylenebisacrylamide (MBAAm), ammonium persulfate (APS), sodium dodecyl sulfate (SDS), 3-aminophenylboronic acid (APBA), and N-(3-dimethylaminopropyl)-N'-ethyl-carbodiimide hydrochloride (EDC), were used as received.

6. 2. 2 Preparation p(NIPAM-AAm-PBA) microgels

The p(NIPAM-AAm-PBA) microgels were synthesized using the procedure described in our previous report.[16a] First, 0.231 g of APBA and 0.231 g of EDC were dissolved in 35 mL of water. The solution was cooled in an ice bath, and then adding 20 mL of purified p(NIPAM-AAm-AA) microgels obtained from the precipitation copolymerization of NIPAM, AAm (7.3 mol%), and AA (7.1mol%) using MBAAm (4.3 mol%) as a crosslinker and APS as an initiator in the presence of SDS. The reaction was kept for 4 h at 0 ℃. The resultant products were purified by dialysis against very frequently changed water for at least 1 week.

6. 2. 3 Preparation of p(NIPAM-AAm-PBA)-CdS hybrid microgels

The p(NIPAM-AAm-PBA)-CdS hybrid microgels were prepared as follows: the mixture of 0.1431 g $Cd(ClO_4)_2 \cdot H_2O$ with 20 mL p(NIPAM-AAm-PBA) microgel suspensions was stirred at room temperature for 1 day under a N_2 purge. After that, excess $Cd(ClO_4)_2$ was removed by centrifugation, decantation, and dialysis against water for 2 days. The microgels loaded with Cd^{2+} ions were then heated to 60 ℃ under a N_2 purge and stirring. After 30 min, a CH_3CSNH_2 solution (0.073 g/5 ml water) was dropwisely added. The temperature was then raised to 85 ℃, and the color gradually turned to brilliant yellow. The mixture was further stirred for 1 h. The resulting hybrid microgels were then purified by centrifugation, decantation, and dialysis against frequently changed water for 3 days.

6. 2. 4 Characterization

The UV-vis absorption spectra were obtained on a Thermo Electron Co. Helios β UV-vis Spectrometer. The PL spectra of the hybrid microgel dispersions under different conditions were obtained on a JOBIN YVON Co. FluoroMax®-3 Spectrofluorometer. The TEM images were taken on a FEI TECNAI transmission electron microscope at an accelerating voltage of 120 kV. Dynamic light scattering (DLS) was performed on a BI-200SM light scattering spectrometer with a He-Ne laser (35mW, 633 nm) as the light source. To confirm the reversibility of the glucose-induced optical property change, the optical spectra of the p(NIPAM-AAm-PBA)-CdS hybrid microgel dispersions were measured for three cycles with dialysis/glucose adjustment. The optical spectra were reproducible after the dialysis (pH ≈ 6) and glucose adjustment, indicating that the glucose-sensitive optical property change is reversible. We have also repeated the experiments three times from batch to batch to make sure the reproducibility of the results.

6. 3 Results and discussion

6. 3. 1 Glucose sensitivity of microgels

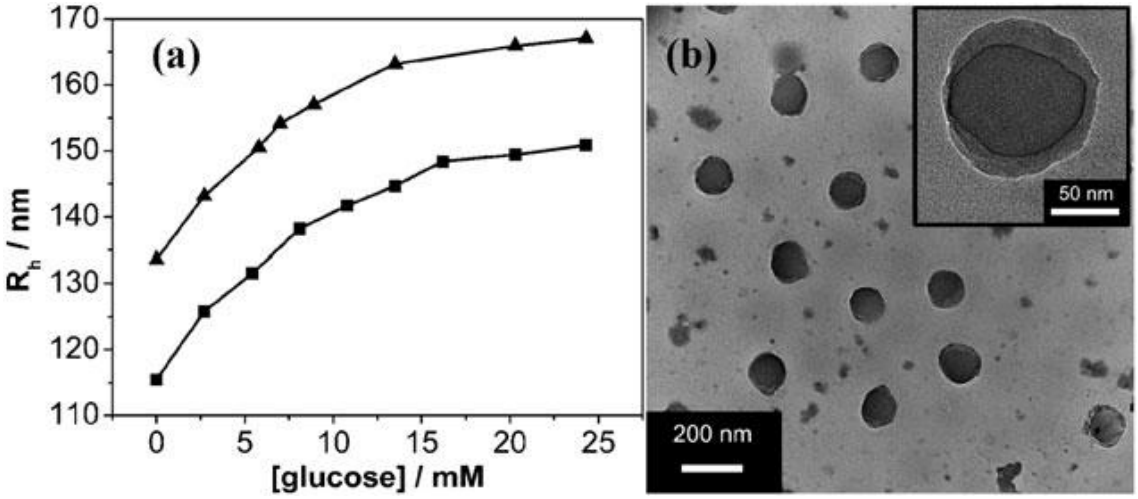

Figure 6-1 (a) Average R_h of p(NIPAM-AAm-PBA) (■), and p(NIPAM-AAm-PBA)–CdS microgels (▲) as a function of glucose concentration, measured at 22.1 °C, pH = 8.8, and a scattering angle θ= 60°. (b) TEM images of the p(NIPAM-AAm-PBA)–CdS hybrid microgels.

The p(NIPAM-AAm-AA) microgels were functionalized with PBA through the coupling of 3-aminophenylboronic acid to the –COOH groups of the AA units under EDC (1-ethyl-3-(3-dimethylaminopropyl)-carbodiimide) catalysis. The complexation of PBA with 1,2-cis-diols such as glucose produces a thermodynamically favorable anionic boronate to form, resulting in an increase in the degree of ionization that builds up a Donnan potential causing the microgels to swell. Figure 6-1a shows the glucose induced swelling curve of the p(NIPAM-AAm-PBA) microgels, in terms of the hydrodynamic radius (R_h) measured in a 0.005 M phosphate buffer solution (PBS) of pH = 8.8. When the glucose concentration is above 16 mM, the microgel network chains stretch to near maximum. This reversible volume phase transition allows us to change the interactions of the CdS QDs with the polymer ligands and the local surface

environments of the QDs embedded in the microgels in response to glucose concentration change.

The p(NIPAM-AAm-PBA)–CdS hybrid microgels were synthesized through the in situ formation of CdS QDs in the interior of the microgels at pH = 5.9, at which the PBA groups were nearly uncharged. Our motivation is to use the amide groups in the AAm units to complex the Cd^{2+} ions into the microgels from the external precursor $Cd(ClO_4)_2$ solution and to protect the obtained CdS QDs from agglomeration or release. The TEM images of the p(NIPAM-AAm-PBA)–CdS hybrid microgels (Figure 6-1b) clearly indicate a core–shell structure with a CdS QD rich core (higher contrast). The hybrid microgels are still glucose-sensitive after the immobilization of CdS QDs (Figure 6-1a), but become larger in size. This could be related to the relatively compact structure of the p(NIPAM-AAm-PBA) template microgels due to the hydrophobic PBA groups and the high cross-linking density. The in situ formed CdS QDs filled the relatively compact chain networks, and thus increased the total volume of the microgels. Importantly, the hydrophilic AAm segments prevented the hybrid microgels from aggregation in PBS even at the shrunk states for 2 months at room temperature.

6. 3. 2 Glucose-sensitive UV-Vis absorption properties of the p(NIPAM-AAm-PBA)–CdS hybrid microgels

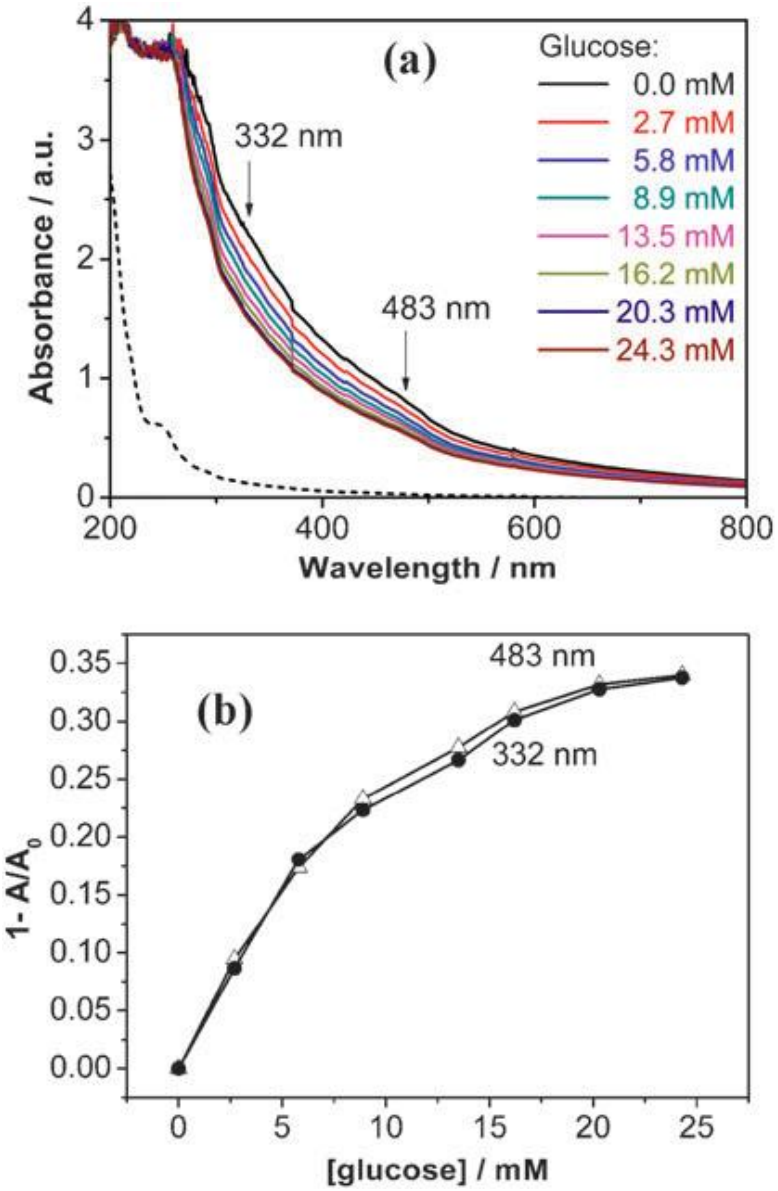

Figure 6-2 (a) UV-vis absorption spectra and (b) the relative transmittance at 332 nm (△) and 483 nm (•), respectively, of the p(NIPAM-AAm-PBA)–CdS hybrid microgels at different glucose concentrations in PBS at pH = 8.8. A and A_0 represent the absorbance of the hybrid microgels in the presence and absence of glucose. The dashed line in (a) shows the absorption spectrum of the template p(NIPAM-AAm-PBA) microgels.

Figure 6-2 shows the glucose-sensitive UV-Vis absorption properties of the p(NIPAM-AAm-PBA)–CdS hybrid microgels. A hump observed around 332 nm is assigned to the

excitonic transition, which possibly results from the $1P_h$–$1P_e$ transition,[18] while the hump at 483 nm is possibly related to the $1S_h$–$1S_e$ transition. The CdS QDs exhibit extremely strong quantum confinement in the microgels. Two effects were observed with a gradual increase in glucose concentration: (1) a decrease in absorbance at both low and long wavelengths; and (2) the gradual disappearance and featurelessness of the high-energy hump. Both effects are likely to arise from a decrease in the refractive index of the hybrid microgels during their swelling, which results in a decrease in the Rayleigh scattering due to a smaller refractive index contrast with the solvent, as well as a decrease in the local refractive index around the CdS QDs, leading to a weakening and featureless absorption. Interestingly, the glucose-induced increase in the transmittance of the p(NIPAM-AAm-PBA)–CdS hybrid microgels qualitatively reproduces the glucose-induced swelling curves (Figure 6-2b).

6. 3. 3 Effect of glucose-induced volume phase transition on PL properties of hybrid microgels

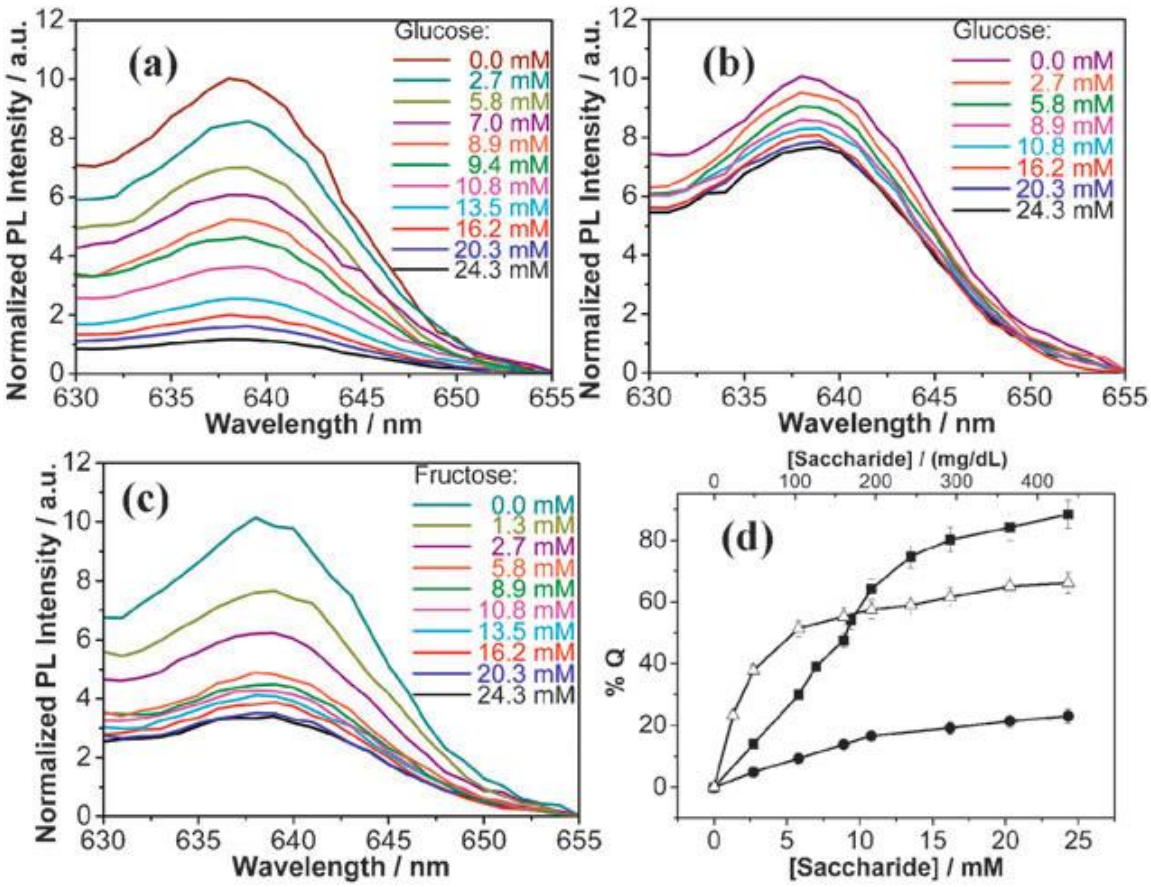

Figure 6-3 Characteristic PL response of the p(NIPAM-AAm-PBA)–CdS hybrid microgels at 638 nm in the presence of saccharides: (a) D-glucose at pH = 8.8, (b) D-glucose at pH = 7.4, and (c) D-fructose at pH = 7.4. (d) Quenched PL at 638 nm as a function of the concentration of glucose (●: pH = 7.4, ■: pH = 8.8) and fructose (△: pH = 7.4), respectively. The excitation wavelength was 390 nm.

The glucose-induced volume phase transition of the hybrid microgels could also significantly affect the photoluminescence (PL) properties of the CdS QDs embedded in the interior of the microgels. Figure 6-3(a-c) shows the evolution of PL emissions, centered at 638 nm, of the p(NIPAM-AAm-PBA)-CdS hybrid microgels in the presence of D-glucose and D-fructose at different concentrations and pH values. It is clear that the PL of CdS QDs was gradually quenched when the microgels gradually swelled up in the presence of D-glucose or D-

fructose. Figure 6-3d summarizes the glucose and fructose sensitivity based on the fluorescence quenching of the CdS QDs embedded in the p(NIPAM-AAm-PBA) microgels. At pH = 7.4, the percentage of the charged boronate complexes produced with PBA was ca. 30% for D-glucose and ca. 80% for D-fructose,[19] thus the fluorescence quenching of the CdS QDs showed a stronger sensitivity to D-fructose over D-glucose. At pH = 8.8, the complexation between D-glucose and the PBA groups in the microgels was almost complete, resulting in a high swelling degree of the microgels. Consequently, the fluorescence quenching of the CdS QDs can reach as high as 90%. The luminescence quenching of the QDs almost linearly increased with the glucose concentration from 0 to 13.5 mM, and then the rate of fluorescence quenching slowed down at higher glucose concentrations when the microgel network chains stretched to near maximum. It should be mentioned that glucose in the tested concentration range 0-50 mM had no effect on the fluorescence of the CdS QDs (see Figure 6-4), which is consistent with the recent report that glucose by itself has no effect on the fluorescence of CdSe/ZnS QDs.[15]

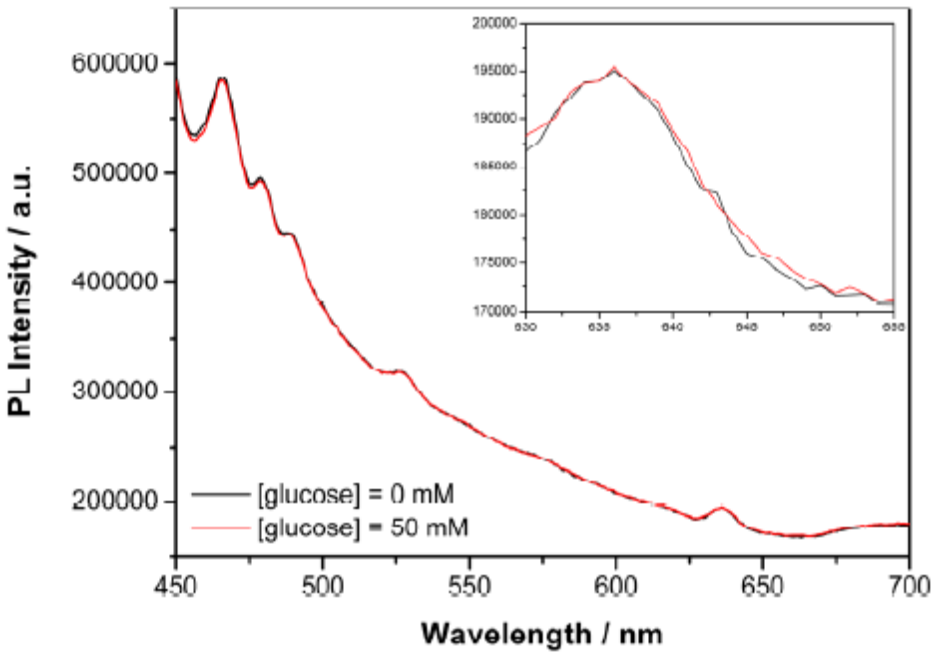

Figure 6-4 The PL spectra of the CTAB-capped CdS QDs in the absence of glucose and presence of 50 mM glucose.

We believe that the increase in the number of emission quenching centers located on the polymer–CdS QD interface provides the essential scenario for the PL quenching during the microgel swelling. At low glucose concentrations, the polymer is less soluble and the polymer chain networks have less elastic tension. In the swollen states at higher glucose concentrations, the polymer chain tends to dissolve; however, the cross-linkage of the polymer chains hinders the network expansion, creating elastic tensions localized at the cross-linking points. Because of the binding between the polymer ligands and the CdS QDs, the CdS QDs also act as cross-linking points, introducing an elastic tension in the bond that could stretch the polymer–CdS QD interface, creating interfacial states that quench the PL (Scheme 6-1). This phenomenon is similar to the temperature induced quenching of QDs,[20] where the freezing of the solvent (water) induces strain in the capping shell and the short stabilizer molecules (2-mercaptoethanolamine) propagate the strain to the surface of the nanocrystals, creating surface quenching states.

6. 3. 4 TEM Images of p(NIPAM-AAm-PBA)-CdS hybrid microgels at High Glucose Concentration

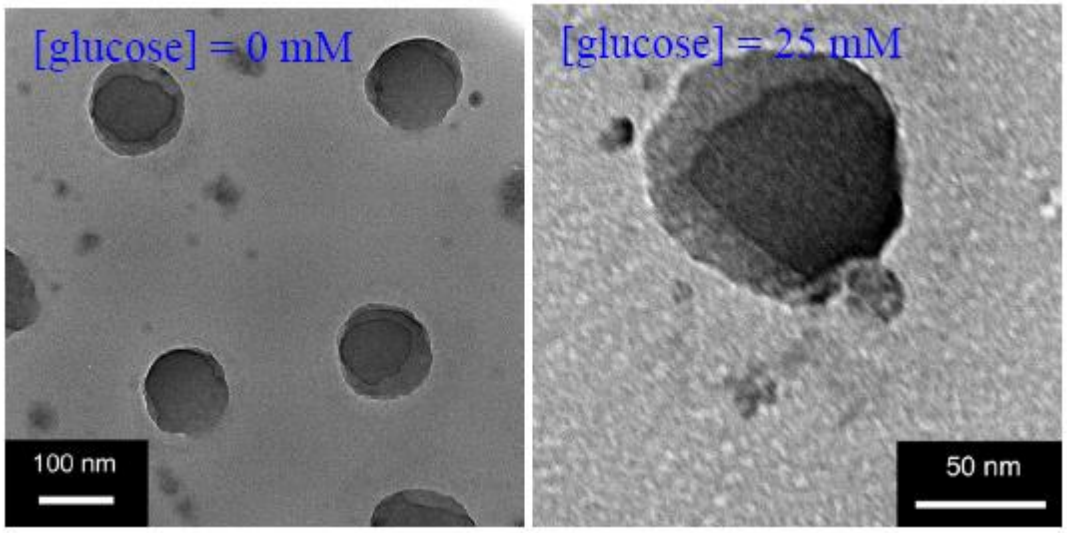

Figure 6-5 TEM Images of p(NIPAM-AAm-PBA)-CdS hybrid microgels at different Glucose Concentrations.

The polyacrylamide (pAAm) segments in the copolymer microgels has been designed to complex with Cd^{2+} ions for the uptake of Cd^{2+} precursors and to stabilize the CdS quantum dots (QDs) in the microgels. Indeed, TEM observations indicate that the swelling of the p(NIPAM-AAm-PBA)-CdS hybrid microgels at high glucose concentrations does not induce the release of CdS QDs. The core-shell structure with a CdS rich core of the hybrid microgels is very stable. No sediment was observed after ~3 months' placement.

6. 4 Conclusion

In summary, we demonstrate a new molecular recognition motif based on the fluorescence quenching of CdS QDs immobilized in glucose-sensitive microgels in the physiologically important glucose concentration range 1–25 mM, which shows a promise for continuous non-invasive in vivo glucose sensing system. We expect that the hybrid microgels prepared by a PBA analogue that can strongly bind D-glucose at physiological pH will enable

the detection of glucose at physiological conditions. Future studies should examine how the different cross-linking degrees and AAm/PBA contents of the microgels affect the size and content of the QDs as well as the sensing range of glucose concentration to provide a controllable glucose sensing range under physiological conditions.

6. 5 Reference

(1) Glucose Sensing (Topics in Fluorescence Spectroscopy), ed. C. D. Geddes and J. R. Lakowicz, Springer, New York, **2006**, vol. 11.

(2) V. R. Kondepati and H. M. Heise, Anal. Bioanal. Chem., **2007**, 388, 545.

(3) A. Heller and B. Feldman, Chem. Rev., **2008**, 108, 2482.

(4) A. P. Davis and R. S. Wareham, Angew. Chem., Int. Ed., **1999**, 38, 2979.

(5) (a)W. Yang, H. He and D. G. Drueckhammer, Angew. Chem., Int. Ed., **2001**, 40, 1714; (b) B. Peng and Y. Qin, Anal. Chem., **2008**, 80, 6137.

(6) E. Shoji and M. S. Freund, J. Am. Chem. Soc., **2002**, 124, 12486.

(7) (a) S. A. Asher, V. L. Alexeev, A. V. Goponenko, A. C. Sharma, I. K. Lednev, C. S. Wilcox and D. N. Finegold, J. Am. Chem. Soc., **2003**, 125, 3322S. A. Asher, V. L. Alexeev, A. V. Goponenko, A. C. Sharma, I. K. Lednev, C. S. Wilcox and D. N. Finegold, Anal. Chem., **2003**, 75, 2316; (b)M.M.W.Muscatello, L. E. Stunja and A. A. Asher, Anal. Chem., **2009**, 81, DOI: 10.1021/ac900006x.

(8) (a) S. Kabilan, A. J. Marshall, F. K. Sartain, M. C. Lee, A. Hussain, X. Yang, J. Blyth, N. Karangu, K. James, J. Zeng, D. Smith, A. Domschke and C. R. Lowe, Biosens. Bioelectron., **2004**, 20, 1602; (b) X. Yang, M. C. Lee, F. Sartain, X. Pan and C. R. Lowe, Chem.–Eur. J., **2006**, 12, 8491.

(9) J. T. Suri, D. B. Cordes, F. E. Cappuccio, R. A. Wessling and B. Singaram, Angew. Chem., Int. Ed., **2003**, 42, 5857.

(10) D. Roy, J. N. Cambre and B. S. Sumerlin, Chem. Commun., **2009**, 2106.

(11) (a) W. C. Chan and S. M. Nie, Science, 1998, 281, 2016; (b) W. C. Chan, D. J. Maxwell, X. Gao, R. E. Bailey, M. Han and S. M. Nie, Curr. Opin. Biotechnol., **2002**, 13, 40.

(12) I. L. Medintz, A. R. Clapp, F. M. Brunel, T. Tiefenbrunn, H. T. Uyeda, E. L. Chang, J. R. Deschamps, P. E. Dawson and H. Mattoussi, Nat. Mater., **2006**, 5, 581.

(13) D. Bardelang, Md. B. Zaman, I. L. Moudrakovski, S. Pawsey, J. C. Margeson, D. Wang, X. Wu, J. A. Ripmeester, C. I. Ratcliffe and K. Yu, Adv. Mater., **2008**, 20, 4517.

(14) (a) D. B. Cordes, S. Gamsey and B. Singaram, Angew. Chem., Int. Ed., **2006**, 45, 3829; (b) B. Tang, L. Cao, K. Xu, L. Zhou, J. Ge and L. Yu, Chem.–Eur. J., **2008**, 14, 3637.

(15) R. Gill, L. Bahshi, R. Freeman and I. Willner, Angew. Chem., Int. Ed., **2008**, 47, 1676.

(16) (a) Y. Zhang, Y. Guan and S. Q. Zhou, Biomacromolecules, **2006**, 7, 3196Y. Zhang, Y. Guan and S. Q. Zhou, Biomacromolecules, 2007, 8, 3842; (b) T. Hoare and R. Pelton, Macromolecules, **2007**, 40, 670.

(17) (a) P. Yez-Sedeo and J. M. Pingarrn, Anal. Bioanal. Chem., **2005**, 382, 884; (b) D. Mandal, H. Hosoi, U. Chatterjee and T. Tahara, J. Chem. Phys., **2009**, 130, 034902.

(18) (a) Y. Nosaka, J. Phys. Chem., **1991**, 95, 5054; (b) H. Matsumoto, T. Sakata, H. Mori and H. Yoneyama, J. Phys. Chem., **1996**, 100, 13781.

(19) S. A. Baker, A. K. Chopra, B. W. Hatt and P. J. Somers, Carbohydr. Res., **1973**, 26, 33.

(20) S. R. Wuister, C. M. Donega′ and A. Meijerink, J. Am. Chem. Soc., **2004**, 126, 10397.

Chapter 7

Engineering of Core-shell Microgels to Control the Onset of Glucose Responsive Volume Phase Transition

7. 1 Introduction

Stimuli-responsive polymer microgels have attracted major scientific interest in many areas, for instance, drug delivery[1-4], diagnostics[5], reaction templates[6-8] and sensors[9-13]. These microgels undergo quick, reversible microstructure changes when exposed to external stimuli such as changes in heat,[14,15] pH,[16] temperature,[17,18] light[19] and electrical field[20]. In recent years, the polymer microgels bearing phenylboronic acid (PBA) functional groups that respond to glucose concentration change in the surrounding environment, have gained great attention[21-30] due to the potential applications in diabetes management such as self-regulated insulin delivery. As shown in scheme 7-1, PBA is in equilibrium between the undissociated (or uncharged) and the dissociated (or charged) forms in aqueous solution. Both forms undergo reaction reversibly with 1, 2-cis-diols such as glucose. Compared with the charged form, complexation of the uncharged form with glucose is not stable since it is highly susceptible to hydrolysis, but the binding with glucose causes the thermodynamically more favorable charged form. As a result, the dissociation equilibrium of PBA moves to the right and its pKa decreases. For a microgel modified with PBA

groups, the binding of 1, 2-cis-diols increases the degree of ionization on the hydrogel and builds up a Donnan potential for the microgel to swell. The swollen microgel network with large mesh size allows the drug molecules to diffuse out easily. The higher the glucose concentration, the larger the swelling degree of the microgel network, which makes it possible to self-regulate the insulin release rate in response to different glucose level. So far, most of the glucose-sensitive polymer microgels are based on the copolymers of poly(N-isopropylacrylamide-co-acrylamido phenylboronic acid) [P(NIPAM-PBA)]. While the PBA component enabled the microgels exhibiting a rapid, reversible, and sensitive glucose responsibility even at very low glucose concentration, the major component of PNIPAM is necessary because its thermo-responsive property with a lower critical solution temperature (LCST) around 32 °C in water enabled a very simple synthesis of the monodispersed microgel particles from the precipitation polymerization under a mild condition (e.g., 60-70 °C in water).

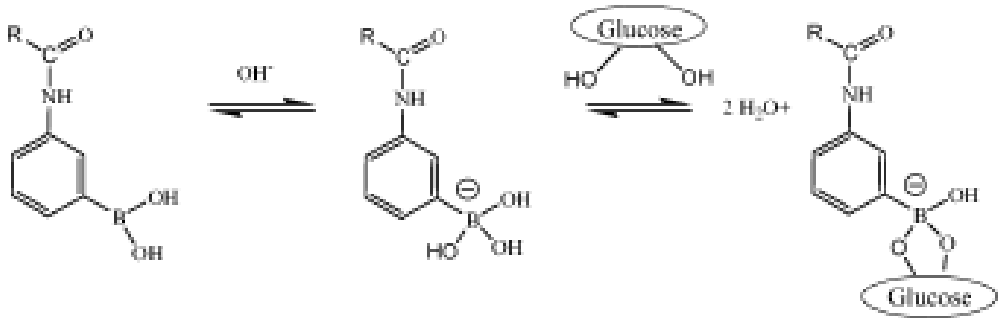

Scheme 7-1 Complexation Equilibrium between the alkylamidophenylboronic acid and glucose in aqueous solution.

A significant problem in the treatment of insulin-dependent diabetes mellitus is the difficulty in controlling the insulin dosage. It would be most desirable for drug release to match a patient's physiological needs at the proper time. The normal blood glucose level is 4-8 mM.[31,32]

Therefore, the ideal insulin delivery carrier is supposed to response quickly when the glucose concentration is beyond the normal blood glucose level. Although the currently developed P(NIPAM-PBA) copolymer microgels have the potential to regulate the insulin release (e.g., the higher the glucose level, the more the insulin to be release), these microgels start to swell at very low glucose concentration. It can be expected that the insulin molecules loaded in these P(NIPAM-PBA) microgels will start to release significantly even at the glucose concentration is well below the normal blood glucose level. In such a case, an overdose of insulin can result in an excessive decrease in blood sugar that may lead to serious hypoglycemia. In order to overcome this critical barrier, it is in an urgent need to develop novel glucose-sensitive microgel insulin delivery system that cannot only regulate the insulin release in response to appropriate glucose level, but also initiate the response only after the glucose concentration is beyond the normal level. In this work, we aim to develop a series of core-shell structured microgels composing of a glucose responsive PBA-based microgel as core and a nonlinear poly(ethylene glycol) (PEG) gel layer as shell to achieve a controllable onset of the glucose-induced volume phase transitions, which should enable the microgel-based insulin delivery system to initiate the insulin release only after the glucose concentration is above the normal blood glucose level. The glucose sensitive core will be based on the P(NIPAM-PBA) microgel but copolymerized with about 10 mol% acrylamide (AAm) to improve the glucose sensitivity of the microgels at physiological pH, denoted as P(NIPAM-AAm-PBA). The nonlinear PEG gel shell mainly composed of carbon-carbon back bone and oligo(ethylene glycol) side chains are biocompatible and thermo-sensitive with a tunable LCST depending on the oligo(ethylene glycol) side chain length.[33-36] The thermoresponsive PNIPAM and nonlinear PEG polymers allows us to apply a simple stepwise precipitation polymerization method in water to prepare the core-shell structured microgels.

While the PBA moieties in the P(NIPAM-AAm-PBA) mcirogel core are designed to complex with glucose to form the negative charges on the core network chains for microgels to swell, the ethylene glycol side chains on the nonlinear PEG gel shell are designed to form hydrogen bonds with the glucose through the ether oxygen of the ethylene glycol units and the hydroxyl groups of glucose molecules, which will not induce the microgel to swell. Kinetic studies show that the formation and dissociation of intermolecular hydrogen bond in liquid solutions is ultrafast (e.g., on a picoseconds time scale).[37] On the other hand, the kinetics of the glucose-induced swelling of the P(NIPAM-PBA) microgels is on a time scale of 100 second due to the slow complexation reaction between the PBA groups and glucose molecules.[29] From these reported results, we predict that the kinetics of the hydrogen bonding association between the glucose molecules and the ethylene glycol units will be much faster than that of the PBA-glucose complexing association. In such a situation, when the newly designed core-shell microgels, denoted as P(NIPAM-AAm-PBA)@PEG, are put into the glucose solution, the glucose molecules will firstly associate with the nonlinear PEG gel shell. Only when the ether oxygen atoms of the the PEG side chains are saturated with glucose molecules, the free glucose molecules will start to bind with the PBA groups located in the core of microgels, at which the core-shell microgels will exhibit glucose-sensitivity. Based on this design, we expect that the more ethylene glycol units are presented on the gel shell, the more glucose molecules will be consumed to saturate the ether oxygen in the gel shell. As a result, the core-shell microgels with thicker nonlinear PEG gel shell should start to swell at relatively higher glucose concentrations. Therefore, it is possible to tune the onset point of glucose sensitivity of the microgels by adjusting the feeding amount of shell component in the synthesis of core-shell microgels. In other words, the onset of glucose-induced swelling of microgels could be controlled by the thickness of the nonlinear PEG gel

shell. The core-shell structured glucose-sensitive P(NIPAM-AAm-PBA)@PEG microgels presented here will have great potential to be used for the smart insulin delivery system for self-regulated insulin release.

7. 2 Experimental

7. 2. 1 Materials

All reagents were purchased from Sigma-Aldrich. Oligo(ethylene glycol)methyl ether methacrylate (M_n = 300 g/mol, MEO_5MA), and poly(ethylene glycol) dimethacrylate (PEGDMA, $M_n \approx 550$ g/mol, crosslinker) were purified with neutral Al_2O_3. Acryamide (AAm), 3-aminophenylboronic acid, N-(3-dimethylaminopropyl)-N-ethyl-carbodiimide hydrochloride (EDC), d(+)-Glucose, N,N'-methylenebisacrylamide (BIS), sodium dodecyl sulfate (SDS) and ammonium persulfate (APS) were used as received. Acrylic acid (AA) was purified by distillation under reduced pressure. N-isopropylacryamide (NIPAM) was recrystallized from the mixture of hexane and acetone (1:1) prior to use.

7. 2. 2 Synthesis of poly(NIPAM-AAm-AA) microgels

The P(NIPAM-AAm-AA) microgels were synthesized by free radical precipitation polymerization. Briefly, 1.403 g of NIPAM, 0.115 g of AA, 0.102 g of AAm, 0.074 g of BIS, and 0.070 g of SDS were dissolved in 80 mL of water. The reaction mixture was transferred to a three necked round-bottom flask equipped with a condenser and a nitrogen inlet and heated to 70 ℃ under a gentle stream of nitrogen. After 1 h, 1 mL of 0.5 M APS solution was added to initiate the polymerization and crosslinking. The reaction was allowed to proceed for 5 h. The

resultant microgels were purified by dialysis (cutoff 12000-14000) against water for at least 1 week. This P(NIPAM-AAm-AA) microgel sample has a feeding AA content of 10.0 mol %.

7. 2. 3 Synthesis of poly(NIPAM-AAm-PBA) microgels

The PBA-functionalized p(NIPAM-AAm-PBA) microgels were then synthesized via the EDC catalyzed coupling of APBA to the COOH groups in AA units. First, 50ml p(NIPAM-AAm-AA) microgel dispersionwas cooled in an ice-water bath, then 0.002 mol of APBA and 0.002 mol of EDC were added. The coupling reaction was allowed to proceed for 4 h in ice water bath. The resultant products were purified by dialysis against very frequently changed water for at least 1 week and then diluted to 100 ml.

7. 2. 4 Synthesis of P(MEO_5MA -AAm-PBA) Microgels

First, P(MEO_5MA-AAm-AA) microgels were synthesized by free radical precipitation polymerization. Briefly, 1.771 ml of MEO_5MA, 0.0573 g of AA, 0.0509 g of AAm, 0.0368 g of BIS, and 0.070 g of SDS were dissolved in 80 mL of water. The reaction mixture was transferred to a three necked round-bottom flask equipped with a condenser and a nitrogen inlet and heated to 70 ℃ under a gentle stream of nitrogen. After 1 h, 0.05 mL of 0.5 M APS solution was added to initiate the polymerization and crosslinking. The reaction was allowed to proceed for 5 h. The resultant microgels were purified by dialysis (cutoff 12000-14000) against water for at least 1 week. Then, the PBA-functionalized p(MEO_5MA-AAm-PBA) microgels were synthesized via the EDC catalyzed coupling of APBA to the COOH groups in AA units. First, 50ml p(MEO_5MA-AAm-AA) microgel dispersion was cooled in an ice-water bath, then 0.002 mol of APBA and 0.002 mol of EDC were added. The coupling reaction was allowed to proceed for 4 h

in ice water bath. The resultant products were purified by dialysis against very frequently changed water for at least 1 week and then diluted to 100 ml.

7. 2. 5 Synthesis of P(NIPAM-AAm-PBA)@PEG core-shell microgels

The P(NIPAM-AAm-PBA)@PEG core-shell microgels were respectively synthesized according to the recipes listed in Table 7-1, which have been coded as CSM1, CSM2, and CSM3 in terms of a gradual increase in the feeding amount for the nonlinear PEG gel shell. Typically, 20 ml P(NIPAM-AAm-PBA) core microgel dispersion, MEO_5MA monomer, PEGDMA crosslinker, and SDS (0.01g) were mixed in 60 mL deionized water. The mixture was heated to 70 ℃ under a N_2 purge. After 1 h, APS (3.0×10^{-4} mol) was added to the solution to initiate the polymerization and crosslinking of MEO_5MA and PEGDMA to add the nonlinear PEG gel shell to the core. The reaction was allowed to proceed for 5 h. The obtained core-shell microgels were purified by dialysis against very frequently changed water for at least 1 week to remove the unreacted small molecules and SDS surfactant molecules, and further diluted to 100 ml with deionized water.

Table 7-1 Feeding composition of the Core-shell microgels

	core, ml	MEO_5MA, ml	PEGDMA, ml	SDS, g
CSM1	20	0.143	0.0072	0.01
CSM2	20	0.286	0.0144	0.01
CSM3	20	0.572	0.0288	0.01

7. 2. 6 Characterization

The FTIR spectra were recorded with a Nicolet Instrument Co. MAGNA-IR 750 Fourier transform infrared spectrometer. The morphology of the core-shell microgels was characterized

with transmission electron microscopy (TEM). The TEM images were taken on a Zeiss EM 902 transmission electron microscope operating at an accelerating voltage of 120 kV. Approximately 20 μL of the diluted microgel suspension was dropped on a Formvar-covered copper grid (300 meshes) and then air-dried at room temperature for the TEM measurements. The pH values were obtained on a METTLER TOLEDO SevenEasy pH meter. The size and size distribution of the microgels under different conditions were measured using a standard light scattering spectrometer (BI-200SM) equipped with a BI-9000 AT digital time correlator (Brookhaven Instrument, Inc.). A He-Ne laser (35 mW, 633 nm) was used as the light source. The diluted microgel dispersion solutions were passed through 0.45 μm PVDF filters to remove dust.

7. 3 Results and Discussion

7. 3. 1 Synthesis of P(NIPAM-AAm-PBA)@PEG core-shell Microgels

The preparation of glucose-sensitive P(NIPAM-AAm-PBA) microgels core involves the first synthesis of a P(NIPAM-AAm-AA) microgel, followed by modification with the glucose-sensing moiety APBA. The preparation of nearly monodisperse P(NIPAM-AAm-AA) microgels with well-controlled size and compositions has been well established from the precipitation polymerization in water.[38] It has been reported that the AA contents in the microgels are nearly equal to the feeding ratios of the AA and NIPAM comonomers.[39] Dialysis has been proved to be an effective purification procedure. The purified P(NIPAM-AAm-AA) microgel was then functionalized with PBA through the coupling of 3-aminophenylboronic acids (APBA) to the AA units in the microgels under EDC catalysis. Using this P(NIPAM-AAm-PBA) microgel as core template, the biocompatible thermo-sensitive nonlinear PEG shell was added through the precipitation polymerization of MEO_5MA in the presence of PEGDMA crosslinker and the

P(NIPAM-AAm-PBA) core microgels. Figure 7-1 shows the FTIR spectra of the dried P(NIPAM-AAm-AA) microgels, the corresponding P(NIPAM-AAm-PBA) microgels and P(NIPAM-AAm-PBA)@PEG core-shell microgels, respectively. In addition to the absorption maxima of amide I at 1650 cm^{-1} and amide II at 1525 cm^{-1}, the P(NIPAM-AAm-AA) microgels present a peak at 1704 cm^{-1} with a shoulder at 1722 cm^{-1}, which was assigned to the stretching of the uncharged dimerized or associated form of carboxylic group (-COOH) of AA units. After functionalized with APBA, both the P(NIPAM-AAm-PBA) microgels and the P(NIPAM-AAm-PBA)@PEG core-shell microgels only present the absorption maxima of amide I at 1638 cm^{-1} and amide II at 1543 cm^{-1}. The disappearance of the peak at 1704 cm^{-1} indicates that the -COOH groups in the P(NIPAM-AAm-AA) precursor microgels are almost completely reacted with APBA. The higher frequency amide I and the lower frequency amide II bands in the P(NIPAM-AAm-AA) microgels as compared to the corresponding P(NIPAM-AAm-PBA) microgels are attributed to the hydrogen bonding between PNIPAM and PAA.[40]

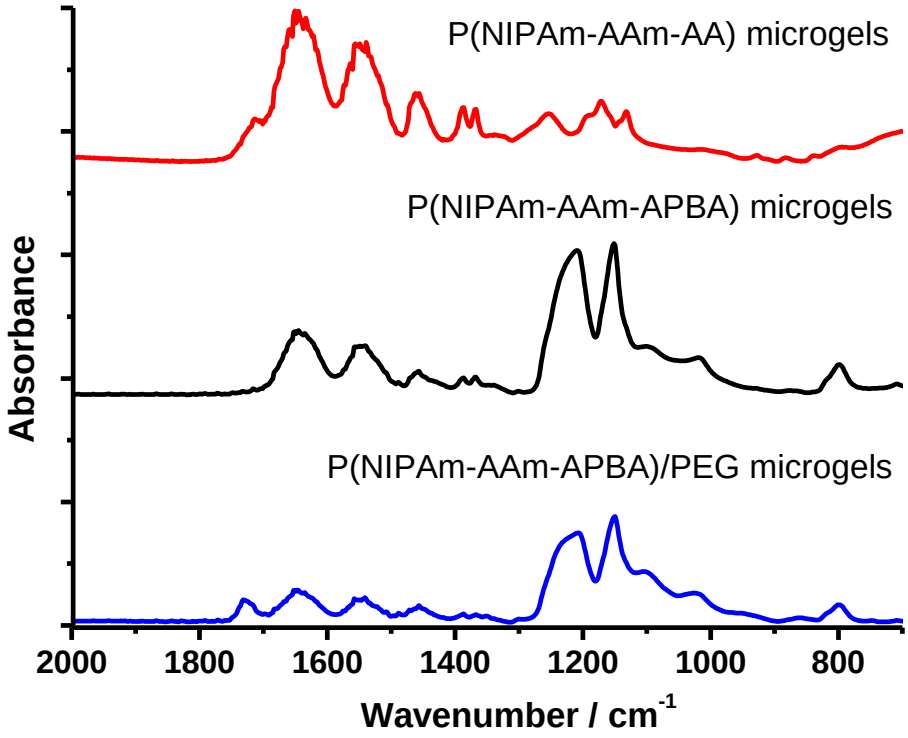

Figure 7-1 FTIR spectra of P(NIPAM-AAm-AA), P(NIPAM-AAm-PBA), and P(NIPAM-AAm-PBA)@PEG microgels.

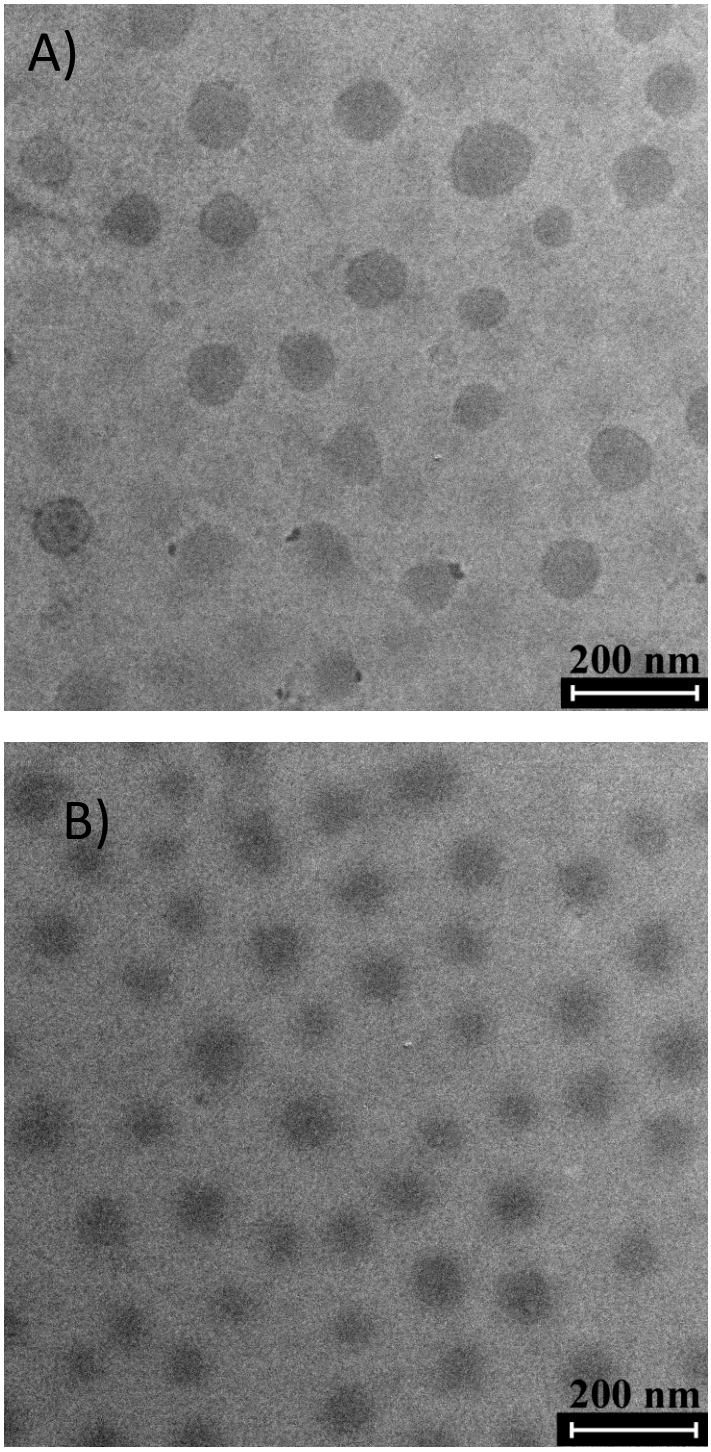

Figure 7-2 Typical TEM image of A) P(NIPAM-AAm-PBA) core microgels; B) P(NIPAM-AAm-PBA)@PEG core-shell microgels (CSM3).

The typical TEM images of resultant microgels are shown in Figure 7-2, respectively. Both P(NIPAM-AAm-PBA) core and P(NIPAM-AAm-PBA)@PEG core-shell microgel particles show a spherical morphology with a very narrow size distribution and no clear core-shell structure has been observed for CSM3 due to the low contrast. The DLS characterization further confirmed that the microgels are nearly monodispersed with the polydispersity index $\mu_2/<\Gamma>^2 < 0.1$ under all measurement conditions. In addition, all microgel dispersions are very stable with neglectable change in polydispersity index after setting for several months at room temperature.

7. 3. 2 Glucose-Sensitivity of P(NIPAM-AAm-PBA) microgels

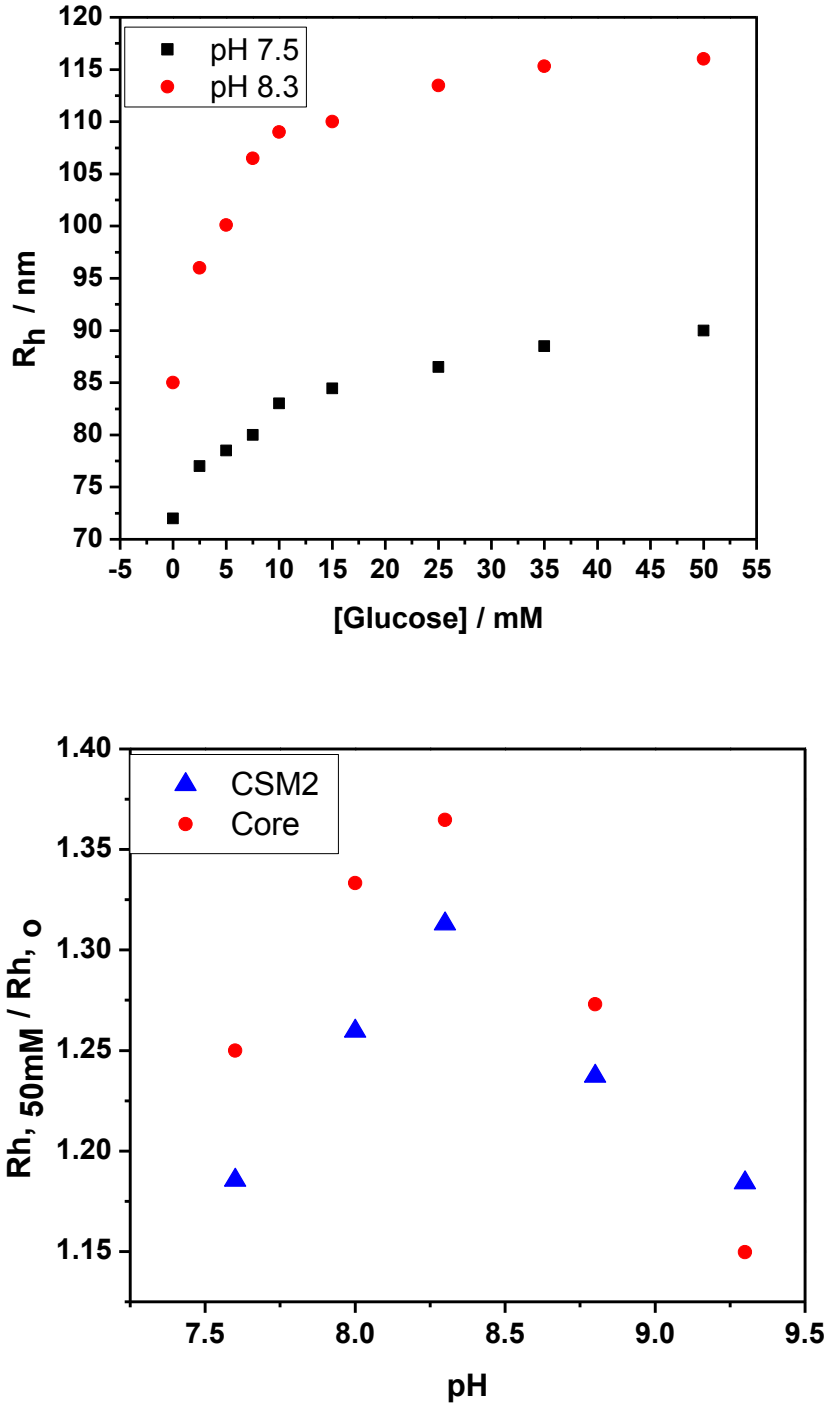

Figure 7-3 A) R_h values of P(NIPAM-AAm-PBA) core microgels as a function of glucose concentration at 37 ^{o}C; B) glucose-induced swelling ratio, $R_{h,50mM}/R_{h,0}$, of the P(NIPAM-AAm-

PBA) core and corresponding P(NIPAM-AAm-PBA)@PEG core-shell microgels as a function of pH value at 37 °C.

The pH value of the media shows a significant effect on the glucose-sensitivity of the microgels modified with PBA group. It was found that the glucose sensors made from the phenylborated polyacrylamide hydrogels embedded with crystalline colloid array are only responsive to glucose concentration change in the pH range of $7.0 < pH < 9.5$. [41] When $pH < 7.0$, the majority of PBA groups are in the uncharged form, while at $pH > 9.5$, almost all of the PBA groups are transferred to the charged form. Therefore, the PBA-based glucose-sensors will lose their sensitivity under these conditions. Figure 7-3A shows the glucose-induced swelling behavior of the P(NIPAM-AAm-PBA) core microgels at two different pH values. At pH = 7.5, the glucose-induced swelling ratio, in terms of the hydrodynamic radius ratio of microgels in the presence of 50 mM and 0 mM glucose ($R_{h,50mM}/R_{h,0}$), of the core is 1.2.When the pH was increased to 8.3 that is closer to the pK_a of PBA groups, the glucose induced swelling is much more significant. Figure 3B shows the pH dependence of the swelling ratio $R_{h,50mM}/R_{h,0}$ of the microgels, which more clearly reflects the pH effect on the overall glucose-sensitivity of the P(NIPAM-AAm-PBA) core microgels and the P(NIPAM-AAm-PBA)@PEG core-shell microgels (CSM2). The glucose-sensitivity of the microgels increases with the increase in pH, reaches a maximum at pH=8.3, and then decreases as pH further increases. The addition of the nonlinear PEG gel shell to the glucose sensitive core microgels did not change the trend, but reduced the glucose-induced swelling ratio, which is understandable because the shell is insensitive to glucose and may also restrict the swelling of core microgels.

7. 3. 3 Glucose Sensitivity of P(MEO_5MA-AAm-PBA) microgels

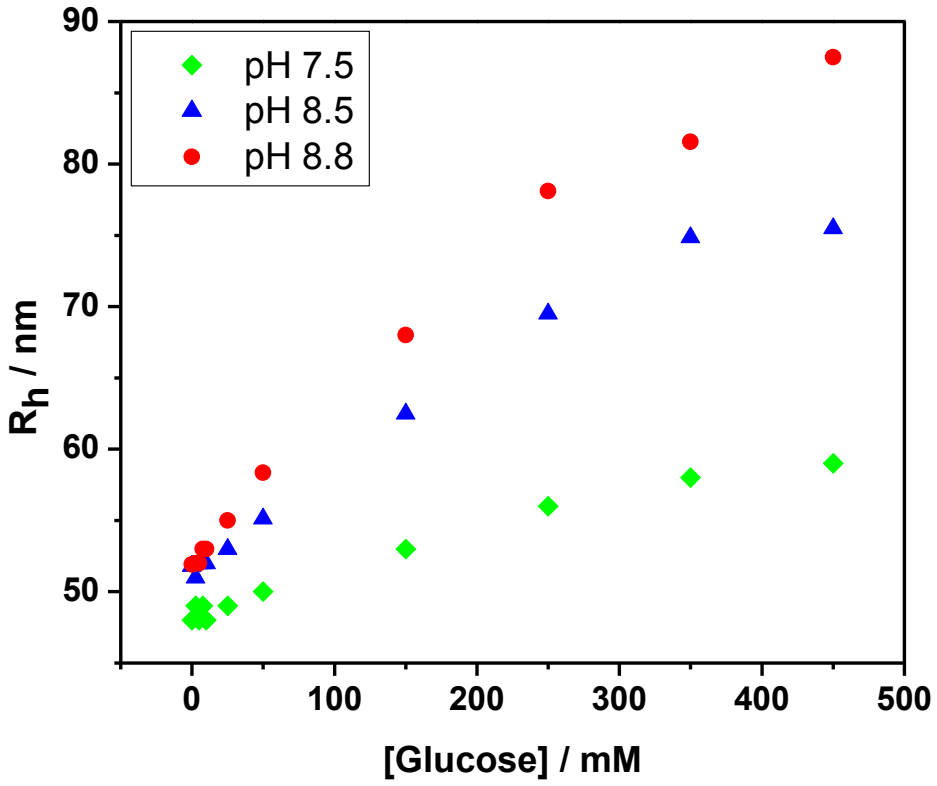

Figure 7-4 R_h values of P(MEO_5MA-AAm-PBA) microgels as a function of glucose concentration at different pH values and 37 ^oC.

As we proposed, the presence of the ether oxygen of the side PEG chains in microgels has the priority to bind with glucose molecules over the PBA groups due to the rapid hydrogen bonding interaction. To verify our hypothesis, P(MEO_5MA-AAm-PBA) microgels with nonlinear PEG as a major component and PBA as glucose-sensitive moieties have been prepared to investigate the glucose responsive volume phase transition. Figure 7-4 shows the R_h change of the P(MEO_5MA-AAm-PBA) microgels as a function of glucose concentration at different pH values. When the glucose concentration is below 25 mM, the size of microgels has no obvious change. Only when the glucose concentration is above 25 mM, the size of microgels starts to

increase significantly with the increase in glucose concentration until reaching nearly a maximum value at 350 mM. This result indicates that the P(MEO_5MA-AAm-PBA) mcirogels only demonstrate good glucose sensitivity in the glucose concentration range of 25-350 mM, which is not desirable for diabetic therapy since the normal blood glucose level is in the range of 4-8 mM. The insensitivity to glucose concentration change of the P(MEO_5MA -AAm-PBA) microgels at glucose concentration below 25 mM support our hypothesis that the glucose molecules will firstly bind to the side PEG chains through the hydrogen bonding interactions, which causes negligible size change of microgels. Only after the ether oxygen of the PEG side chains in the microgels are saturated with glucose, the glucose molecules will bind to the PBA groups to form negatively charged complexes, inducing the microgels to swell due to the Donnan potential.

7. 3. 4 Effect of shell thickness on glucose sensitivity of P(NIPAM-AAm-PBA)@PEG core-shell microgels

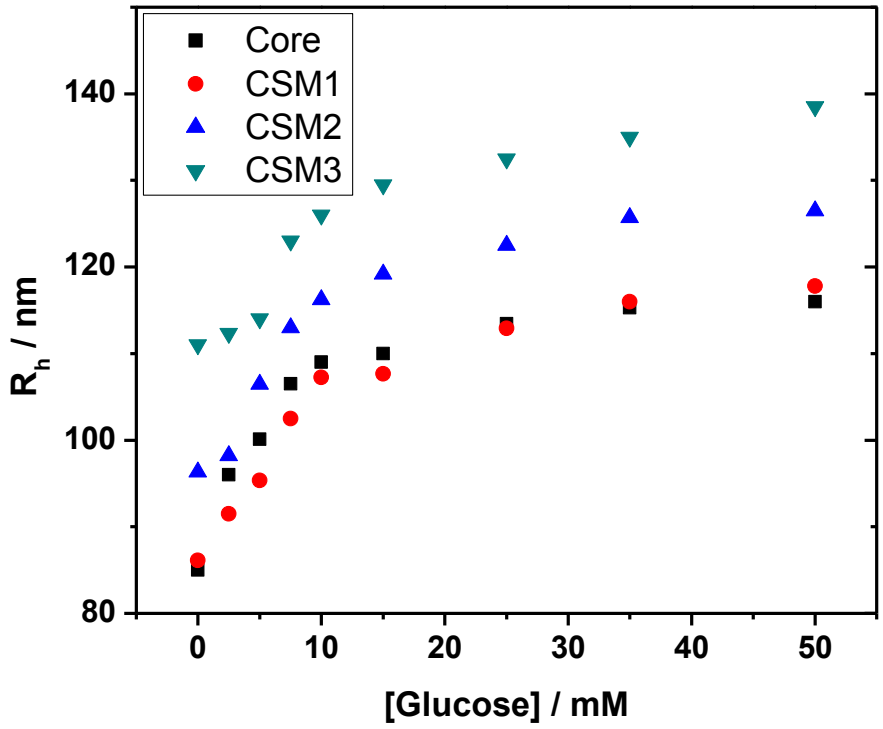

Figure 7-5 R_h values of the P(NIPAM_AAm-PBA) core microgels and the P(NIPAM-AAm-PBA)@PEG core-shell microgels with different shell thickness as a function of glucose concentrationat 37 ^{o}C and pH 8.3.

Three P(NIPAM-AAm-PBA)@PEG core-shell microgels were synthesized using the same batch of P(NIPAM-AAm-PBA) microgels as core template and different feeding amount of MEO_5MA monomers for shell synthesis (see recipes in Table 7-1). Obviously, the increase in the feeding amount of shell components increases the thickness of the resultant nonlinear PEG gel shells. To investigate the effect of the PEG gel shell thickness on the glucose sensitivity of core-shell microgels, we have monitored the glucose-induced size change of all the three core-shell microgels at 37 ^{o}C and pH 8.3, where the microgels should have the best glucose-sensitivity. Two features should be noted in Figure 7-5. Firstly, the R_h difference between the core-shell microgels and the parent core microgels can be attributed to the addition of PEG gel shell. Thus,

the thickness of the PEG gel shell could be estimated for the core-shell microgels. For example, at 37 ℃ and pH 8.3, the increase in R_h from 85 nm for the core microgel to 87 nm (CSM1), 96 nm (CSM2) and 111 nm (CSM3), respectively, which corresponds to a shell thickness of 2 nm, 11 nm and 26 nm for the CSM1, CSM2, and CSM3, respectively. Secondly, the core-shell microgels with different shell thickness exhibited different glucose responsive swelling behavior. As proposed, the addition of the PEG gel shell does shift the onset of the glucose-responsive volume phase transition of the microgels. The thicker the PEG gel shell, the higher the glucose concentration required to induce the core-shell microgels to swell. As shown in Figure 7-5, the core only P(NIPAM-AAm-PBA) microgels exhibited a significant increase in particle size even at a very low glucose concentration. In comparison with this parent core, the CSM1 microgels with the thinnest shell showed slower increase in particle size with the gradual addition of glucose. For example, the Rh of core microgels increased by 15 nm when glucose concentration was added to 5 mM, while the R_h of CSM1 only increased by 8 nm at the same glucose level. For CSM2 and CSM3 microgels, apparently retarded glucose sensitivity was observed. The addition of glucose to a concentration at 2.5 mM did not cause significant change of the particle size for CSM2 (just 2 nm). Only after the glucose concentration was larger than 2.5 mM, the microgels started to swell dramatically with an excellent glucose-sensitivity. For CSM3 microgels with the thickest PEG gel shell, the onset of the glucose responsive volume phase transition further shifted to a higher glucose concentration. Only at the glucose concentration above 5 mM, a significant glucose-induced increase in R_h was clearly observed. According to our previous work,[42] the nonlinear PEG microgel synthesized from the MEO_5MA monomers should have a LCST above 50 ^oC. At our study temperature of 37 °C, the PEG gel shell is in a swollen state, which should not compress the swelling of core microgels. Therefore, the nonresponse of the

CSM2 and CSM3 microgels to the glucose addition at glucose concentration below 2.5 mM and 5 mM, respectively, should be attributed to the prior hydrogen bonding between the glucose and PEG gel shell. Only after the ether oxygens of the PEG gel shell were saturated with glucose molecules, the extra glucose molecules will start to bind with the PBA moieties in the core microgels to induce the swelling of microgels. Our results indicate that the thickness of the PEG gel shell could control the onset of glucose sensitive volume phase transition of the core-shell microgels, which is very important to regulate the insulin release when these microgels are used as insulin delivery carriers.

7. 4 Conclusion

Well-defined glucose-sensitive core-shell microgels with the P(NIPAM-AAm-PBA) microgel as core and the nonlinear PEG gel layer as shell in different thickness could be successfully synthesized via a simple precipitation polymerization method in water. The presence of PEG gel shell could retard the glucose-sensitive core network from swelling because the rapid hydrogen bonding between the glucose molecules and the ether oxygens in the PEG shell is prior to the glucose binding to the PBA groups in the core microgels. The thicker the PEG gel shell, the higher the glucose concentration required to induce the glucose sensitive volume phase transition. Therefore, the onset point of glucose sensitivity of the microgels could be controlled through the adjustment of the feeding amount of PEG gel shell component. These newly designed core-shell structured glucose sensitive microgels are promising for insulin delivery carriers, which can regulate the insulin release from the microgel only after the glucose level is above critical zone in diabetes management.

7. 5 Reference

(1) Oh, J. K.; Drumright, R.; Siegwart, D. J.; Matyjaszewski, K. *Progress in Polymer Science* **2008**, *33*, 448-477.

(2) Otsuka, H.; Nagasaki, Y.; Kataoka, K. *Adv. Drug Deliv. Rev* **2003**, *55*, 403-419.

(3) Malmsten, M. *Soft Matter* **2006**, *2*, 760-769.

(4) Kost, J.; Langer, R. *Advanced Drug Delivery Reviews* **2001**, *46*, 125-148.

(5) Oishi, M.; Nagasaki, Y. *Nanomedicine* **2010**, *5*, 451-468.

(6) Yu, W. W. *Expert Opin. Biol. Ther.* **2008**, *8*, 1571-1581.

(7) Zhou, W.; Schwartz, D. T.; Baneyx, F. *Journal of the American Chemical Society* **2010**, *132*, 4731-4738.

(8) Dagallier, C.; Dietsch, H.; Schurtenberger, P.; Scheffold, F. *Soft Matter* **2010**, *6*, 2174.

(9) Sorrell, C. D.; Carter, M. C. D.; Serpe, M. J. *Advanced Functional Materials* **2011**, *21*, 425-433.

(10) Chan, Y.-H.; Wu, C.; Ye, F.; Jin, Y.; Smith, P. B.; Chiu, D. T. *Analytical Chemistry* **2011**, *83*, 1448-1455.

(11) Liu, T.; Hu, J.; Yin, J.; Zhang, Y.; Li, C.; Liu, S. *Chemistry of Materials* **2009**, *21*, 3439-3446.

(12) Steiner, M.S.; Duerkop, A.;Wolfbeis, O. S. *Chem. Soc. Rev.*, **2011**, *40*, 4805–4839.

(13) Ye, F.; Wu, C.; Jin, Y.; Chan, Y.-H.; Zhang, X.; Chiu, D. T. *Journal of the American Chemical Society* **2011**, *133*, 8146-8149.

(14) Okano, T.; Bae, Y. H.; Jacobs, H.; Kim, S. W. *Journal of Controlled Release* **1990**, *11*, 255-265.

(15) Katono, H.; Maruyama, A.; Sanui, K.; Ogata, N.; Okano, T.; Sakurai, Y. *Journal of Controlled Release* **1991**, *16*, 215-227.

(16) Shin, B. C.; Jhon, M. S.; Lee, H. B.; Yuk, S. H. *European Polymer Journal* **1998**, *34*, 1675-1681.

(17) Shen, W.; Chang, Y.; Liu, G.; Wang, H.; Cao, A.; An, Z. *Macromolecules* **2011**, *44*, 2524-2530.

(18) Tian, H.; Yan, J.; Wang, D.; Gu, C.; You, Y.; Chen, X. *Macromolecular Rapid Communications* **2011**, *32*, 660-664.

(19) Jochum, F. D.; zur Borg, L.; Roth, P. J.; Theato, P. *Macromolecules* **2009**, *42*, 7854-7862.

(20) Sudaxshina, M. *Journal of Controlled Release* **2003**, *92*, 1-17.

(21) Ge, H.; Ding, Y.; Ma, C.; Zhang, G. J. Phys. Chem. B, **2006**, *110*, 20635-20639.

(22) Matsumoto, A.; Yamamoto, K.; Yoshida, R.; Kataoka, K.; Aoyagi, T.; Miyahara, Y. *Chem. Commun.* **2010**, *46*, 2203-2205.

(23) Zhang, Y.; Guan, Y.; Zhou, S. *Biomacromolecules* **2006**, *7*, 3196-3201.

(24) Zhang, Y.; Guan, Y.; Zhou, S. *Biomacromolecules* **2007**, 8, 3842-3847.

(25) Hoare, T; Pelton, R. Macromolecules, **2007**, 40, 67-678.

(26) Hoare, T; Pelton, R. Biomacromolecules, **2008**, 9, 733-740.

(27) Lapeyre, V.; Gosse, I.; Chevreux, S.; Ravaine, V. *Biomacromolecules* **2006**, 7, 3356-3363.

(28) Ancla, C.; Lapeyre, V.; Gosse, I.; Catargi, B.; Ravaine, V. Langmuir, **2011**, 27, 12693-12701.

(29) Xing, S.; Guan, Y.; Zhang Y. Macromolecules, **2011**, 44, 4479-4486.

(30) Wu, W; Zhou, T.; Zhou, S. Chem. Comm., **2009**, 4390-4392

(31) Thomé-Duret, V.; Reach, G.; Gangnerau, M. N.; Lemonnier, F.; Klein, J. C.; Zhang, Y.; Hu, Y.; Wilson, G. S. *Anal. Chem.* **1996**, *68*, 3822-3826.

(32) Tierney, S.; Falch, B. M. H.; Hjelme, D. R.; Stokke, B. T. *Anal. Chem.* **2009**, *81*, 3630-3636.

(33) Lutz, J. *Journal of Polymer Science Part A: Polymer Chemistry* **2008**, *46*, 3459-3470.

(34) Lutz, J.-F.; Hoth, A. *Macromolecules* **2006**, *39*, 893-896.

(35) Ishizone, T.; Seki, A.; Hagiwara, M.; Han, S.; Yokoyama, H.; Oyane, A.; Deffieux, A.; Carlotti, S. *Macromolecules* **2008**, *41*, 2963-2967.

(36) Badi, N.; Lutz, J.-F. *J Control Release* **2009**, *140*, 224-229.

(37) Zheng, J.; Kwak, K.; Chen, X.; Fayer, M. D., J. Am. Chem. Soc., 2006, 128, 2977-2987.

(38) Pich, A.; Richtering, W. In *Chemical Design of Responsive Microgels*; Pich, A.; Richtering, W., Eds.; Springer Berlin Heidelberg: Berlin, Heidelberg, **2010**, 234, 1-37.

(39) Christensen, M. L.; Keiding, K. *Colloids and Surfaces A: Physicochemical and Engineering Aspects* **2005**, *252*, 61-69.

(40) Hyk, W.; Ciszkowska, M. *J. Phys. Chem. B* **2002**, *106*, 11469-11473.

(41) Asher, S. A.; Alexeev, V. L.; Goponenko, A. V.; Sharma, A. C.; Lednev, I. K.; Wilcox, C. S.; Finegold, D. N. *J. Am. Chem. Soc.* **2003**, *125*, 3322-3329.

(42) Zhou, T.; Wu, W.; Zhou, Q. *Polymer*, **2010**, *51*, 3926-3933.

Chapter 8

Summary

The overall goal of the work in this dissertation was to investigate the design, properties and applications of multi-responsive microgels, especially, their role act as particular carriers for controlled and targeted drug delivery system and response to different glucose level.

Well-defined oligo(ethylene glycol)-based thermosensitive core-shell microgels with the P(MEO_2MA) microgel as a hydrophobic core and the P(MEO_2MA-co-MEO_5MA) gel layer as a hydrophilic shell were discussed in Chapter 3. The presence of P(MEO_2MA-co-MEO_5MA) hydrophilic shell could prevent the hydrophobic core network from collapsing, resulting in a shift of the VPTT of P(MEO_2MA) core to higher temperatures in comparison with the free parent core microgels. This unique structure of hydrophobic core with the open network (or large mesh size) in the core-shell microgels can dramatically improve the loading capacity for hydrophobic drugs, which indicates that both the drug-core hydrophobic interactions and the mesh size of core networks are important to determine the drug loading efficiency. The DIP-loaded core-shell microgels significantly enhanced the in vitro cytotoxicity against tumor cells.

In Chapter 4, PEG-chitosan gel nanoparticles with semi-IPN structure and tunable diameter were successfully prepared by in-situ free radical polymerization and crosslinking of the monomers containing short oligo(ethylene glycol) side chains in the solution of natural biopolymer chitosan. The PEG-chitosan semi-IPN nanogels can adapt with high-sensitivity to different pH values and temperatures over the physiologically relevant ranges of 5.0-7.4 and 36-40 ^{o}C, respectively. The PEG-chitosan nanogels cannot only provide a high drug loading capacity of the model anticancer drug 5-FU, but also offer pH and temperature dual-triggered drug delivery possibilities. The drug release kinetics studies demonstrate that the multifunctional nanogels show drug sustained properties and the release could be triggered by the pH and temperature dual-responsive volume phase transition of the gel. In vitro cytotoxicity tests indicate that the empty nanogels have very low cytotoxicity, while the 5-FU-loaded nanogels have high anticancer activity. These characteristics are important in both fundamental research and practical applications. The properly designed dual-responsive nanogels as delivery vehicles should enhance our ability to address the complexity of biological systems, and thus offer broad opportunities for biomedical applications.

Inorganic QDs has been involved within microgels in Chapter 5. Multifunctional core-shell structured ZnO@PEG-chitosan hybrid microgels composed of PEG stabilized ZnO QDs as core and semi-IPN PEG-chitosan gel layer as shell were successfully prepared by free radical polymerization of shell components onto the colloidal ZnO particles. The presence of PEG-chitosan gel shell at appropriate ratios enables the hybrid microgels highly sensitive to pH values and temperatures over the physiologically relevant ranges of 5.0-7.4 and 36-40 ^{o}C, respectively. Therefore, the pH and temperature dual-triggerable drug delivery becomes possible. The drug releasing studies demonstrated that the hybrid microgels show drug sustained properties and the

release could be triggered by the pH and temperature dual-responsive volume phase transition of the PEG-chitosan gel shell. Meanwhile, the encapsulated ZnO QDs in the core extend the application to cell imaging. The resultant hybrid microgels can enter intracellular region successfully. In vitro cytotoxicity tests indicate that the empty hybrid microgels have very low cytotoxicity, while the 5-FU-loaded microgels have high anticancer activity. These characteristics are important in both fundamental research and practical applications.

In Chapter 6, we demonstrate a new molecular recognition motif based on the fluorescence quenching of CdS QDs immobilized in glucose-sensitive microgels in the physiologically important glucose concentration range 1-25 mM, which shows a promise for continuous non-invasive in vivo glucose sensing system. We expect that the hybrid microgels prepared by a PBA analogue that can highly bind D-glucose at physiological pH will enable the detection of glucose at physiological conditions. Future studies should examine how the different cross-linking degrees and AAm/PBA contents of the microgels affect the size and content of the QDs as well as the sensing range of glucose concentration to provide a controllable glucose sensing range under physiological conditions.

The effect of the presence of PEG on glucose sensitivity of microgels has been discussed in Chapter 7.Well-defined glucose-sensitive core-shell microgels with the P(NIPAM-AAm-PBA) microgel as core and the nonlinear PEG gel layer as shell were synthesized. The presence of PEG gel shell could retard the glucose-sensitive core network from swelling because the rapid hydrogen bonding between the glucose molecules and the ether oxygens in the PEG shell is prior to the glucose binding to the PBA groups in the core microgels. The thicker the PEG gel shell, the higher the glucose concentration required to induce the glucose sensitive volume phase transition. Therefore, the onset point of glucose sensitivity of the microgels could be controlled

through the adjustment of the feeding amount of PEG gel shell component. These newly designed core-shell structured glucose sensitive microgels are promising for insulin delivery carriers, which can regulate the insulin release from the microgel only after the glucose level is above critical zone in diabetes management.

Bibliography

Chapter 1

(1) Saunders *Advances in Colloid and Interface Science* **1999**, *80*, 1-25.

(2) Baker, W. O. *Ind. Eng. Chem.* **1949**, *41*, 511-520.

(3) Staudinger, H.; Huseman, E. *Ber.* **1935**, *68*, 1618.

(4) Das, M.; Zhang, H.; Kumacheva, E. *Annu. Rev. Mater. Res.* **2006**, *36*, 117-142.

(5) Saunders, B. R.; Laajam, N.; Daly, E.; Teow, S.; Hu, X.; Stepto, R. *Adv Colloid Interface Sci* **2009**, *147-148*, 251-262.

(6) Nayak, S.; Lyon, L. A. *Angewandte Chemie International Edition* **2005**, *44*, 7686-7708.

(7) Dalmont, H.; Pinprayoon, O.; Saunders, B. R. *Langmuir* **2008**, *24*, 2834-2840.

(8) Pelton, R. *Adv Colloid Interface Sci* **2000**, *85*, 1-33.

(9) Zhang, Y.; Guan, Y.; Zhou, S. *Biomacromolecules* **2006**, *7*, 3196-3201.

(10) Hennink, W. E.; van Nostrum, C. F. *Adv. Drug Deliv. Rev* **2002**, *54*, 13-36.

(11) Wang, D.; Liu, T.; Yin, J.; Liu, S. *Macromolecules* **2011**, *44*, 2282-2290.

(12) Peter, G. *Carbohydrate Polymers* **1988**, *8*, 161-182.

(13) Goosen, M. F. A.; O'Shea, G. M.; Gharapetian, H. M.; Chou, S.; Sun, A. M. *Biotechnology and Bioengineering* **1985**, *27*, 146-150.

(14) Wee; Gombotz, W. *Advanced Drug Delivery Reviews* **1998**, *31*, 267-285.

(15) Wu, C.; Zhou, S. *Macromolecules* **1995**, *28*, 8381-8387.

(16) Zhou, S.; Chu, B. *J. Phys. Chem. B* **1998**, *102*, 1364-1371.

(17) Pich, A.; Richtering, W. In *Chemical Design of Responsive Microgels*; Pich, A.; Richtering, W., Eds.; Springer Berlin Heidelberg: Berlin, Heidelberg, 2010; Vol. 234, pp. 1-37.

(18) Welsch, N.; Ballauff, M.; Lu, Y. In Chemical Design of Responsive Microgels; Pich, A.; Richtering, W., Eds.; Springer Berlin Heidelberg: Berlin, Heidelberg, 2010; Vol. 234, pp. 129-163.

(19) Hu, Z. B.; Cai, T.; Chi, C.L. *Soft Matter* **2010**, 6, 2115-2123.

(20) Cai, T.; Marquez, M.; Hu, Z. *Langmuir* **2007**, 23, 8663-8666.

(21) Chi, C.; Cai, T.; Hu, Z. *Langmuir* **2009**, 25, 3814-3819.

(22) Cai, T.; Wang, G.; Thompson, S.; Marquez, M.; Hu, Z. *Macromolecules* **2008**, 41, 9508-9512.

(23) Asua, J. M. *Journal of Polymer Science Part A: Polymer Chemistry* **2004**, *42*, 1025-1041.

(24) Lally, S.; Mackenzie, P.; LeMaitre, C. L.; Freemont, T. J.; Saunders, B. R. *J Colloid Interface Sci* **2007**, *316*, 367-375.

(25) Kashyap, N.; Kumar, N.; Kumar, M. N. V. R. *Crit Rev Ther Drug Carrier Syst* **2005**, *22*, 107-149.

(26) Peppas, N. A.; Wood, K. M.; Blanchette, J. O. *Expert Opin Biol Ther* **2004**, *4*, 881-887.

(27) Shivakumar, H.; Satish, C.; Satish, K. *Indian J Pharm Sci* **2006**, *68*, 133.

(28) Vinogradov, S. V. *Curr Pharm Des* **2006**, *12*, 4703-4712.

(29) Wu, W.; Zhou, S. *Nano Reviews* **2010**, *1*.

(30) Chan, Y.-H.; Wu, C.; Ye, F.; Jin, Y.; Smith, P. B.; Chiu, D. T. *Analytical Chemistry* **2011**, *83*, 1448-1455.

(31) Liu, T.; Hu, J.; Yin, J.; Zhang, Y.; Li, C.; Liu, S. *Chemistry of Materials* **2009**, *21*, 3439-3446.

(32) Yin, J.; Guan, X.; Wang, D.; Liu, S. *Langmuir* **2009**, *25*, 11367-11374.

(33) Suzuki, D.; McGrath, J. G.; Kawaguchi, H.; Lyon, L. A. *J. Phys. Chem. C* **2007**, *111*, 5667-5672.

(34) Green, N. L.; Kaya, D.; Maloney, C. E.; Islam, M. F. *Phys. Rev. E* **2011**, *83*, 051404.

(35) Xu, S.; Zhang, J.; Paquet, C.; Lin, Y.; Kumacheva, E. *Advanced Functional Materials* **2003**, *13*, 468-472.

(36) Lyon, L. A.; Debord, J. D.; Debord, S. B.; Jones, C. D.; McGrath, J. G.; Serpe, M. J. *J. Phys. Chem. B* **2004**, *108*, 19099-19108.

(37) Zhang, J.; Sun, Z.; Yang, B. *Current Opinion in Colloid & Interface Science* **2009**, *14*, 103-114.

(38) Zhang, J.; Xu, S.; Kumacheva, E. *J. Am. Chem. Soc.* **2004**, *126*, 7908-7914.

(39) Bromberg, L.; Temchenko, M.; Hatton, T. A. *Langmuir* **2003**, *19*, 8675-8684.

(40) Mizrahi, B.; Irusta, S.; McKenna, M.; Stefanescu, C.; Yedidsion, L.; Myint, M.; Langer, R.; Kohane, D. S. *Advanced Materials* **2011**, *23*, H258-H262.

(41) Lutz, J. F.; Hoth, A. *Macromolecules* **2006**, 39, 893-896.

(42) Lutz, J. F.; Okdemir, O.; Hoth, A. *J. Am. Chem. Soc.* **2006**, 128, 13046-13047.

(43) Lutz, J. F.; Weichenhan, K.; Akemir, O.; Hoth, A. *Macromolecules* **2007**, 40, 2503-2508.

(44) Lutz, J. F.; Hoth, A.; Schade, K. *Des. Monomers Polym.* **2009**, 12, 343-353.

(45) Zarafshani, Z.; Obata, T.; Lutz, J. F. *Biomacromolecules* **2010**, 11, 2130-2135. (28) Jones, C. D.; Lyon, L. A. *Macromolecules* **2000**, 33, 8301-8306.

(46) Welsch, N.; Ballauff, M.; Lu, Y. In *Chemical Design of Responsive Microgels*; Pich, A.; Richtering, W., Eds.; Springer Berlin Heidelberg: Berlin, Heidelberg, **2010**; Vol. 234, pp. 129-163.

(47) Wu, W.; Shen, J.; Banerjee, P.; Zhou, S. *Adv. Func. Material.* **2011**, 21, 2830-2839.

(48) Hu, J.; Liu, S. *Macromolecules* **2010**, *43*, 8315-8330.

(49) Lee, Y. K.; Kopelman, R. *Wiley Interdisciplinary Reviews: Nanomedicine and Nanobiotechnology* **2009**, *1*, 98-110.

(50) Ye, F.; Wu, C.; Jin, Y.; Chan, Y.-H.; Zhang, X.; Chiu, D. T. *Journal of the American Chemical Society* **0**, *0*.

(51) Pringsheim, E.; Zimin, D.; Wolfbeis, O. S. *Advanced Materials* **2001**, *13*, 819-822. (52) Wu, W.; Zhou, T.; Shen, J; Zhou, S. *Chem. Comm.* **2009**, 4390-4392.

(53) Wu, W.; Mitra, N.; Yan, E. C. Y.; Zhou, S. *ACS Nano* **2010**, 4, 4831-4839.

(54) Honarkar, H.; Barikani, M. *Monatshefte für Chemie Chemical Monthly* **2009**, *140*, 1403-1420.

(55) Das, M.; Mardyani, S.; Chan, W. C. W.; Kumacheva, E. *Advanced Materials* **2006**, *18*, 80-83.

(56) Biondi, M.; Ungaro, F.; Quaglia, F.; Netti, P. A. *Advanced Drug Delivery Reviews* **2008**, *60*, 229-242.

(57) Zhang, H.; Mardyani, S.; Chan, W. C. W.; Kumacheva, E. *Biomacromolecules* **2006**, *7*, 1568-1572.

(58) Das, M.; Zhang, H.; Kumacheva, E. *Annual Review of Materials Research* **2006**, *36*, 117-142.

(59) Van Thienen, T. G.; Raemdonck, K.; Demeester, J.; De Smedt, S. C. *Langmuir* **2007**, *23*, 9794-9801.

(60) Kost, J.; Langer, R. *Advanced Drug Delivery Reviews* **2001**, *46*, 125-148.

(61) Malmsten, M. *Soft Matter* **2006**, *2*, 760-769.

(62) Alvarez-Lorenzo, C.; Concheiro, A.; Dubovik, A. S.; Grinberg, N. V.; Burova, T. V.; Grinberg, V. Y. *Journal of Controlled Release* **2005**, *102*, 629-641.

(63) Oh; Drumright, R.; Siegwart, D. J.; Matyjaszewski, K. *Progress in Polymer Science* **2008**, *33*, 448-477.

(64) Jones, C. D.; Lyon, L. A. *Macromolecules* **2000**, 33, 8301-8306.

(65) Hu, X.; Tong, Z.; Lyon, L. A. *J. Am. Chem. Soc.* **2010**, 132, 11470-11472.

(66) Nayak, S.; Gan, D.; Serpe, M.; Lyon, L. A. *Small* **2005**, 1, 416-421.

(67) Smith, M. H.; Herman, E. S.; Lyon, L. A. *J. Phys. Chem. B* **2011**, 115, 3761-3764.

(68) Smith, M. H.; South, A. B.; Gaulding, J. C.; Lyon, L. A. *Anal. Chem.* **2009**, 82, 523-530.

(69) South, A. B.; Lyon, L. A. *Chem. Mater.* **2010**, 22, 3300-3306.

(70) Nayak, S.; Lee, H.; Chmielewski, J.; Lyon, L. A. *J. Am. Chem. Soc.* **2004**, 126, 10258-10259.

(71) Duracher, D.; Sauzeddde, F.; Elaissari, A.; Pichot, C.; Nabzar, L. *Colloid, Polym. Sci.* **1998**, 276, 920-929.

Chapter 2

(1) Pich, A.; Richtering, W. In *Chemical Design of Responsive Microgels*; Pich, A.; Richtering, W., Eds.; Springer Berlin Heidelberg: Berlin, Heidelberg, 2010; Vol. 234, pp. 1-37.

(2) Schärtl, W. *Light scattering from polymer solutions and nanoparticle dispersions*; Springer, 2007.

(3) Williams, D. B.; Carter, C. B. In *Transmission Electron Microscopy*; Springer US: Boston, MA, 2009; pp. 3-22.

(4) Fujimoto, J. G.; Farkas, D.; Farkas, D. L. *Biomedical Optical Imaging*; Oxford University Press, 2009.

(5) Wu, W.; Aiello, M.; Zhou, T.; Berliner, A.; Banerjee, P.; Zhou, S. *Biomaterials* **2010**, *31*, 3023-3031.

(6) Xiong, H.-M.; Xu, Y.; Ren, Q.-G.; Xia, Y.-Y. *Journal of the American Chemical Society* **2008**, *130*, 7522-7523.

(7) Wu, W.; Zhou, T.; Aiello, M.; Zhou, S. *Biosensors and Bioelectronics* **2010**, *25*, 2603-2610.

Chapter 3

(1) Das M, Zhang H, Kumacheva E. *Annu. Rev. Mater. Res.* **2006,** 36: 117–42.

(2) Malmsten M. *Soft Matter* **2006**, 2: 760-9.

(3) Oh JK, Drumright R, Siegwart DJ, Matyjaszewski K. *Prog. Polym. Sci.* **2008**, 33: 448-77.

(4) Saunders BR, Laajam N, Daly E, teow S, Hu X, Stepto R. *Adv. Colloid Interface Sci.* **2009**, 147-8: 251-62.

(5) Das M, Mardyani S, Chan WCW, Kumacheva E. *Adv. Mater.* **2006**, 18: 80-3.

(6) Thienen TG, Raemdonck K, Demeester J, De Smedt SC. *Langmuir* **2007**, 23: 9794-801.

(7) Shi L, Khondee S, Linz TH, Berkland C. *Macromolecules* **2008**, 41: 6546-54.

(8) Ghugare S, Mozetic P, Paradossi G. *Biomacromolecules* **2009**, 10: 1589-96.

(9) Nolan CM, Serpe MJ, Lyon LA. *Biomacromolecules* **2004**, 5: 1940-6.

(10) Das M, Sanson N, Fava D, Kumacheva E. *Langmuir* **2007**, 23: 196-201.

(11) Nolan CM, Reyes C, Debord J, Garcia A, Lyon LA. *Biomacromolecules* **2005**, 6: 2032-9

(12) Nolan C, Gelbaum LT, Lyon LA. *Biomacromolecules* **2006**, 7:2918-22.

(13) Snowden M J. *J Chem Soc Chem Comm* **1992**, 11: 803-4.

(14) Huo D, Li Y, Kobayashi T. *Adv Mat Res* **2006**, 11-12: 299-302.

(15) Wu JY, Liu SQ, Heng PW, Yang YY. *J Controlled Release* **2005**, 102: 361-72.

(16) Zhou J, Wang G, Zou L, Tang L, Marquez M, Hu Z. *Biomacromolecules* **2008**, 9: 142-8.

(17) Hoare T, Pelton R. *Langmuir* **2008**, 24: 1005-12.

(18) Pelton R. *Adv. Colloid Interface Sci.* **2000**, 85: 1-33.

(19) Castro-Lopez V, Hadgraft J, Snowden MJ. *Int. J Pharm.* **2005**, 292: 137-47.

(20) Zhang Y, Guan Y, Zhou S. *Biomacromolecules* **2007**, 8: 3842–7.

(21) Harsh DC, Gehrke SH. *J Controlled Release* **1991**, 17: 175-85.

(22) Lutz JF, Hoth A. *Macromolecules* **2006**, 39:893-6.

(23) Lutz JF, Akdemir O, Hoth A. *J. Am. Chem. Soc.* **2006**, 128: 13046-7.

(24) Lutz JF, Weichenhan K, Akdemir O, Hoth A. *Macromolecules* **2007**, 40: 2503-8.

(25) Lutz JF. *J Polym. Sci. Part A: Polym. Chem.* **2008**, 46: 3459-70.

(26) Han S, Hagiwara M, Ishizone T. *Macromolecules* **2003**, 36: 8312-9.

(27) Ishiznoe T, Seki A, Hagiwara M, Han S, Yokoyama H, Oyane A, Deffieux A, Carlotti S. *Macromolecules* **2008**, 41: 2963-7.

(28) Badi N, Lutz JF. *J Controlled Release* **2009**, 140: 224-9.

(29) Cai T, Marquez M, Hu Z. *Langmu*ir **2007**, 23: 8663-6.

(30) Chi C, Cai T, Hu Z. *Langmuir* **2009**, 25: 3814-9.

(31) (a) Jones CD, Lyon A. *Macromolecules* **2000**, 33: 8301-6. (b) Jones CD, Lyon A. *Macromolecules* **2003**, 36: 1988-93. (c) Jones CD, Lyon A. *Langmuir* **2003**, 19: 4544-7.

(32) (a)Gan D, Lyon A. *J. Am. Chem. Soc.* **2001,** 123: 8203-9. (b) Jones CD, McGrath JG, Lyon A. *J. Phys. Chem. B* **2004**, 108: 12652-7.

(33) Berndt I, Richtering W. *Macromolecules* **2003**, 36: 8780-5.

(34) Berndt I, Pedersen JS, Lindner P, Richtering W. *Langmuir* **2006,** 22: 459-68.

(35) Chu B. *Laser Light Scattering*, 2nd ed, Academic Press: New York, **1991**.

(36) Tang Y, Liu SY, Armes SP, Billinghan NC. *Biomacromolecules* **2003**, 4: 1636-45.

(37) Giacomelli C, Le ML, Borsali R, Lai-Kee-Him J, Brisson A, Armes SP, Lewis A. *Biomacromolecules* **2006**,7: 817-28.

(38) Vertzoni M, Pastelli E, Psachoulias D, Kalantzi L, Reppas C. *Pharm. Res.* **2007**, 24: 909-17.

(39) Jiang X, Ge Z, Xu J, Liu H, Liu S. *Biomacromolecules* **2007**, 8: 3184-92.

(40) Marchandt E, Prichard AD, Casanegra P, Lindsay L. *Am. J. Cardiol.* **1984**, 53: 718.

(41) Shalinsky DR, Jekunen AP, Alcaraz JE, Christen RD, Kim S, Khatibi S, Howell SB. *Brit J Cancer* **1993,** 67(1): 30.

(42) Hejna M, Raderer M, Zielinski CC. *J. Natl. Cancer Inst.* **1999,** 91:22.

(43) Siepmann J, Peppas NA. *Adv Drug Delivery Rev.* **2001,** 48: 139.

(44) Giacomelli C, Schmidt V, Borsali R. *Langmuir* **2007**, 23: 6947-55.

(45) Avdeef A, Berger CM, Brownell C. *Pharm. Res.* **2000,** 17: 85-9.

Chapter 4

(1) Shi, J.; Votruba, A.R.; Farokhzad, O.C.; Langer, R. *Nano Lett.* **2010**, *10*, 3223.

(2) Torchilin, V.P. *Pharm. Res.* **2007**, *24*, 1.

(3) Reese, C.E.; Mikhonin, A.V.; Kamenjicki, M.; Tikhonov, A.; Asher, S.A. *J. Am. Chem. Soc.* **2004**, *126*, 1493.

(4) Oh, J.K.; Lee, D.I.; Park, J.M. *Prog. Polym. Sci.* **2009**, *34*, 1361.

(5) Stuart, M.A.C.; Huck, W.T.S.; Genzer, J.; Muller, M.; Ober, C.; Stamm, M.; Sukhorukov,

G.B.; Szleifer, I.; Tsukruk, V.V.; Urban, M.; Winnik, F.; Zauscher, S.; Luzinov, I.; Minko, S. *Nature Mater*. **2010**, *9*, 101.

(6) Wu, W.; Zhou, S. *Nano Review* **2010**, *1*, 5730-DOI:10.3402/nano.v1io.5730.

(7) Tan, B.H.; Tam, K.C. *Adv. Colloid Interface Sci.* **2008**, *136*, 25.

(8) Hu, Z.B.; Cai, T.; Chi, C.L. *Soft Matter* **2010**, *6*, 2115.

(9) Wu, W.; Zhou, T.; Shen, J.; Zhou, S. *Chem. Commun.* **2009**, 4390.

(10) Wu, W.; Mitra, N.; Yan, E.C.Y.; Zhou, S. *ACS Nano* **2010**, *4*, 4831.

(11) Gerweck, L.; Seetharaman, K. *Cancer Res.* **1996**, *56*, 1194.

(12) Stefanadis, C.; Chrysochoou, C.; Markou, D.; Petraki, K.; Panagiotakos, D.; Fasoulakis, C.; Kyriakidis, A.; Papadimitriou, C.; Toutouzas, P. *J. Clin. Oncol.* **2001**, *19*, 676.

(13) Soppimath, K.; Tan, D.; Yang, Y. *Adv. Mater*. **2005**, *17*, 318.

(14) Lo, C.; Lin, K.; Hsiue, G. *J. Control. Release* **2005**, *104*, 477.

(15) Zhang, L.; Guo, R.; Yang, M.; Jiang, X.; Liu, B. *Adv. Mater*. **2007**, *19*, 2988.

(16) Chen, Y.; Ding, D.; Mao, Z.; He, Y.; Hu, Y.; Wu, W.; Jiang, X. *Biomacromolecules* **2008**, *9*, 2609.

(17) Yang, L.; Guo, C.; Jia, L.; Liang, X.; Liu, C.; Liu, H. *J. Colloid Interface Sci.* **2010**, *350*, 22.

(18) Huynh, C.T.; Nguyen, M.K.; Kim, J.H.; Kang, S.W.; Kim, B.S.; Lee, D.S. *Soft Matter* **2011**, *7*, 4974.

(19) Carreira, A.S.; Goncalves, F.A.M.M.; Mendonca, P.V.; Gil, M.H.; Coelho, J.F.J. *Carbohydr. Polym.* **2010**, *80*, 618.

(20) Liu, W.; Huang, Y.; Liu, H.; Hu, Y. *J. Colloid Interface Sci.* **2007**, *313*, 117.

(21) Cao, Y.; Zhang, C.; Shen, W.; Cheng, Z.; Yu, L.; Ping, Q. *J. Control. Release* **2007**, *120*,

186.

(22) Duan, C.; Zhang, D.; Wang, F.; Zheng, D.; Jia, L.; Feng, F.; Liu, Y.; Wang, Y.; Tian, K.; Wang, F.; Zhang, Q. *Int. J. Pharm.* **2011**, *409*, 252.

(23) Jang, J.H.; Choi, Y.M.; Choi, Y.Y.; Joo, M.K.; Park, M.H.; Choi, B.G.; Kang, E.Y.; Jeong, B. *J. Mater. Chem.* **2011**, *21*, 5484.

(24) Zhang, G.Z.; Winnik, F.M.; Wu, C. *Phys. Rev. Lett.* **2003**, *90*, 035506.

(25) Jung, H.; Jang, M.K.; Nah. J.W. *Macromol. Res.* **2009**, *17*, 265.

(26) Wu, W.; Aiello, M.; Zhou, T.; Berliner, A.; Banerjee, P.; Zhou, Q. *Biomaterials* **2010**, *31*, 3023.

(27) Wu, W.; Shen, J.; Banerjee, P.; Zhou, S. *Biomaterials* **2010**, *31*, 8371.

(28) Jiang, J.; Hua, D.; Tang, J. *Int. J. Biol. Macromol.* **2010**, *46*, 126.

(29) Fan, L.; Wu, H.; Zhang, H.; Li, F.; Yang, T.; Gu, C.; Yang, Q. *Carbohydr. Polym.* **2008**, *73*, 390.

(30) Li, F.; Wu, H.; Zhang, H.; Li, F.; Gu, C.; Yang, Q. *Carbohydr. Polym.* **2009**, *77*, 773.

(31) van Vlerken, L.E.; Vyas, T.K.; Amiji, M.M. *Pharm. Res.* **2007**, *24*, 1405.

(32) Zeng, M.; Fang, Z. *J. Membr. Sci.* **2004**, *245*, 95.

(33) Wu, J.; Wei, W.; Wang, L.; Su, Z.; Ma, G. *Biomaterials* **2007**, *28*, 2220.

(34) Lutz, J.F.; Akdemir, O.; Hoth, A. *J. Am. Chem. Soc.* **2006**, *128*, 13046.

(35) Wu, W.; hen, J.; Banerjee, P.; Zhou, S. *Biomaterials* **2010**, *31*, 7555.

(36) Zhou, T.; Wu, W.; Zhou, S. *Polymer* **2010**, *51*, 3926.

(37) Chu, B. *Laser Light Scattering, 2nd ed, Academic Press: New York*, **1991**.

(38) Alexis, F.; Pridgen, E.; Molnar, L.K.; Farokhzad, O.C. *Mol. Pharm.* **2008**, *5*, 505.

(39) Wu, C.; Zhou, S. *Macromolecules* **1997**, *30*, 574.

(40) Nayak, S.; Lyon, L.A. *Angew. Chem. Int. Ed.* **2005**, *44*, 7686.

(41) Longley, D.B.; Harkin, D.P.; Johnston, P.G. *Nature Rev. Cancer* **2003**, *3*, 330.

(42) Parker, J.B.; Stivers, J.T. *Biochemistry* **2011**, *50*, 612.

(43) Duffner, P.K. *J. Biol.* **2006**, *5*, 21.

(44) Han, R.; Yang, Y.M.; Dietrich, J.; Luebke, A.E.; Mayer-Proschel, M.; Noble, M. *J. Biol.* **2008**, *7*, e12.

(45) Siepmann, J.; Peppas, N.A. *Adv. Drug Delivery Rev.* **2001**, *48*, 139.

Chapter 5

(1) Wu, W.; Zhou, T.; Aiello, M.; Zhou, S. *Biosensors and Bioelectronics* **2010**, *25*, 2603-2610.

(2) Yildiz, I.; Deniz, E.; McCaughan, B.; Cruickshank, S. F.; Callan, J. F.; Raymo, F. M. *Langmuir* **2010**, *26*, 11503-11511.

(3) Wu, W.; Zhou, T.; Berliner, A.; Banerjee, P.; Zhou, S. *Angewandte Chemie International Edition* **2010**, *49*, 6554-6558.

(4) Obonyo, O.; Fisher, E.; Edwards, M.; Douroumis, D. *Crit. Rev. Biotechnol.* **2010**, *30*, 283-301.

(5) Vannoy, C. H.; Tavares, A. J.; Noor, M. O.; Uddayasankar, U.; Krull, U. J. *Sensors (Basel, Switzerland)* **2011**, *11*, 9732-9763.

(6) Xiong, H.-M.; Xu, Y.; Ren, Q.-G.; Xia, Y.-Y. *Journal of the American Chemical Society* **2008**, *130*, 7522-7523.

(7) Yuan, Q.; Hein, S.; Misra, R. D. K. *Acta Biomater* **2010**, *6*, 2732-2739.

(8) Fu, Y.-S.; Du, X.-W.; Kulinich, S. A.; Qiu, J.-S.; Qin, W.-J.; Li, R.; Sun, J.; Liu, J. *J. Am. Chem. Soc.* **2007**, *129*, 16029-16033.

(9) Tang, X.; Choo, E. S. G.; Li, L.; Ding, J.; Xue, J. *Chem. Mater.* **2010**, *22*, 3383-3388.

(10) Zhang, P.; Liu, W. *Biomaterials* **2010**, *31*, 3087-3094.

(11) Saunders, B. R.; Laajam, N.; Daly, E.; Teow, S.; Hu, X.; Stepto, R. *Adv Colloid Interface Sci* **2009**, *147-148*, 251-262.

(12) Das, M.; Zhang, H.; Kumacheva, E. *Annu. Rev. Mater. Res.* **2006**, *36*, 117-142.

(13) Baker, W. O. *Ind. Eng. Chem.* **1949**, *41*, 511-520.

(14) Shin, B. C.; Jhon, M. S.; Lee, H. B.; Yuk, S. H. *European Polymer Journal* **1998**, *34*, 1675-1681.

(15) Dalmont, H.; Pinprayoon, O.; Saunders, B. R. *Langmuir* **2008**, *24*, 2834-2840.

(16) Katono, H.; Maruyama, A.; Sanui, K.; Ogata, N.; Okano, T.; Sakurai, Y. *Journal of Controlled Release* **June**, *16*, 215-227.

(17) Okano, T.; Bae, Y. H.; Jacobs, H.; Kim, S. W. *Journal of Controlled Release* **1990**, *11*, 255-265.

(18) Lapeyre, V.; Ancla, C.; Catargi, B.; Ravaine, V. *Journal of Colloid and Interface Science* **2008**, *327*, 316-323.

(19) Torchilin, V. P. *Pharm. Res.* **2007**, *24*, 1-16.

(20) Stefanadis, C.; Chrysochoou, C.; Markou, D.; Petraki, K.; Panagiotakos, D. B.; Fasoulakis, C.; Kyriakidis, A.; Papadimitriou, C.; Toutouzas, P. K. *J. Clin. Oncol.* **2001**, *19*, 676-681.

(21) Gerweck, L. E.; Seetharaman, K. *Cancer Research* **1996**, *56*, 1194 -1198.

(22) Park, J. H.; Saravanakumar, G.; Kim, K.; Kwon, I. C. *Advanced Drug Delivery Reviews* **2010**, *62*, 28-41.

(23) Honarkar, H.; Barikani, M. *Monatshefte für Chemie Chemical Monthly* **2009**, *140*, 1403-1420.

(24) Polk, A.; Amsden, B.; De Yao, K.; Peng, T.; Goosen, M. F. A. *Journal of Pharmaceutical Sciences* **1994**, *83*, 178-185.

(25) Lutz, J.-F.; Hoth, A. *Macromolecules* **2006**, *39*, 893-896.

(26) Hu, Z.; Cai, T.; Chi, C. *Soft Matter* **2010**, *6*, 2115.

(27) Lutz, J. *Journal of Polymer Science Part A: Polymer Chemistry* **2008**, *46*, 3459-3470.

(28) Badi, N.; Lutz, J.-F. *J Control Release* **2009**, *140*, 224-229.

(29) Buyukserin, F.; Camli, S. T.; Yavuz, M. S.; Budak, G. G. *Journal of Colloid and Interface Science* **2011**, *355*, 76-80.

(30) Wu, W.; Aiello, M.; Zhou, T.; Berliner, A.; Banerjee, P.; Zhou, S. *Biomaterials* **2010**, *31*, 3023-3031.

(31) Chung, T.-W.; Lin, S.-Y.; Liu, D.-Z.; Tyan, Y.-C.; Yang, J.-S. *Int J Pharm* **2009**, *382*, 39-44.

(32) Dong, Y.; Hassan, W.; Zheng, Y.; Saeed, A. O.; Cao, H.; Tai, H.; Pandit, A.; Wang, W. *J Mater Sci Mater Med* **2011**.

(33) Chu, B. *Laser light scattering: basic principles and practice*; Academic Press, 1991.

(34) Lutz, J.-F.; Akdemir, Ö.; Hoth, A. *J. Am. Chem. Soc.* **2006**, *128*, 13046-13047.

(35) Scartozzi, M.; Maccaroni, E.; Giampieri, R.; Pistelli, M.; Bittoni, A.; Del Prete, M.; Berardi, R.; Cascinu, S. *Pharmacogenomics* **2011**, *12*, 251-265.

(36) Longley, D. B.; Harkin, D. P.; Johnston, P. G. *Nat. Rev. Cancer* **2003**, *3*, 330-338.

(37) Parker, J. B.; Stivers, J. T. *Biochemistry* **2011**, *50*, 612-617.

(38) Duffner, P. K. *J. Biol.* **2006**, *5*, 21.

(39) Han, R.; Yang, Y. M.; Dietrich, J.; Luebke, A.; Mayer-Pröschel, M.; Noble, M. *J. Biol.* **2008**, *7*, 12.

(40) Siepmann, J.; Peppas, N.A. *Adv. Drug Delivery Rev.* **2001**, *48*, 139.

Chapter 6

(1) Glucose Sensing (Topics in Fluorescence Spectroscopy), ed. C. D. Geddes and J. R. Lakowicz, Springer, New York, **2006**, vol. 11.

(2) V. R. Kondepati and H. M. Heise, Anal. Bioanal. Chem., **2007**, 388, 545.

(3) A. Heller and B. Feldman, Chem. Rev., **2008**, 108, 2482.

(4) A. P. Davis and R. S. Wareham, Angew. Chem., Int. Ed., **1999**, 38, 2979.

(5) (a)W. Yang, H. He and D. G. Drueckhammer, Angew. Chem., Int. Ed., **2001**, 40, 1714; (b) B. Peng and Y. Qin, Anal. Chem., **2008**, 80, 6137.

(6) E. Shoji and M. S. Freund, J. Am. Chem. Soc., **2002**, 124, 12486.

(7) (a) S. A. Asher, V. L. Alexeev, A. V. Goponenko, A. C. Sharma, I. K. Lednev, C. S. Wilcox and D. N. Finegold, J. Am. Chem. Soc., **2003**, 125, 3322S. A. Asher, V. L. Alexeev, A. V. Goponenko, A. C. Sharma, I. K. Lednev, C. S. Wilcox and D. N. Finegold, Anal. Chem., **2003**, 75, 2316; (b)M.M.W.Muscatello, L. E. Stunja and A. A. Asher, Anal. Chem., **2009**, 81, DOI: 10.1021/ac900006x.

(8) (a) S. Kabilan, A. J. Marshall, F. K. Sartain, M. C. Lee, A. Hussain, X. Yang, J. Blyth, N. Karangu, K. James, J. Zeng, D. Smith, A. Domschke and C. R. Lowe, Biosens. Bioelectron., **2004**, 20, 1602; (b) X. Yang, M. C. Lee, F. Sartain, X. Pan and C. R. Lowe, Chem.–Eur. J., **2006**, 12, 8491.

(9) J. T. Suri, D. B. Cordes, F. E. Cappuccio, R. A. Wessling and B. Singaram, Angew. Chem., Int. Ed., **2003**, 42, 5857.

(10) D. Roy, J. N. Cambre and B. S. Sumerlin, Chem. Commun., **2009**, 2106.

(11) (a) W. C. Chan and S. M. Nie, Science, 1998, 281, 2016; (b) W. C. Chan, D. J. Maxwell, X. Gao, R. E. Bailey, M. Han and S. M. Nie, Curr. Opin. Biotechnol., **2002**, 13, 40.

(12) I. L. Medintz, A. R. Clapp, F. M. Brunel, T. Tiefenbrunn, H. T. Uyeda, E. L. Chang, J. R. Deschamps, P. E. Dawson and H. Mattoussi, Nat. Mater., **2006**, 5, 581.

(13) D. Bardelang, Md. B. Zaman, I. L. Moudrakovski, S. Pawsey, J. C. Margeson, D. Wang, X. Wu, J. A. Ripmeester, C. I. Ratcliffe and K. Yu, Adv. Mater., **2008**, 20, 4517.

(14) (a) D. B. Cordes, S. Gamsey and B. Singaram, Angew. Chem., Int. Ed., **2006**, 45, 3829; (b) B. Tang, L. Cao, K. Xu, L. Zhou, J. Ge and L. Yu, Chem.–Eur. J., **2008**, 14, 3637.

(15) R. Gill, L. Bahshi, R. Freeman and I. Willner, Angew. Chem., Int. Ed., **2008**, 47, 1676.

(16) (a) Y. Zhang, Y. Guan and S. Q. Zhou, Biomacromolecules, **2006**, 7, 3196Y. Zhang, Y. Guan and S. Q. Zhou, Biomacromolecules, 2007, 8, 3842; (b) T. Hoare and R. Pelton, Macromolecules, **2007**, 40, 670.

(17) (a) P. Yez-Sedeo and J. M. Pingarrn, Anal. Bioanal. Chem., **2005**, 382, 884; (b) D. Mandal, H. Hosoi, U. Chatterjee and T. Tahara, J. Chem. Phys., **2009**, 130, 034902.

(18) (a) Y. Nosaka, J. Phys. Chem., **1991**, 95, 5054; (b) H. Matsumoto, T. Sakata, H. Mori and H. Yoneyama, J. Phys. Chem., **1996**, 100, 13781.

(19) S. A. Baker, A. K. Chopra, B. W. Hatt and P. J. Somers, Carbohydr. Res., **1973**, 26, 33.

(20) S. R. Wuister, C. M. Donega′ and A. Meijerink, J. Am. Chem. Soc., **2004**, 126, 10397.

Chapter 7

(1) Oh, J. K.; Drumright, R.; Siegwart, D. J.; Matyjaszewski, K. *Progress in Polymer Science* **2008**, *33*, 448-477.

(2) Otsuka, H.; Nagasaki, Y.; Kataoka, K. *Adv. Drug Deliv. Rev* **2003**, *55*, 403-419.

(3) Malmsten, M. *Soft Matter* **2006**, *2*, 760-769.

(4) Kost, J.; Langer, R. *Advanced Drug Delivery Reviews* **2001**, *46*, 125-148.

(5) Oishi, M.; Nagasaki, Y. *Nanomedicine* **2010**, *5*, 451-468.

(6) Yu, W. W. *Expert Opin. Biol. Ther.* **2008**, *8*, 1571-1581.

(7) Zhou, W.; Schwartz, D. T.; Baneyx, F. *Journal of the American Chemical Society* **2010**, *132*, 4731-4738.

(8) Dagallier, C.; Dietsch, H.; Schurtenberger, P.; Scheffold, F. *Soft Matter* **2010**, *6*, 2174.

(9) Sorrell, C. D.; Carter, M. C. D.; Serpe, M. J. *Advanced Functional Materials* **2011**, *21*, 425-433.

(10) Chan, Y.-H.; Wu, C.; Ye, F.; Jin, Y.; Smith, P. B.; Chiu, D. T. *Analytical Chemistry* **2011**, *83*, 1448-1455.

(11) Liu, T.; Hu, J.; Yin, J.; Zhang, Y.; Li, C.; Liu, S. *Chemistry of Materials* **2009**, *21*, 3439-3446.

(12) Steiner, M.S.; Duerkop, A.;Wolfbeis, O. S. *Chem. Soc. Rev.*, **2011**, *40*, 4805–4839.

(13) Ye, F.; Wu, C.; Jin, Y.; Chan, Y.-H.; Zhang, X.; Chiu, D. T. *Journal of the American Chemical Society* **2011**, *133*, 8146-8149.

(14) Okano, T.; Bae, Y. H.; Jacobs, H.; Kim, S. W. *Journal of Controlled Release* **1990**, *11*, 255-265.

(15) Katono, H.; Maruyama, A.; Sanui, K.; Ogata, N.; Okano, T.; Sakurai, Y. *Journal of Controlled Release* **1991**, *16*, 215-227.

(16) Shin, B. C.; Jhon, M. S.; Lee, H. B.; Yuk, S. H. *European Polymer Journal* **1998**, *34*, 1675-1681.

(17) Shen, W.; Chang, Y.; Liu, G.; Wang, H.; Cao, A.; An, Z. *Macromolecules* **2011**, *44*, 2524-2530.

(18) Tian, H.; Yan, J.; Wang, D.; Gu, C.; You, Y.; Chen, X. *Macromolecular Rapid Communications* **2011**, *32*, 660-664.

(19) Jochum, F. D.; zur Borg, L.; Roth, P. J.; Theato, P. *Macromolecules* **2009**, *42*, 7854-7862.

(20) Sudaxshina, M. *Journal of Controlled Release* **2003**, *92*, 1-17.

(21) Ge, H.; Ding, Y.; Ma, C.; Zhang, G. J. Phys. Chem. B, **2006**, *110*, 20635-20639.

(22) Matsumoto, A.; Yamamoto, K.; Yoshida, R.; Kataoka, K.; Aoyagi, T.; Miyahara, Y. *Chem. Commun.* **2010**, *46*, 2203-2205.

(23) Zhang, Y.; Guan, Y.; Zhou, S. *Biomacromolecules* **2006**, *7*, 3196-3201.

(24) Zhang, Y.; Guan, Y.; Zhou, S. *Biomacromolecules* **2007**, 8, 3842-3847.

(25) Hoare, T; Pelton, R. Macromolecules, **2007**, 40, 67-678.

(26) Hoare, T; Pelton, R. Biomacromolecules, **2008**, 9, 733-740.

(27) Lapeyre, V.; Gosse, I.; Chevreux, S.; Ravaine, V. *Biomacromolecules* **2006**, 7, 3356-3363.

(28) Ancla, C.; Lapeyre, V.; Gosse, I.; Catargi, B.; Ravaine, V. Langmuir, **2011**, 27, 12693-12701.

(29) Xing, S.; Guan, Y.; Zhang Y. Macromolecules, **2011**, 44, 4479-4486.

(30) Wu, W; Zhou, T.; Zhou, S. Chem. Comm., **2009**, 4390-4392

(31) Thomé-Duret, V.; Reach, G.; Gangnerau, M. N.; Lemonnier, F.; Klein, J. C.; Zhang, Y.; Hu, Y.; Wilson, G. S. *Anal. Chem.* **1996**, *68*, 3822-3826.

(32) Tierney, S.; Falch, B. M. H.; Hjelme, D. R.; Stokke, B. T. *Anal. Chem.* **2009**, *81*, 3630-3636.

(33) Lutz, J. *Journal of Polymer Science Part A: Polymer Chemistry* **2008**, *46*, 3459-3470.

(34) Lutz, J.-F.; Hoth, A. *Macromolecules* **2006**, *39*, 893-896.

(35) Ishizone, T.; Seki, A.; Hagiwara, M.; Han, S.; Yokoyama, H.; Oyane, A.; Deffieux, A.; Carlotti, S. *Macromolecules* **2008**, *41*, 2963-2967.

(36) Badi, N.; Lutz, J.-F. *J Control Release* **2009**, *140*, 224-229.

(37) Zheng, J.; Kwak, K.; Chen, X.; Fayer, M. D., J. Am. Chem. Soc., 2006, 128, 2977-2987.

(38) Pich, A.; Richtering, W. In *Chemical Design of Responsive Microgels*; Pich, A.; Richtering, W., Eds.; Springer Berlin Heidelberg: Berlin, Heidelberg, **2010**, 234, 1-37.

(39) Christensen, M. L.; Keiding, K. *Colloids and Surfaces A: Physicochemical and Engineering Aspects* **2005**, *252*, 61-69.

(40) Hyk, W.; Ciszkowska, M. *J. Phys. Chem. B* **2002**, *106*, 11469-11473.

(41) Asher, S. A.; Alexeev, V. L.; Goponenko, A. V.; Sharma, A. C.; Lednev, I. K.; Wilcox, C. S.; Finegold, D. N. *J. Am. Chem. Soc.* **2003**, *125*, 3322-3329.

(42) Zhou, T.; Wu, W.; Zhou, Q. *Polymer*, **2010**, *51*, 3926-3933.